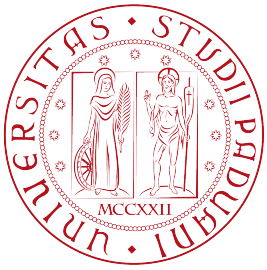

Università degli Studi di Padova

FACOLTÀ DI INGEGNERIA
Corso di Laurea Magistrale in Ingegneria dell'automazione

Tesi di laurea magistrale

Model reduction techniques for large scale nuclear fusion devices

Relatore:
Angelo Cenedese

Candidato:
Massimo Fagherazzi
Matricola 1057031

Anno Accademico 2014/2015

Acknowledgements

At first i want to thank my supervisor Angelo Cenedese, who sustained and supported me during all the period we spent together, giving to me useful hints and technical teachings and moreover allowing me to spend a great period in Barcelona working for F4E (Fusion for Energy) in a very fascinating European research environment.

My deepest gratitude goes to my family for their undeniable and unconditioned support throughout these years.

Finally, I wish to thank all my friends for the time we spent together.

Contents

Abstract

Tokamaks are controlled nuclear fusion devices which are capable of confining a high temperature plasma inside a vacuum toroidal chamber by exploiting the action of magnetic fields on the ionized particles generating the plasma. Numerous control problems are involved in the functioning of these devices. In particular, a crucial role is played by the reconstruction of the position of the plasma inside the chamber as direct contact with the plasma surrounding structures must be avoided. Therefore, the use of feedback for plasma shape control as been widely investigated in the last years, in order to create magnetic fields capable of modifying plasma shape and position (see [10]). Unfortunately, the plasma boundary position is not directly measurable. As a consequence, several plasma boundary reconstruction algorithm have been developed in the last years. Accurate models are needed to describe the plasma behavior and its electromagnetic coupling with the surrounding structures. Thus, such models take into account the massive conducting structures around the vacuum chamber which are modeled by toroidally symmetric elements and consequently the model order rise with the complexity of the structure. This is a drawback when dealing with real-time constraints and also for many standard linear control schemes. Therefore, model order reduction techniques have been developed in the last years, in order to provide a reasonable trade-off between the contrasting needs of reducing the number of states and of reaching a good approximation of the overall system behavior. This work focuses on the analysis and the reduction of the models appearing in the IAIA code, which is an algorithm capable of accurately estimating the plasma shape and boundary position.

This thesis is organized as follows. In the first chapter an introduction on the nuclear fusion is provided together with the key concepts of the plasma shape and position control. Moreover, the state of the art in model order reduction is discussed.

The second chapter focuses on the description of the main components of the ITER tokamak fusion device, which represents the next step in the realization of electricity-producing fusion power plants, and the RFX-mod, a large experimental device built for plasma physics studies and operating in Padua. Furthermore, an insight on the IAIA code is given together with the discussion of some crucial steps adopted in the plasma boundary reconstruction, such as the filamentary models and the passive structures

modeling.

The third chapter lists the main model order reduction techniques that were implemented in the IAIA code as well as their main features and advantages respect to each other.

The fourth chapter provides the main results achieved in the model order reduction process applied to IAIA and RFX-mod systems.

Finally, the fifth chapter introduces another method to optimize the time consumption of the IAIA code, by reducing the number of internal parameters of the plasma filamentary model adopted inside the algorithm. The results achieved in one particular case are provided and discussed.

Chapter 1

Introduction

1.1 Nuclear fusion and tokamaks

Nuclear fusion is, in a certain sense, the opposite of nuclear fission. Nuclear fission is a mature technology, which produces energy through the splitting of heavy atoms like uranium in controlled chain reactions. The drawback is that the by-products of fission are highly radioactive and long lasting. On the other hand, fusion is the process by which the nuclei of two light atoms, like hydrogen, are fused together to form a heavier nucleus (helium), with energy produced as a by-product. For instance, see figure 1.1. Nuclear fusion occurs when two atomic nuclei stay close at a very short distance (about $10^{-15}m$) for a sufficiently long time interval to allow the nuclear strong force to fuse them together, and obtaining a single nucleus. The energy achieved throughout this process can be calculated using the famous Einstein's formula of balance between mass and energy $E = mc^2$. As a matter of fact, in every nuclear reaction reagents mass sum is different from the products one. For this reason, remembering the famous relation above, it's possible to conclude that the missing mass has been transformed into energy. Among all the conceivable fusion reactions, not all are actually realizable or useful. For instance, it's not always possible to create the necessary conditions to make a particular fusion reaction happen. Moreover, not necessarily a fusion reaction is exergonic, which means that not always there is a positive flow of energy from the system to the surroundings. Among the most convenient reactions, in terms of obtained energy and of easiness to create the experimental conditions, there is the deuterium-tritium fusion. When fusing together a nucleus of deuterium with one of tritium, a nucleus of helium is obtained together with a free neutron

$$ {}^{2}_{1}D + {}^{3}_{1}T \rightarrow {}^{4}_{2}He \text{ (3.517 MeV)} + {}^{1}_{0}n \text{ (14.069 MeV)}. $$

The virtue of this nuclear reaction it's huge; by comparing it with the fission reaction, here the neutron possesses a quantity of energy about 14 times greater. Furthermore,

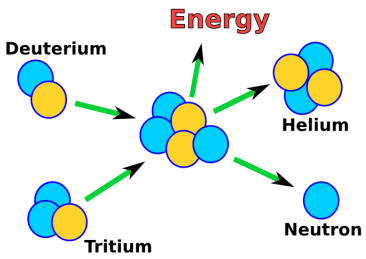

Figure 1.1: *Typical fusion reaction. Protons are shown in yellow, and neutrons are shown in light-blue. In a fusion reaction a deuterium nucleus and a tritium one combine to form a helium nucleus, and a free neutron, while producing excess heat. The excess heat is useful for sustaining additional fusion reactions, while the free neutron is captured by the fusion reactor, and its energy converted to heat.*

conventional methods of electric power generation bring with them some downsides, such as radioactive waste, greenhouse gases, or the use of non-renewable resources. In contrast, the development of a nuclear reactor would offer an almost limitless source of power, without any production of greenhouse gases. Moreover, nuclear fusion has no long-lived reaction by-products such as plutonium.

The aim of achieving controlled fusion is extremely challenging. A fusion power reactor will produce mostly short-term, low-level radioactive waste, and there is an abundant fuel supply available. In contrast to fission, fusion poses no risk of a nuclear accident. Fusion produces no air pollution or greenhouse gases during normal operation since the reaction product is helium. The primary sources of radioactive by-products are neutron-activated materials, which can be safely and easily disposed of within a human lifetime, differently from most fission by-products, which require special storage over thousand of years.

The primary challenge of fusion is to confine a gas comprised of ionized hydrogen isotopes, called a plasma, while it is heated and its pressure increases to initiate and sustain fusion reactions. There are three known ways to confine the plasma.

1. Gravitational confinement, confines the plasma through large gravitational forces. This is what happens in the sun.

2. Second, inertial confinement compresses the hydrogen gases through a controlled implosion, with inertia then holding the gases together long enough for fusion reactions to occur.

3. Finally, magnetic confinement. Here magnetic fields act on hydrogen atoms that have been ionized, so that the magnetic fields can exert a force on the moving particles. Thanks to the Lorentz force, a charged particle immersed in a magnetic field is bounded to move helically along the field lines which forum a cage

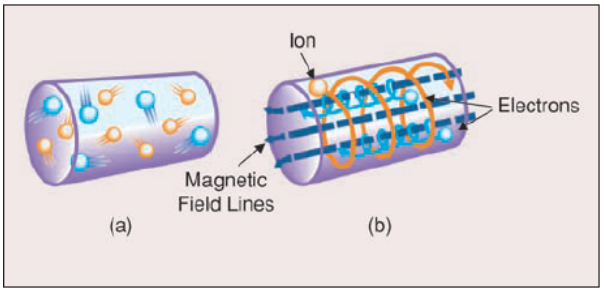

Figure 1.2: *The basic magnetic confinement concept. In (a), gas is unconfined and capable of moving in any direction, while in (b) the ionized gas interacts with a magnetic field externally imposed and is subject to forces that cause the ions to travel along the magnetic field lines while circling around these lines. Because the ions and electrons have opposite charges, these particles move in opposite directions along the field lines. In (b), the particles remain confined by the magnetic field until the field lines end or dissipate, contrary to the desire to keep them confined. Because of this, the tokamak bends the field lines into a torus so that these lines continue forever.*

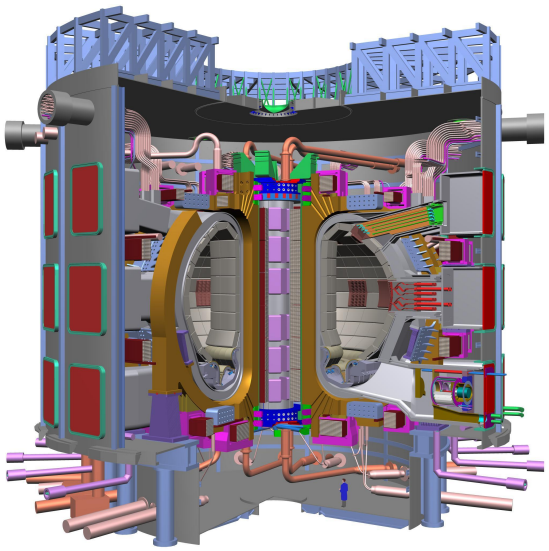

Figure 1.3: *Design of the ITER Tokamak, which is under construction in Cadarache, France. Note the size of the person in figure, relative to the device.*

around the plasma. The result of this interaction between the plasma and the magnetic fields is shown in figure 1.2.

Among all the proposed magnetic confinement devices, tokamaks are the most promising. A tokamak is a magnetic confinement device constructed in the shape of a torus.

Tokamaks are meant to create magnetic fields through currents that flow in large coils which are used to confine the plasma within a fixed volume. The shape of a torus can facilitate the fulfillment of the plasma confinement. Several of these magnetic coils

serve additional purposes of shaping, heating, and driving current in the plasma. In particular, the plasma inside the tokamak is confined by electromagnetic fields generated by a set of Poloidal Field (PF) coils distributed around the vacuum vessel. Voltages applied to these coils drive currents that produce a magnetic field. This field changes the shape and position of the plasma and induces plasma current.

During the last 50 years, tokamaks of various size were built all around the world. Nowadays, tokamaks have reached a point at which it's possible to produce almost as much energy as is expended in heating and confining the plasma. Figure 1.4 illustrates the growth of the fusion power output of tokamaks during the last 30 years. Actually, it is under construction the world's largest tokamak ever built, called International Thermonuclear Experimental Reactor (ITER). The goal of this huge project, funded by European Union, India, Japan, People's Republic of China, Russia, South Korea and the United States, is to demonstrate the feasibility of the use of fusion energy on an industrial scale. Therefore the ITER project aims to make the long-awaited transition from experimental studies of plasma physics to full-scale electricity-producing fusion power plants. ITER is a very complex nuclear fusion device, made of a large number of subsystems which must properly coexist to achieve nuclear fusion reactions. The most important subsystems are the vacuum chamber and the components fixed to it, such as the active coils, indispensable to create the magnetic fields to confine the plasma, the divertor, the additional heating modules, the cryogenic system, essential to create and maintain low-temperature conditions for the magnet, vacuum pumping and some diagnostics systems, the robotic system for maintenance, the general control system of the overall plant, and finally the numerous diagnostics. The next step is the construction and operation of the proposed ITER burning plasma experiment. The goal is to improve understanding of the underlying physics while providing a testbed for developing technology to support high fusion levels.

The performance in currently designed fusion devices, is strongly affected by the environment surrounding them. The plasma-circuit system is a distributed parameter system, consisting of the plasma itself, the surrounding passive structures, and the external circuits, whose dynamic behavior is described by a set of nonlinear PDE. The behavior of each circuit part or subsystem depends not only on its own physical and electrical characteristics, but also on the devices to which it is directly connected to or coupled with, including air and passive structures. This causes the analysis and modeling of these systems to be quite difficult. A tokamak can be seen as the union of three subsystems which interact with each other through electromagnetic fields, the plasma, the control circuits, and the passive conductors. The evolution of the whole system is governed by Maxwell's equations.

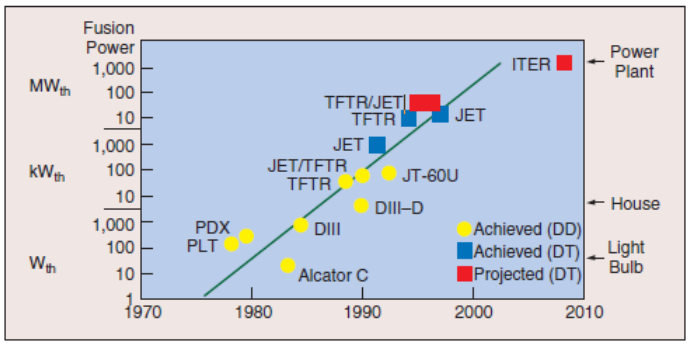

Figure 1.4: *The amount of power generated by tokamak devices has increased by a factor of* 10^8 *in the past* 30 *years. The ITER tokamak which will be the first experimental device able to produce more power than it consumes, appears to be a reasonable objective for the next decade of growth.*

The employment of mathematical models in the context of fusion plasma science and engineering has become of great importance since fusion devices are complex machines, whose operational state and behaviors depend on several controllable and non-controllable interconnected subsystems as, limiting the analysis to the magnetic control: the plasma, the electromagnetic circuits, the passive conducting structures, the magnetic diagnostics. The coupling of these elements give rise to high order, non-linear systems with a large number of instabilities, so there is consensus in the fusion community that active control will be one of the key enabling technologies, whence the need of accurate models derives. To simplify the analysis of the plasma position and current, and the design of plasma controllers, various assumptions are usually made. The two most important assumptions are the following.

1. The plasma-circuit system in a tokamak is assumed to be axisymmetric;
2. The plasma current profile can be described by means of a finite number of global parameters.

In particular, the first assumption let us reduce the question of plasma boundary reconstruction to a two-dimensional problem. These assumptions will be considered always verified in the following.

1.2 Plasma control

To achieve the deuterium-tritium reaction, temperatures higher than 100 million degrees Celsius are needed. To obtain these very high temperatures and maintain the plasma purity in a practical engineering system, the plasma must avoid any contact with the surrounding structures. The essential task of a tokamak is to confine and to heat the plasma so that sustained fusion reactions can occur. This confinement is basically possible due to the fact that the plasma is an ionized gas and therefore capable of interacting with externally generated magnetic fields. The charged particles composing the plasma are subjected to a magnetic field which confines them because they follow magnetic field lines. The effect of electric current flowing in the toroidal and PF coils and in the plasma produces helical magnetic field lines which provide a path for the ionized particles, which never leave the torus. In a tokamak, the plasma confinement is obtained through a complex system of magnetic fields which form a cage around the plasma. The toroidal field coils produce the main component of the magnetic field. This field, together with the one produced by the plasma current, create the basis of the magnetic confinement system. In addition to the toroidal field coils, there are also the PF coils. These coils are used modify the shape and position of the plasma inside the vacuum vessel.

In a simplified axisymmetric toroidal geometry, The dynamic of the plasma is that of a fluid conductor whose behavior is regulated by the Grad-Shafranov (GS) equation, this equation is a two-dimensional, nonlinear, elliptic PDE and describes the equilibrium between the kinetic pressure of the plasma and the Lorentz force. In the representation of plasma, discrete filamentary models and FE free boundary plasma models that can solve the GS equation have been successfully tested (For instance, see [27]). In particular, FE models proved to be more accurate because of their capacity of modeling the current distribution inside the plasma boundary with a higher number of degrees of freedom.

The toroidal fields are the dominant confining fields; they are typically on the order of a few Tesla. The coils are wound with many turns of conductors which carry several kilo amperes of current, producing an equivalent of many mega amperes of flux-producing current. Depending on the resistance of the coils (typically copper, but sometimes superconductors for newer tokamaks), the voltages required to drive the copper-borne currents range from a few volts to hundreds of volts in steady state. The magnetic fields produce an external magnetic pressure that balances the kinetic pressure created by the plasma.

Slight irregularities in the magnetic field confining the gas may allow plasma bulges that can grow exponentially over time if not actively suppressed. A large number of

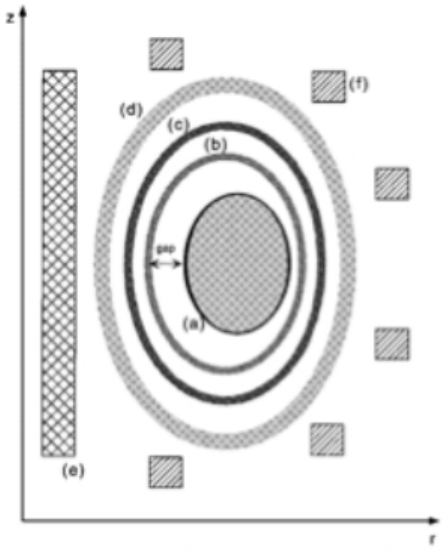

Figure 1.5: *Cross section of a standard tokamak. The plasma (a) is kept inside the vacuum vessel (b) and is coupled with the central solenoid (e). Toroidal (d) and poloidal (f) field coils contribute to shape the plasma and create the desired magnetic configuration. Metallic structures (c) are also present between the vessel and the magnet systems.*

such plasma instabilities can be predicted using ideal Magnetohydrodynamics (MHD) theory.

A key concept in plasma characterization is the plasma boundary, which is defined as the outermost closed flux surface entirely contained inside the vacuum chamber, not crossing any solid object. The plasma boundary usually needs to be as close as possible to the plasma surrounding structures, to enhance passive stabilization and to maximize the plasma volume. The use of magnetic measurements outside the plasma has traditionally been a simple and reliable method for finding the plasma configuration in fusion experiments. Unfortunately, numerical codes developed for full MHD equilibrium reconstruction from external magnetic measurements require too high computational effort which isn't suited with real-time constraints. For this reason, alternative methods, based on simpler and faster algorithms, have been developed to comply with the specific requirements of real-time plasma contour identification such as Equivalent Currents [29], Toroidal Harmonics [30], Local Field Expansion [20], or their combination into modular frameworks ([5], [6]).

By the way, recently, it has been developed a new filamentary model capable of controlling the degrees of freedom of the problem through SVD regularization combined within an iterative scheme. This allow the representation of advanced configurations with strongly non-homogeneous current distribution while keeping the model sufficiently compact. This algorithm is called Iterative Axisymmetric Identification Algorithm (IAIA).

In this respect, the estimation of the currents flowing in the passive structures is a key issue, because it may be misinterpreted by the external sensors as a contribution of the plasma itself, and can lead to wrong comprehension over the role of the passive stabilization that counteracts plasma instabilities while active control fields penetrate the vessel shielding.

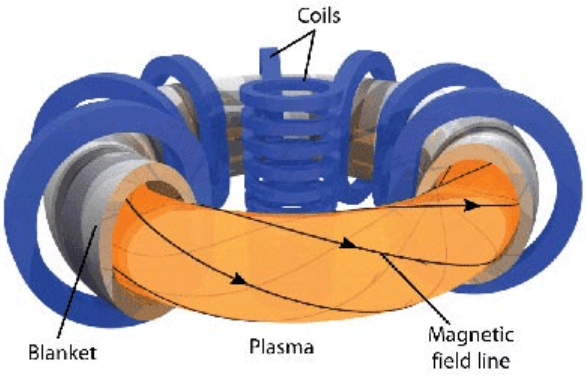

Figure 1.6: *Thanks to the shape of a torus, some of the magnetic field lines never leave the tokamak vacuum chamber.*

The use of feedback for plasma position, current, and shape control has been extensively investigated in the last few decades. These control systems are used to maintain the plasma at a desired equilibrium configuration. Controller design for these systems is usually based on low-order, linear, time-invariant models. This task can be simplified by reducing the order of the original system and by approximating it with a lower order model. In recent years, much research has been done in order reduction of large scale systems with application to circuit simulation, micro-electro-mechanical systems and more. Such systems, composed of several elements or sub-systems, need to be accurately modeled, including the electro-magnetic couplings existing between the different elements. The electro-magnetic based modeling procedures usually rely on a discretization of the governing equations, in this case Maxwell's equations, in the domain of interest. A FE model of the conducting structures can provide a state space model that well matches the filamentary plasma model to follow dynamic evolution and scenario transitions. When in the description of a physical system the required or desired level of detail rises above a certain threshold, the resulting mathematical system becomes too complex, causing, for instance, numerical issues or too much expensive time requirements. To compute and/or simulate the phenomena of interest. This is particularly unwanted when we have to deal with real-time constraints. In fact, the simulation, analysis and controller design of high order control systems are quite complicated. From this considerations emerge the necessity to develop simpler models which well approximate the starting ones.

In the context of space-state representations of linear systems of high dimension the objective of Model Order Reduction (MOR) is the development of a new model of the linear system of much smaller dimension than the original one, yet capable of describing the behavior of the original model with acceptable accuracy over a broad frequency bandwidth, or at least along the band of interest. The discretization of the spatial derivatives in Maxwell's time-dependent equations using finite methods results in state space semi-discrete approximations of the electromagnetic system, which approximately describe the relations between the elements in the environment of interest.

MHD equations

Magnetohydrodynamics (MHD) is the branch of plasma physics that describes the basic behavior of the plasma, in terms of interaction among currents, magnetic fields, and forces exerted on and by the plasma. MHD treats the plasma as a fluid, without distinction between the ions and electrons comprising the fluid. In particular, ideal MHD [34] starts from the assumption that the plasma has zero electrical resistance (only partially satisfied). However, this branch of MHD is sufficiently accurate to prompt its use as a first approximation in a wide range of analysis done for tokamak plasma physics, including definition of plasma magnetic evolution equations, estimation of plasma shape and position control and studies of plasma magnetic instabilities. MHD applies both to axisymmetric and nonaxisymmetric plasma behavior. An important consequence of ideal MHD is that contours of constant axisymmetric poloidal flux are nested, as shown in figure 1.7. For the sake of generality, resistive MHD equations are reported, where a conductivity coefficient σ is defined. The quantities involved are the electric field $\mathbf{E}$, magnetic field $\mathbf{B}$, current density $\mathbf{J}$, fluid velocity $\mathbf{v}$, pressure p and mass density ρ. $\mathbf{E}_i$ is the impressed field, defined to model external forces per unit charge. Maxwell equations give reason of the interaction with external fields, and Navier-Stokes equation models fluid dynamics.

$$\nabla \times \mathbf{E} = -\frac{\partial \mathbf{B}}{\partial t}$$

$$\nabla \times \mathbf{B} = \mu_0 \mathbf{J}$$

$$\nabla \cdot \mathbf{E} = 0$$

$$\nabla \times \mathbf{B} = 0$$

$$\mathbf{J} = \sigma(\mathbf{E} + \mathbf{v} \times \mathbf{B} + \mathbf{E}_i)$$

$$\rho(\frac{\partial \mathbf{v}}{\partial t} + \mathbf{v} \cdot \nabla \mathbf{v}) = \mathbf{J} \times \mathbf{B} - \nabla p$$

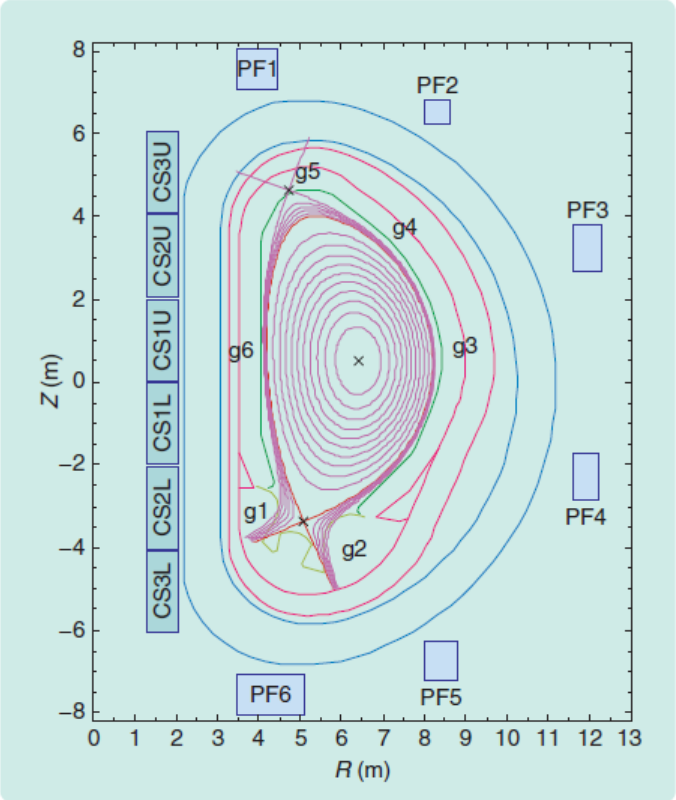

Figure 1.7: *ITER poloidal cross section. The contours of constant axisymmetric poloidal flux (magenta lines) are nested.*

1.3 State of the art in model order reduction

Nowadays, simulation has become an important part of the technological world, and it is considered as the third discipline, besides the classical disciplines of theory and experiment. Computer simulations are now performed routinely for several kind of processes, and virtual design environments have been set up in order to ease the work of designers and engineers. In this way it's possible to design new products, in a more reliable way, and without the need to produce costly prototypes. Numerical simulation of large-scale dynamical systems plays a fundamental role in the study of a wide range of complex physical phenomena; however, the large-scale nature of several models leads to an unmanageable computational burden. In engineering, the modeling of a dynamic process plays a crucial role in the whole study. Depending on the specific application, the model can vary over a wide range of complexity being described by few equations (e.g. as derived by lumped parameters model) or by several thousands of equations (as obtained by 2D or 3D finite elements models). When deciding on the model complexity, one has to reach a compromise between the detailed representation of the phenomena of interest and the model complexity. In any case, simpler models are often preferred due to their better suitability with computer simulations and real-

time constraints. Moreover, a high model complexity leads to high order models and this is a drawback for many standard linear control schemes such as linear quadratic Gaussian. The consequence is that reduced models are obtained starting from more detailed ones through some MOR technique, without affecting the relevant features of the starting models. Once a detailed model is derived, the reduction procedure should lead to a simpler model, whose output, for the same input signals, mimics the one of the original system. This consistency, between the input-output behavior of the original and simplified systems must be guaranteed over the whole range of operating conditions of interest for the system to be studied.

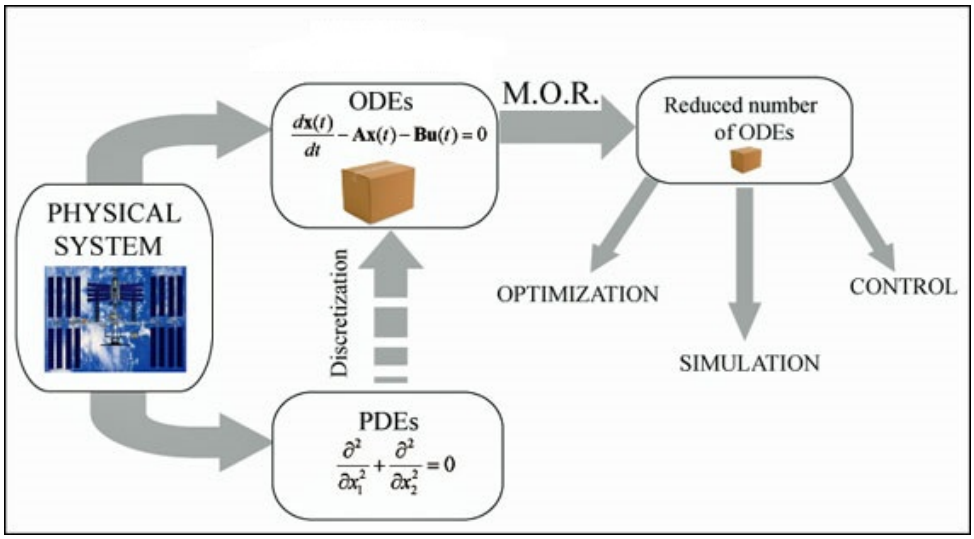

Figure 1.8: *Basic steps in the study of complex physical systems. First a set of ODE describing the system behavior is derived. After this, due to the system complexity, a MOR step is required to simplify the analysis, simulation and controller design.*

In order to understand this idea from a mathematical point of view, it is useful to restrict the attention to linear, time invariant systems. A state-space representation of a system $S = (A, B, C, D)$ is given by

$$\dot{x}(t) = Ax(t) + Bu(t)$$
$$y(t) = Cx(t) + Du(t)$$

and its transfer function $G(s) = C(sI - A)^{-1}B + D$ describes the input-output system behavior in the frequency domain. The high order model is considered exact and the purpose is to find and compute low order approximations. The system order n can be very large. As a consequence, since low order models give more efficient[1] simulations and lead to low order optimal controllers, an important question is whether is possible to simplify the high order model without an excessive loss of accuracy. The fundamental task of every model reduction procedure is to compute, for a given $r < n$, a reduced

[1] In terms of execution times as well as limited numerical issues.

system S_r, of order r, which approximates S. A space-state representation of S_r is

$$\dot{x}_r(t) = A_r x_r(t) + B_r u(t)$$
$$\hat{y}(t) = C_r x_r(t) + D_r u(t)$$

And its transfer function is $G_r(s) = C_r(sI - A_r)^{-1}B_r + D_r$. More in general, an optimal reduction problem aims to find a system of low order r with transfer function G_r that, among all systems of McMillan degree r, minimizes $||G - G_r||_p$ for some p. By the way, there are several aspects that play a role in MOR:

- Usually, the most important requirement is that the output signal $y(t)$ is well approximated by the low order model respect to some given input signal $u(t)$ (i.e. time domain behavior).
- Instead of the approximation in time domain, one can require that the Bode-plots of the transfer function for the original and reduced systems are as similar as possible (i.e. frequency domain behavior).
- Sometimes there are also requirement on the input-state behavior, so that the state trajectory $x(t)$ is approximated by the reduced order model.
- Finally, it may be required that the state variables of the reduced model have some physical meaning, just like the variables of the full-order model.

If we consider only the first aspect, the input-output behavior, then the question is which parts of the model can be neglected without affecting too much the transfer function of the original system. First of all, it is clear that the uncontrollable and unobservable parts of the system can be easily removed without even modifying the transfer function. This concept can be better understood by focusing on a SISO system:

$$\begin{cases} \dot{z} = T^{-1}ATz + T^{-1}Bu = \begin{bmatrix} \lambda_1 & & \\ & \ddots & \\ & & \lambda_n \end{bmatrix} z + \begin{bmatrix} \bar{b}_1 \\ \vdots \\ \bar{b}_n \end{bmatrix} u \\ y = CTz = \begin{bmatrix} \bar{c}_1 & \dots & \bar{c}_n \end{bmatrix} z \end{cases}$$

It's clear that a state variable z_i can be easily removed when it appears to be uncontrollable ($\bar{b}_i = 0$), or unobservable ($\bar{c}_i = 0$), or both. When all the uncontrollable and unobservable state-variables are removed, a so-called *minimal realization* of the space-state model is obtained. The real MOR step occurs when removing also weakly controllable or observable state variables.

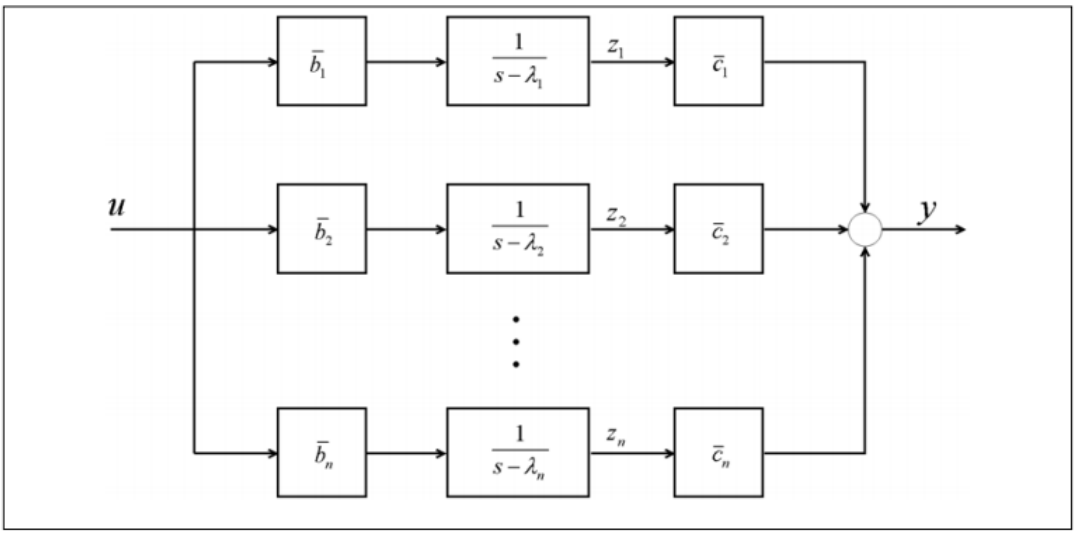

Figure 1.9: *If either $\bar{b}_i = 0$ or $\bar{c}_i = 0$, or both, the $i-th$ path can be removed and the input-output behavior doesn't change.*

In doing so, we can typically obtain a relevant reduction of the number of state variables, with the advantage of preserving those variables which are the most influential on the overall input-output behavior.

Fusion devices are complex machines, whose operational states and behaviors depend on several controllable and non-controllable interconnected subsystems as: the plasma, the electromagnetic circuits, the passive conducting structures, the magnetic diagnostics. The coupling of the elements composing the various subsystems give rise to high order systems with a large number of instabilities. Furthermore, the massive conducting structures around the vacuum chamber are usually modeled by toroidally symmetric elements of finite cross section (e.g. finite elements methods (FEM) models). The number of such elements, and therefore the model order, rapidly increases with the level of detail chosen to describe the passive structure and this is a drawback for many standard linear control schemes. Hence, as the level of detail and complexity increases, the computational effort might become too high. To cope with this problem, the fundamental idea is to derive models of reduced order, capable of giving an accurate description of the real system and at the same time allowing to simplify the design of the controller. The complexity reduction of these models, is one major issue to be addressed. In the past, several approaches have been followed ([16], [**?**]), and model reduction techniques are available from linear state-space control theory, among which it is worth mentioning state aggregation methods, balanced truncation and optimal Hankel norm approximation, Krylov based techniques, selective modal analysis. Actually, this field of research is very active, and in practice new methods and optimizations of existing approaches are often generated from specific application

needs and requirements.

A great number of MOR algorithms has emerged to generate macromodels for fast circuit simulation. In relation to their different application areas, these MOR algorithms can be classified into the following three groups.

1. Linear MOR. Linear model reduction of dynamical systems has reached a good level of maturity during the last 50 years. These techniques are mostly used to reduce the complexity of parasitic networks (For instance, RLC networks or discretized EM models) or chip packagings. Linear MOR can be implemented by exploiting numerous approaches, such as modal truncation, gramian-based reduction techniques (Truncated Balanced Realization (TBR), optimal Hankel norm approximation), Krylov-subspace projection, proper orthogonal decomposition reduction. All these are popular methods based on space projection, but because of the change of basis over the space state they have the drawback of losing the physical meaning of the starting model variables. For this reason other methods have been developed, such as Selective Modal Analysis (SMA), which allow to preserve this meaning resorting to a state selection according to the contribution of the single states to the model modes. For instance, in tokamak models, the state variables represent currents, voltages, fluxes and so on. They have a clear physical meaning in the overall system. Therefore it would be important not to loose this valuable feature while reducing the order of the system. Moreover, physical intuition on the system it's useful during the controller tuning and design phase. Techniques from linear system theory actually provide a reasonable trade-off between the contrasting needs of reducing the number of states to ease the controller design and of reaching a good approximation of the overall system behavior.

2. Nonlinear MOR. These techniques are mainly used to simplify the mathematical models of nonlinear devices (e.g., transistors, micro electro-mechanical systems devices) or systems. There are lots of examples of nonlinear systems in circuit design, such as almost all analog and radio-frequency blocks, amplifiers, mixers, oscillators, and so on.

3. Parametric MOR (pMOR). Parametric model reduction is a new and important research area. This kind of model reduction is linked with the class of problems where the equations governing the system behavior depend on a certain set of parameters. pMOR aims to generate low cost but accurate models capable of characterizing the system response for different values of the parameters. One advantage of pMOR is that it can be applied to both linear and nonlinear systems.

1.4 Objective and structure

Given this preliminary overview, the aim of this work is twofold:

- on the one side, we want to study a modeling technique for large scale tokamaks and in particular related to the ITER machine. Such model needs to be suited for plasma control and stabilization;
- on the other side, we want to develop a procedure for model reduction that allows us to employ the reduced models in real-time for diagnostics and/or control purposes as a kind of software in the loop.

This thesis is organized as follows. In the first chapter an introduction on the nuclear fusion is provided together with the key concepts of the plasma shape and position control. Moreover, the state of the art in model order reduction is discussed.

The second chapter focuses on the description of the main components of the ITER tokamak fusion device, which represents the next step in the realization of electricity-producing fusion power plants, and the RFX-mod, a large experimental device built for plasma physics studies and operating in Padua. Furthermore, an insight on the IAIA code is given together with the discussion of some crucial steps adopted in the plasma boundary reconstruction, such as the filamentary models and the passive structures modeling.

The third chapter lists the main model order reduction techniques that were implemented in the IAIA code as well as their main features and advantages respect to each other.

The fourth chapter provides the main results achieved in the model order reduction process applied to IAIA and RFX-mod systems.

Finally, the fifth chapter introduces another method to optimize the time consumption of the IAIA code, by reducing the number of internal parameters of the plasma filamentary model adopted inside the algorithm. The results achieved in one particular case are provided and discussed.

Chapter 2

Machine structure and system modeling

The entire performance of a nuclear fusion device system is obviously strictly depending on the real-time control of the plasma position and shape inside the vacuum chamber. Unfortunately, direct contact with the surrounding structures would cause huge damages and introduce impurities in the plasma itself. Due to the impossibility of direct evaluation, several algorithm have been developed to identify the plasma shape and boundary position, which make use of other sets of data, such as magnetic measurements (flux or field, or both) outside the vacuum chamber.

In almost all tokamak devices an axysimmetric geometry is assumed. In this way it is possible to ignore the toroidal coordinate ϕ in a cylindrical system $\{r, \phi, z\}$ and to consider a 2D flux map to describe the magnetic configuration and to locate the plasma boundary and shape inside the poloidal cross section of the machine. This allows to successfully make use of a 2D filamentary plasma model. In fact, in this work the plasma is considered as modeled using an appropriate set of filamentary currents placed well inside the vacuum vessel. Even though this model is quite different from the natural plasma distribution, outside the plasma boundary the filaments yield a magnetic field that can be made nearly indistinguishable from that of the real plasma. A fast and accurate identification of the plasma geometry is fundamental to achieve a robust control system and in the following we will study an appropriate modeling to this aim.

2.1 The International Thermonuclear Experimental Reactor (ITER)

Among the various nuclear fusion approaches, tokamaks have proved to be the most promising fusion devices. In a tokamak, a plasma is magnetically confined in order to achieve nuclear fusion. In a tokamak reactor, plasma is located inside a vacuum chamber, and several magnetic fields are applied to confine it. The dominant component of the magnetic field is the toroidal magnetic field, which is generated by a set of coils named TF coils. Unfortunately, a plasma placed in such a field can't come to an equilibrium force balance. Because of this, an additional magnetic field component is added to confine the plasma, the Poloidal Field (PF).

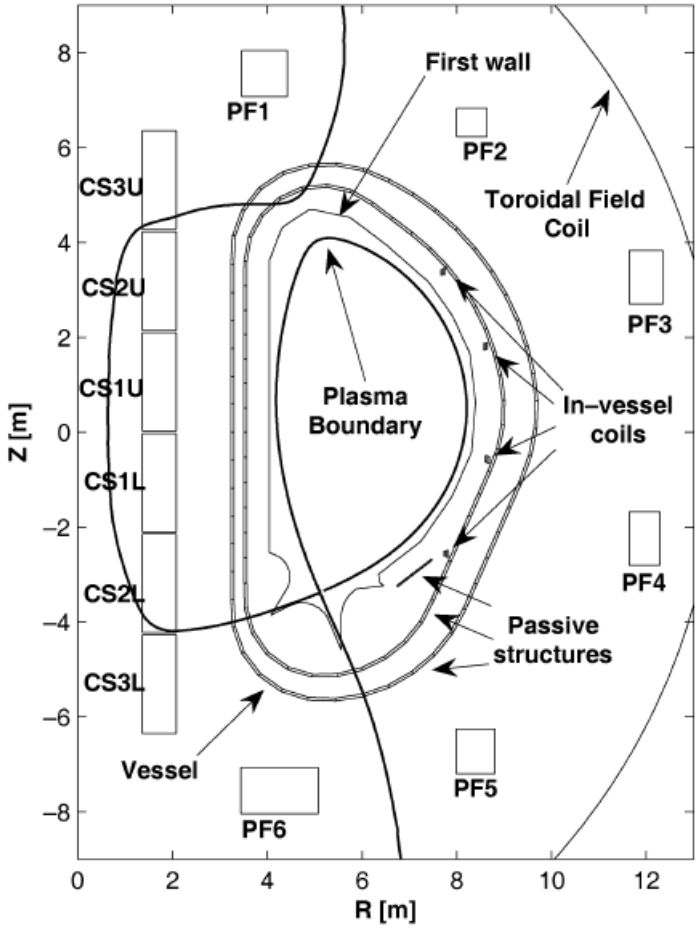

Figure 2.1: *ITER poloidal cross section. The figure shows in particular the location of the PF coils (PF 1-6) and the Central Solenoid (CS) six-coil stack.*

Such magnetic field component is given by the PF coils. This additional component is useful to both achieve the desired plasma configuration and to control the plasma shape and position. Therefore, the plasma is confined by a combination of magnetic fields with three different origins: TF coils, PF coils and plasma current.

The International Thermonuclear Experimental Reactor is the next step tokamak in the realization of electricity-producing fusion power plants. The main goal of the ITER tokamak is to achieve plasma burning condition, and produce about 500 MW of fusion generate-power for more than 1000 s. There are three main component in the structure of the ITER tokamak:

1. **Magnetic field coils**. The nested magnetic surfaces are able to confine a plasma equivalent to a few atmospheres, with a density that 10^6 times smaller than in the atmosphere. All the magnetic coils in ITER are superconducting. The TF coils are composed by Nb_3S_n, cooled at 4.5K by a flow of supercritical helium at about 0.6 MPa. The total magnetic energy in the toroidal field is of about 40 GJ, and therefore its confinement leads to significant forces exerted on each coil restrained by a thick steel case to resist circumferential tension. The coils are connected together using bolted structures and by two rings made of unidirectional glass fibers. The reason of a such robust assembly is that the TF coils must resist to the toroidal forces induced by the interaction of the TF coil current with the transverse poloidal field from plasma and PF coils. The plasma shape is modified by the currents distributed inside the six modules of the Central Solenoid (CS) and the six large PF coils. These axisymmetric coils are made of superconductors cooled by a flow of supercritical helium at 4.5K and 0.6 MPa. Nb_3S_n is used to build the CS modules, while N_bT_i can be exploited in the PF coils. Furthermore, another set of coils, named "Correction coils" is used, in order to correct possible imperfections in the magnetic field symmetry, due to a not perfect positioning of the PF, CS and TF coil currents. These coils (figure 2.2) are composed of three sets of six saddle coils, which are located between PF and TF coils. They are able to produce a field of about 10^{-5} times the TF value.

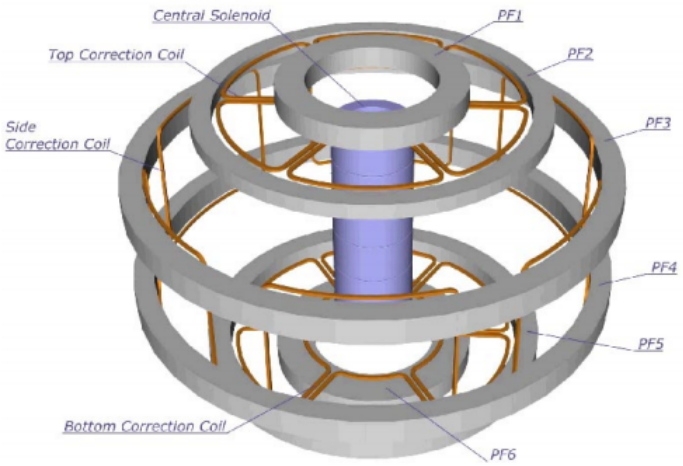

Figure 2.2: *ITER PF and correction coils.*

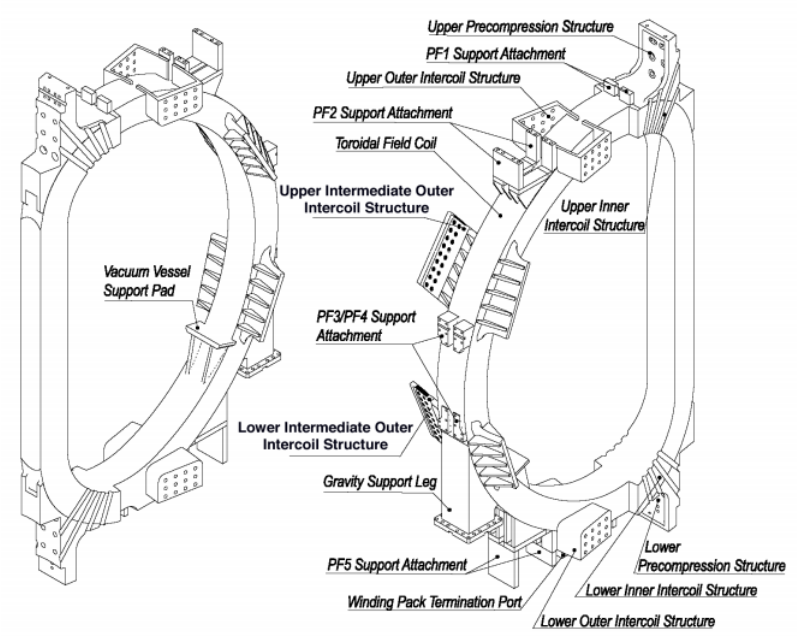

Figure 2.3: *TF coils structure.*

2. **Blanket modules**. The shielding blanket is composed of two parts: the back part is a shield made of steel and water, with a thickness of about 30 cm. The front part, named "first wall", include different materials: 1 cm thick beryllium armor protection, 1 cm thick copper, and about 10 cm of steel structure. This is a crucial component because, due to its proximity with the plasma, it is the most activated and tritium-contaminated in the entire ITER device. In particular it can suffer damage caused by the heat locally deposited, thus needing frequent maintenance operation. in order to allow practical maintenance, the blanket wall is modular (about 420 modules in total), with a maximum weight of 4.5 tons.

3. **Vacuum Vessel**. The vacuum vessel serves several functions:

   - It provides a boundary consistent with the generation and maintenance of a high quality vacuum, necessary to limit impurity flux into the plasma.
   - It participates in the shielding against neutrons.
   - it is a support for the in-vessel components and their mechanical loads.
   - It provides the access to the plasma through ports, for heating system, diagnostic, pumping, etc.
   - It provides the first confinement barrier for tritium and activated dust with a high reliability.

Other important components of the ITER machine are the divertor and the cryogenic pumps. More details on the ITER tokamak can be found in [14].

Superconducting TF coils	Nb_3S_n in circular stainless steel jacket grooved in radial plates
Superconducting Central Solenoid (CS)	Nb_3S_n in square Incoloy jacket, or in circular T_i/SS jacket. Segmented into six modules each built from 3 double or 1 hexa-pancakes, wind react and transfer technologies
Superconducting PF coils	N_bt_i in square stainless steel conduit
Vacuum vessel	Double-wall, welded ribbed shell, with internal shield plates and ferromagnetic inserts for TF ripple reduction
First wall/blanket	Single curvature faceted separate FW attached to shielding block which is fixed to vessel. Materials: Be armour, Cu-alloy heat sink, stainless steel
Divertor	Single null, modular cassettes with separable high heat flux components. Materials: W alloy and C plasma facing components
Cryostat	Reinforced cylinder with flat ends: 28 m diameter, 24 m height
Tokamak cooling water system	750 MW at 3 and 4.2 MPa water pressure
Electrical Power Supply	Total pulsed active/reactive power from grid: 500 MW. Total steady state active/reactive power: 110 MW

Table 2.1: *Main engineering features.*

The passive structures

The passive structures surrounding the plasma inside a tokamak play a fundamental role in the stabilization of the plasma. In ITER four different passive structures are considered, namely, the inner vessel, the outer vessel, the triangular structure and the vertical structure. These structures can be approximated by using toroidally symmetric elements of finite cross section, given the substantially axisymmetric nature of a tokamak device. For instance, see figure 2.4, where the passive structure is partitioned in 110 axisymmetric elements (50 elements both inner and outer vessel and 5 elements both vertical and triangular structure). Obviously the number of elements can

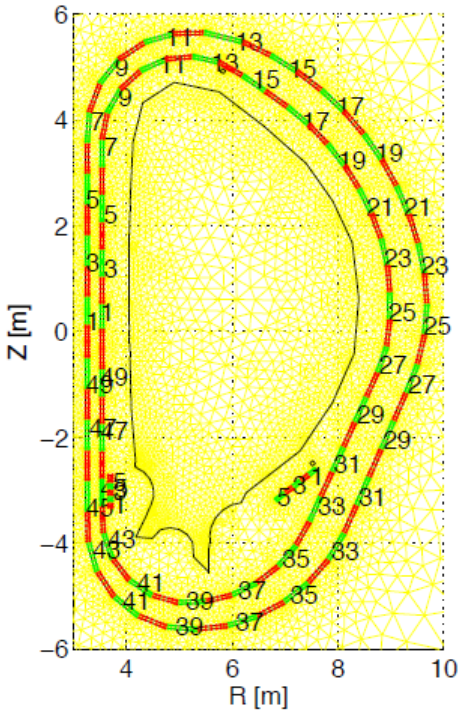

Figure 2.4: *Map of the passive structures divided in 110 toroidally symmetric elements.*

be arbitrarily chosen depending on the level of detail desired to describe the structure. Accordingly, the 110 elements can be split or fused together to obtain a higher or lower number of elements, respectively.

2.2 RFX-mod experiment

RFX-mod is an experimental device built to study Reverse Field Pinch (RFP) operation at high plasma current (up to 2MA). From the point of view of the the plasma current profile there is no difference between the RFX-mod and a general tokamak configuration. In the RFX-mod the plasma is formed in a toroidal vacuum chamber internally covered with graphite tiles. The vacuum vessel is closely surrounded by a thin copper

Transformer core material	air
Material composing the vacuum vessel	inconel
FW material	graphite
Shell material	copper
Coils conducting material	copper
Coils non-conducting material	fiberglass and kapton
Torus major radius	$2m$
Vacuum vessel volume	$8.31m^3$
Max. plasma current	2 MA
Max. magnetic toroidal field	0.7 T
Stored inductive energy	72.5 MJ
Chamber vacuum level	10^{-12} bar

Table 2.2: *Main RFX-mod specifications.*

shell, meant to stabilize fast-growing unstable MHD modes. The main difference that distinguish the RFX-mod from a tokamak is that it is possible to induce in the plasma ring a extremely high current, up to 2MA. In this way, together with a voltage applied to the toroidal loop, it is possible to achieve a huge dissipated power of about 40MW. Therefore, there is no need to use any further heating subsystem, which is typical in tokamak fusion devices.
Table 2.2 shows the main components of the RFX, which are:

- The plasma containment system, named "vacuum chamber", which contains the plasma gas that is then ionized. The vacuum chamber is constantly pumped by a pumping system which grant an high vacuum level.
- The First Wall (FW), which is the inner surface of the vacuum chamber, immediately in contact with the plasma, consist of 2016 trapezoidal graphite tiles, able to resist to temperatures up to 3000 °C.
- The shell, made of copper, which completely envelops the outer surface of the vacuum chamber. Due to the good electrical conductivity of copper, guarantees the magnetohydrodynamics plasma stability on a time scale of 50 ms.
- The magnetic system, made of several coils, which serve to induce the plasma current and produce the toroidal magnetic field.

The TF coils are used to provide stability to the plasma in the first phase of a RFP pulse. The toroidal circuit is composed of two identical groups, each feeding 6 of the

12 toroidal winding sectors. The TF coils circuit is designed to allow field reversal during RFP discharges, and a maximum toroidal field of 0.67 T can be produced. The PF coil system is composed by a magnetizing circuit (M coils), which serves to provide transformer action on the plasma and induce plasma current without generating a magnetic field in the plasma region, and field shaping circuit (F coils) which is used to control the plasma shape without providing a transformer action. For instance see figure 2.5. The systems is perfectly top-down symmetric. As a consequence, no net horizontal field can be generated on the equatorial plane of the machine. One advantage of the RFX-mod is that it can operate also in a tokamak configuration. In this case, it is not necessary to pre-charge the M coils, since the machine will operate at much lower plasma current ($\sim$100 kA for the Tokamak, 2 MA max. for normal RFP working conditions). The transformer action is provided by generating a growing (negative in sign) current in the M coils.

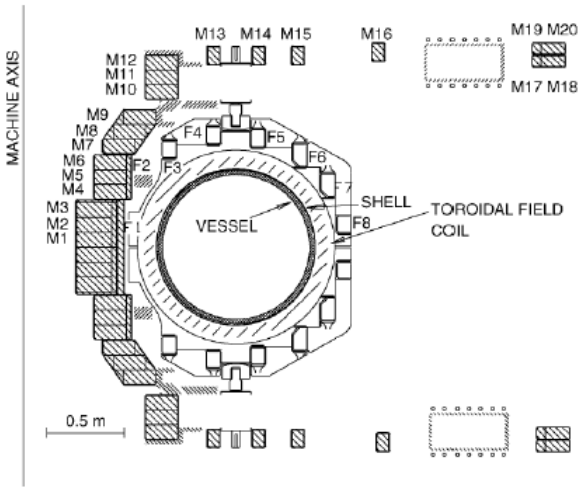

Figure 2.5: *RFX cross section.*

2.2.1 RFX-mod linear model

The derivation of a linear model for the RFX-mod device is presented in [7]. The resulting linear model is also stabilized with a closed-loop controller because of two unstable eigenvalues relative to horizontal and vertical plasma displacements instabilities. The model consist of 12 inputs, 250 states and 23 outputs. The inputs consist of voltages on F and saddle coils. The outputs are the plasma current, plasma current centroid position, 8 gap positions, 8 F coils currents and 4 saddle coils currents. The vessel and shell are both divided into 60 elements, and the structure is divided in two layers of 60 elements as shown in figure 2.6.

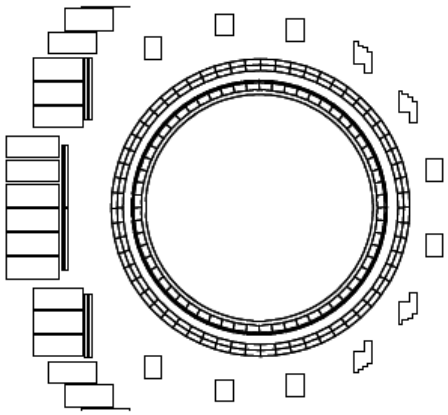

Figure 2.6: *Discretized mesh of the RFX-mod, used to derive the linear model.*

2.3 Current moments evaluation

The magnetic field map generated by the contemporary presence of plasma current, active coil currents and eddy currents is a fundamental element for the magnetic diagnostic system, constituted of field and flux sensors. By exploiting these measurements it is possible to obtain indirect measurements of, for instance, plasma current value and current centroid position. The current moment method [23] allows to measure some distribution of field sources inside the plasma, while distinguishing them from external ones. The current moment q_i can be associated to an external magnetic field B (where B_T and B_N are its tangential and normal components, respectively) as

$$q_i = \int_{\Omega_p} g j_p \cdot d\Omega = \oint_l (g B_T + r f B_N) \cdot dl$$

where Ω_P is the plasma cross section, l is a closed countour surrounding Ω_p, j_ϕ is the plasma current density, (g, f) is a couple of scalar functions solving the equation. The standard choice for g is a series of polynomial functions of the geometric coordinates:

$$\{g_n\} = \{1, z, r^2 z, r^2 z^2 - 0.25 r^4, \dots\}$$

The lower order moments give useful informations on the plasma such as total current (q_0), current centroid position (q_1, q_2), skew and vertical ellipticity (q_3, q_4), upward and outward triangularity (q_5, q_6). In particular, for the first three moments we have the following relations:

$$q_0 = \int_{\Omega_P} j_\phi \, d\Omega = I_p \qquad \longrightarrow \qquad \text{Plasma Current}$$

$$q_1 = \int_{\Omega_P} z \cdot j_\phi \, d\Omega = Z_p \cdot I_p \qquad \longrightarrow \qquad \text{Vertical Position}$$

$$q_2 = \int_{\Omega_P} r^2 \cdot j_\phi \, d\Omega = R_p^2 \cdot I_p \qquad \longrightarrow \qquad \text{Horizontal Position}$$

where I_p is the total plasma current and (R_p, Z_p) is the plasma centroid position.

From a more practical point of view, the integrals that appear in the moment equations must be discretized because of the availability of a finite number of measures, so the integrals over a continuous line reduce to a finite summation:

$$q_i \approx \hat{q}_i = \sum_{j=0}^{N_T} g_{T,j} B_{T,j} + \sum_{j=0}^{N_N} g_{N,j} B_{N,j} = \sum_{j=0}^{N_s} g_{s,j} s_j$$

where $B_{T,j}$ ($B_{N,j}$) is the $j-th$ measurement of the tangential field at one of the N_T (N_N) different positions, and $g_{T,j}$ ($g_{N,j}$) are suitable coefficients.

Since an approximation is exploited by using a finite sets of sensor measurements and suitable weighting coefficients, these moments are indicated as *estimated* moments: $\hat{q}_i$.

2.4 Filamentary model description

Recently, filamentary models for the plasma have been proposed in combination with low-order FE models of the conducting structures which allows the representation of advanced plasma configurations and scenario transitions [11]. The filamentary models allow a fast and easy description of the plasma shape inside the vacuum vessel with a relatively simple mathematical model. A basic filamentary model can be defined by a triple R_e, Z_e, I_e, of radial and vertical position of the filaments ($(R_e(ii) = r_{ii}$, $Z_e(ii) = z_{ii})$) and value of the filament current ($(I_e(ii))$: with a model composed of N_e filaments, this translates into a solution of $3N_e$ unknowns. The simplest possible filamentary model is composed by a single filament, of which the position (R_1, Z_1) and current (I_1) can be suitably and easily evaluated by exploiting the current moments, in order to obtain a basic description of the plasma shape:

$$\hat{q_0} = I_1$$
$$\hat{q_1} = Z_1 \cdot I_1$$
$$\hat{q_2} = R_1^2 \cdot I_1$$

Obviously the use of a single filament (and therefore only three degrees of freedom) allows to accurately describe only a small number of plasma shape. Also, only the first three moments can be exploited in this way. For this reason filamentary models are usually developed considering a sufficiently high number of filaments, in order to describe several plasma shapes. In any case, a typical choice is to use a filamentary model where the positions of the filaments are fixed. In such models, the relation between the currents in the filaments and the moments can be rewritten as:

$$Q = G \cdot I$$

where Q is the moment vector, G is a matrix containing the values of the g functions evaluated at the position of the filaments, and I are the filamentary currents. Typically, the number of unknowns (currents) is greater than the equations (moments). Therefore, in order to obtain the solution a pseudo-inverse G^{+} or optimization methods relative to the problem are considered.

2.5 Passive structures modeling

In dynamic conditions eddy currents are induced in the passive structures surrounding the plasma. The structures surrounding the plasma inside the vacuum chamber play a crucial role in the stabilization of the plasma. In fact, in dynamic conditions eddy currents are induced in the passive structures surrounding the plasma. These currents are usually of the order of several kilo-amperes, thus affecting the magnetic measurements used in the moments evaluation. Hence, the fast and accurate computation of these currents is crucial, in particular when the magnetic measurements are employed to determine the values of the parameters of a filamentary model in order to describe the plasma shape. The whole passive structure can be discretized into N_c triangular mesh elements according to a FE procedure, while the plasma is discretized using a filamentary model suitably defined.

Starting from a set of plasma currents $\mathbf{I_p}$ and the source currents flowing in the active circuits $\mathbf{I_s}$, and naming the flux linked by the passive elements as $\mathbf{\Psi_c}$, the following relations can be written for the passive structures:

$$\dot{\mathbf{\Psi}}_\mathbf{c} + \mathbf{R_c I_c} = 0 \Rightarrow \left(\mathbf{M_{cc}} \dot{\mathbf{I}}_\mathbf{c} + \mathbf{M_{cp}} \dot{\mathbf{I}}_\mathbf{p} + \mathbf{M_{cs}} \dot{\mathbf{i}}_\mathbf{s} \right) + \mathbf{R_c I_c} = 0,$$

$$\mathbf{I_c} = \mathbf{M_{cc}^{-1}} (\mathbf{\Psi_c} - \mathbf{M_{cp} I_p} - \mathbf{M_{cs} i_s}).$$

where:

- $\mathbf{M_{cc}} \in \mathbb{R}^{N_c \times N_c}$: inductance matrix of the passive structure elements;
- $\mathbf{M_{cp}} \in \mathbb{R}^{N_c \times N_p}$: inductance matrix linking the plasma elements to the passive structure;
- $\mathbf{M_{cs}} \in \mathbb{R}^{N_c \times n_s}$: inductance matrix linking the active coils to the passive structure;
- $\mathbf{R_c} \in \mathbb{R}^{N_c \times N_c}$: diagonal resistance matrix of the passive structure elements;

If we take the flux $\mathbf{\Psi_c}$ the system can be written in state space form as follows:

$$\dot{\mathbf{\Psi}}_\mathbf{c} = -\mathbf{R_c M_{cc}^{-1}} \mathbf{\Psi_c} + \mathbf{R_c M_{cc}^{-1} M_{cp} I_p} + \mathbf{R_c M_{cc}^{-1} M_{cs} i_s}$$

$$\mathbf{I_c} = \mathbf{M_{cc}^{-1}\Psi_c} - \mathbf{M_{cc}^{-1}M_{cp}I_p} - \mathbf{M_{cc}^{-1}M_{cs}i_s}$$

hence:

$$\begin{cases} \dot{\mathbf{\Psi}}_\mathbf{c} = A\mathbf{\Psi_c} + [B_p \; B_s] \begin{bmatrix} \mathbf{I_p} \\ \mathbf{i_s} \end{bmatrix} \\ \mathbf{I_c} = C\mathbf{\Psi_c} + [D_p \; D_s] \begin{bmatrix} \mathbf{I_p} \\ \mathbf{i_s} \end{bmatrix} \end{cases}$$

where the matrices A, B_p, B_s, C, D_p and D_s are suitably defined. It is important to stress the fact that the number of variables of the state-space systems directly depends on the number of elements that are considered in the vessel model. Therefore it is clear that by increasing the number of elements a more detailed model is obtained, with the drawback of having a more complex model, less suitable for real-time implementation. Model order reduction of this system is of crucial importance to improve the real-time performance of the entire algorithm.

2.6 Plasma measurements

In general the magnetic measurements $\mathbf{m}$ are the effects of the plasma current, the active coil currents $\mathbf{i_s}$ and the passive structure currents $\mathbf{i_c}$, respectively $\mathbf{m_p}$, $\mathbf{m_s}$, and $\mathbf{m_c}$:

$$\mathbf{m} = \mathbf{m_p} + \mathbf{m_s} + \mathbf{m_c},$$

which reduces to the following in the static case:

$$\mathbf{m} = \mathbf{m_p} + \mathbf{m_s}.$$

Then, since the active coil currents are known and the passive structure currents can be estimated, the magnetic measurements can provide the information related only to the plasma current contribution.

2.7 The Iterative Axisymmetric Identification Algorithm (IAIA)

The IAIA code is a fast and robust algorithm capable of accurately estimating the plasma shape and boundary position in an axisymmetric toroidal plasma geometry. The algorithm is based on a filamentary plasma model that is iteratively optimized and a SVD-based regularization scheme, in order to fit the magnetic measurements while avoiding ill-conditioned issues. More in detail, the IAIA code is a 2D reconstruction

algorithm based on a model of the machine that considers both the active coils and the passive structures (inner and outer vessels, vertical and triangular structures), takes the signals coming from both the magnetic sensors and the active coils as input, and provide the boundary location as a set of gap distances as output together with flux information at specified points on the poloidal plane. Given the knowledge of the currents flowing in the passive structures, the iterative procedure is able to accurately provide the location and shape of the plasma boundary using a unique fixed radial grid of possible equivalent plasma currents. In particular, the algorithm converges to a correct solution within three iterations, with errors in the 24 gaps almost always in the $\pm$10mm range. Moreover, the code used in the analysis appears to be suitable for real-time implementation and able to reconstruct both diverted and limiter plasmas. The code is structured into five cascading modules (see figure 2.7) and the core of the procedure is the approximation of the plasma with an equivalent filamentary model that is computed iteratively and allows to describe a wide variety of plasma current distributions, from the peaked ones, to the pedestal current ones.

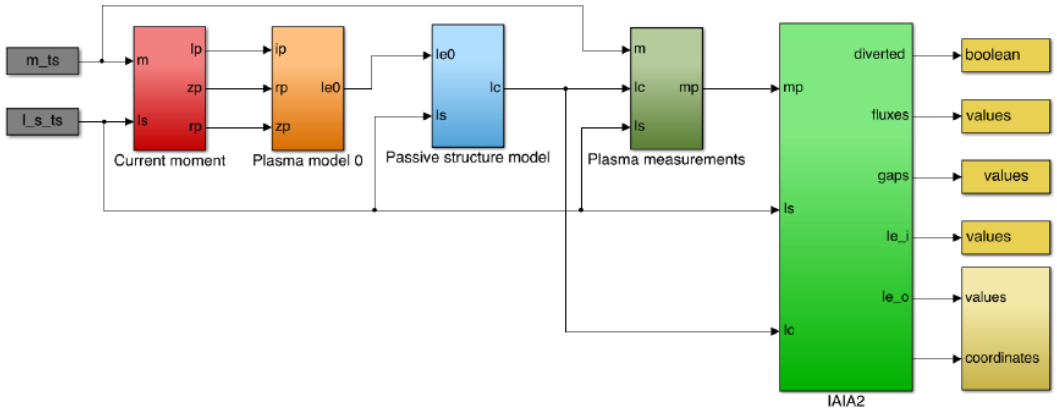

Figure 2.7: *Schematic drawing of the algorithm.*

The algorithm takes as inputs/outputs the following:

- Inputs (gray blocks in Figure 2.7):
  1. sensor measurements as timeseries (m), e.g. from pickup coils and/or flux loops;
  2. active coils signals as timeseries (I_s).
- Outputs (yellow blocks in Figure 2.7):
  1. diverted/limiter flag (*diverted*);
  2. flux values at a predefined set of positions (*fluxes*);

3. gap values at a predefined set of positions (*gaps*);
4. filamentary current plasma model (I_{e_i}, I_{e_o}).

With reference to figure 2.7, the IAIA algorithm works as follows:

1. At first, the inputs, which represents the available data, are used to compute the first three estimated plasma current moments (red block in figure 2.7)
2. After the moments are computed, they are taken by a new module (orange block in Figure 2.7) as input, in order to calculate a first guess plasma model.
3. With this filamentary plasma model as input, together with the active coils currents, a third module (light-blue block in figure 2.7) provides as output the passive currents in a discretized vessel model.
4. a fourth module receives as input the magnetic measurements, the active coils currents, and the passive current distribution provided by the third block, and calculates the magnetic measurements due to the plasma only.
5. The final module (light green block in figure 2.7) takes the active coil currents and the measurements due to the plasma only in input and provides the plasma shape descriptions (in terms of plasma-firstwall distances along predefined lines, i.e. gaps), position of the magnetic $x-point$ and other flux information outside the plasma, using a filamentary model that is iteratively optimized. The module procedure is explained in section 2.8.

The first 4 blocks rely on the considerations made in the previous sections. More in detail, the first guess plasma model is defined by a triple R_e, Z_e, I_e, of radial and vertical position of the filaments $((R_e(ii) = r_{ii}, Z_e(ii) = z_{ii}))$ and value of the filament current $(I_e(ii))$. For the sake of simplicity, the filaments position is chosen a priori, so that the problem boils down to the current distribution computation $(N_e$ unknowns$)$. In this spirit, to approximate the first three moments with a preliminary current distribution, it is possible to proceed by employing a fixed position filamentary model and fitting a sinusoidal current distribution of the kind:

$$I_e(ii) = I_0 + I_{\cos}(ii) + I_{\sin}(ii),$$

where I_0 is a current bias, and the $I_{\cos}$ and $I_{\sin}$ are sinusoidal contributions, with respect to the filament position:

$$I_{\cos}(ii) = I_{cos} \cos\theta_{ii}$$
$$I_{\sin}(ii) = I_{sin} \sin\theta_{ii}$$

being (r_{ii}, z_{ii}) the position of the $ii-th$ filament:

$$r_{ii} = r_0 + a\cos\theta_{ii}$$
$$z_{ii} = z_0 + b\sin\theta_{ii}$$

Given these assumptions:

$$\hat{q_0} = \sum_{ii=1}^{N_e} I_0$$
$$\hat{q_1} = z_0 N_e I_0 + b I_{\sin}\frac{N_e}{2}$$
$$\hat{q_2} = r_0^2 N_e I_0 + a^2 I_0 \frac{N_e}{2} + a r_0 I_{\cos} N_e$$

The parameters of this model are r_0, a, b, N_e. It follows:

$$\begin{cases} I_0 = \frac{1}{N_e}\hat{q_0} \\ I_{\sin} = \frac{2}{bN_e}(\hat{q_1} - z_0\hat{q_0}) \\ I_{\cos} = \frac{1}{ar_0N_e}\left(\hat{q_2} - \left(r_0^2 + \frac{a^2}{2}\right)\hat{q_0}\right) \end{cases} .$$

And so, by using the first three plasma moments, the first guess plasma filamentary model is computed.

2.8 Iterative procedure

The procedure implemented in the last module of IAIA is based on an Iterative Axisymmetric Identification Algorithm that adaptively allocates the equivalent currents to obtain the best estimate of the plasma contour.

The approach adopted to obtain this model is based on a static best fitting of the available magnetic measurements to compute the model parameters. This calculation involves the computation of the eigenvalues of a map between the equivalent currents $\mathbf{I_e}$ and the measurement contribution due to the plasma only $\mathbf{m_p}$: the larger the eigenvalues, the stronger the relation between the two sets of quantities. The cardinality N_e of the filamentary model and the positions of the equivalent current set are degrees of freedom of the inverse identification problem and they must be *a priori* assigned. The input quantities (known terms) of the identification problem are a set of n_m magnetic measurements (flux loops and pick-up probes) distributed inside and outside the vacuum vessel.

Then, for a given arrangement, the values of the equivalent currents $\mathbf{I_e}$ can be calculated as the solution of the following inverse problem:

$$\mathbf{m_p} = \mathbf{G_{mp}}\mathbf{I_e} \Rightarrow \mathbf{I_e} = \mathbf{G_{mp}^{-1}}\mathbf{m_p}$$

unfortunately G_{mp} is usually not-invertible (due to the fact that the chosen measurements are not linearly independent that translates into a rank-deficient matrix or to a number of unknowns different from the number of measurement data, i.e. undetermined/overdetermined problems).

Therefore, the problem is translated into an optimization one: in other words, starting from the observational data $\mathbf{m_p}$, we want to find the best distribution $\hat{I}_e$ that allows to approximate (and no longer to exactly match) the measurements $\mathbf{m_p}$:

$$\hat{\mathbf{I}}_\mathbf{e} = \min_{\mathbf{I_e}} ||\mathbf{G_{mp}}\mathbf{I_e} - \mathbf{m_p}||_\mathbf{2}$$

This problem has the following solution:

$$\hat{\mathbf{I}}_\mathbf{e} = \left(\mathbf{G}^\mathbf{T}_\mathbf{mp}\mathbf{G_{mp}}\right)^{-\mathbf{1}}\mathbf{G}^\mathbf{T}_\mathbf{mp}\mathbf{m_p}$$

In general, it may happen that the problem is ill-conditioned, where the extent of the ill-conditioning strongly depends both on the probe locations and on the arrangement selected for the equivalent currents. A singular value decomposition technique is usually adopted to approximate the ill-conditioned matrix $\mathbf{G_{mp}}$ with a better-conditioned one.

2.8.1 Iterative algorithm

Unfortunately, the matrix $\mathbf{G_{mp}}$ needs to be computed on-line since the choice of the filaments occurs in real time.

To locate the equivalent plasma currents within the plasma domain, a discrete set of rays is defined which starts at the machine center and extends towards the first wall. Along these lines (called *rad-lines*), filamentary currents are selected according to the iterative procedure described as follows:

- first, a set of equivalent currents is placed at the beginning of the current rays, well inside the plasma domain, in an area that is basically included in any plasma cross section shape;
- the current distribution I_{ei} on this inner set is computed according to the optimization problem seen before;
- given this current distribution, a flux map is generated and a first guess of the plasma boundary is computed;
- then, iteratively:

- a second set of equivalent currents is placed along the rays, midway between the starting point of the rays and the currently identified boundary (in order to avoid local artifacts induced by the filamentary model, the equivalent currents are in any case kept at a minimum distance from the identified boundary);
- the current distribution I_{eo} on this outer set is computed together with a new I_{ei} according to the usual optimization problem;
- a further boundary is computed;
- the procedure is iterated.

It can be chosen to have a fixed number of iterations (experimentally three iterations are sufficient to reconstruct plasmas with edge current distributions), or setting a convergence criterion with reference to some distance measurement between two consecutive iterations.

2.9 Passive structures model - explicit magnetic measurements

The overall structure of the algorithm analyzed until now can be partially compressed by considering the measurement term

$$\mathbf{m} = \mathbf{m_p} + \mathbf{m_s} + \mathbf{m_c},$$

where $\mathbf{G_{mp}}$, $\mathbf{G_{ms}}$, and $\mathbf{G_{mc}}$ are the Green matrices related respectively to the pairs measurements-plasma, measurements-active coils, and measurements-passive structures. From here, the $\mathbf{I_p}$ term can be obtained as

$$\mathbf{I_p} = \mathbf{G_{mp}^{+}}(\mathbf{m} - \mathbf{G_{ms}}\mathbf{I_s} - \mathbf{G_{mc}}\mathbf{I_c})$$

where the pseudoinverse of the matrix $\mathbf{G_{mp}}$ is used. Then, remembering

$$\mathbf{I_c} = -\mathbf{R_c}\dot{\mathbf{\Psi}}_\mathbf{c}$$

It follows

$$\dot{\mathbf{\Psi}}_\mathbf{c} = -\mathbf{R_c}\mathbf{M_{cc}^{-1}}\mathbf{\Psi_c} + \mathbf{R_c}\mathbf{M_{cc}^{-1}}\mathbf{M_{cp}}\mathbf{G_{mp}^{+}}\left(\mathbf{m} - \mathbf{G_{ms}}\mathbf{I_s} + \mathbf{G_{mc}}\mathbf{R_c^{-1}}\dot{\mathbf{\Psi}}_\mathbf{c}\right) + \mathbf{R_c}\mathbf{M_{cc}^{-1}}\mathbf{M_{cs}}\mathbf{i_s}$$

$$\mathbf{I_c} = \mathbf{M_{cc}^{-1}}\mathbf{\Psi_c} - \mathbf{M_{cc}^{-1}}\mathbf{M_{cp}}(\mathbf{m} - \mathbf{G_{ms}}\mathbf{i_s} - \mathbf{G_{mc}}\mathbf{I_c}) - \mathbf{M_{cc}^{-1}}\mathbf{M_{cs}}\mathbf{i_s}$$

And then a compact space-state model is obtained

$$\begin{cases} \dot{\mathbf{\Psi}}_\mathbf{c} = \bar{A}\mathbf{\Psi}_\mathbf{c} + [\bar{B}_p \ \bar{B}_s] \begin{bmatrix} \mathbf{m} \\ \mathbf{i_s} \end{bmatrix} \\ \mathbf{I_c} = \bar{C}\mathbf{\Psi}_\mathbf{c} + [\bar{D}_p \ \bar{D}_s] \begin{bmatrix} \mathbf{m} \\ \mathbf{i_s} \end{bmatrix} \end{cases}$$

with the following definitions:

$$\begin{cases} \bar{A} = -(\mathbf{I} - \mathbf{R_c}\mathbf{M_{cc}^{-1}}\mathbf{M_{cp}}\mathbf{G_{mp}^{+}}\mathbf{G_{mc}}\mathbf{R_c^{-1}})^{-1}\mathbf{R_c}\mathbf{M_{cc}^{-1}} \\ \bar{B}_m = (\mathbf{I} - \mathbf{R_c}\mathbf{M_{cc}^{-1}}\mathbf{M_{cp}}\mathbf{G_{mp}^{+}}\mathbf{G_{mc}}\mathbf{R_c^{-1}})^{-1}\mathbf{R_c}\mathbf{M_{cc}^{-1}}\mathbf{M_{cp}}\mathbf{G_{mp}^{+}} \\ \bar{B}_s = (\mathbf{I} - \mathbf{R_c}\mathbf{M_{cc}^{-1}}\mathbf{M_{cp}}\mathbf{G_{mp}^{+}}\mathbf{G_{mc}}\mathbf{R_c^{-1}})^{-1}(\mathbf{R_c}\mathbf{M_{cc}^{-1}}\mathbf{M_{cs}} - \mathbf{R_c}\mathbf{M_{cc}^{-1}}\mathbf{M_{cp}}\mathbf{G_{mp}^{+}}\mathbf{G_{ms}}) \\ \\ \bar{C} = (\mathbf{I} - \mathbf{M_{cc}^{-1}}\mathbf{M_{cp}}\mathbf{G_{mp}^{+}}\mathbf{G_{mc}})^{-1}\mathbf{M_{cc}^{-1}} \\ \bar{D}_m = -(\mathbf{I} - \mathbf{M_{cc}^{-1}}\mathbf{M_{cp}}\mathbf{G_{mp}^{+}}\mathbf{G_{mc}})^{-1}\mathbf{M_{cc}^{-1}}\mathbf{M_{cp}}\mathbf{G_{mp}^{+}} \\ \bar{D}_s = -(\mathbf{I} - \mathbf{M_{cc}^{-1}}\mathbf{M_{cp}}\mathbf{G_{mp}^{+}}\mathbf{G_{mc}})^{-1}(\mathbf{M_{cc}^{-1}}\mathbf{M_{cs}} - \mathbf{M_{cc}^{-1}}\mathbf{M_{cp}}\mathbf{G_{mp}^{+}}\mathbf{G_{ms}}) \end{cases}$$

Thanks to this manipulation, the first three blocks of the IAIA scheme can be grouped in a single one. Actually this model shows to be unstable depending on the chosen magnetic measurements as input. The reason of this behavior needs to be further investigated.

Chapter 3

Model order reduction techniques

In the IAIA code, as well as in other real-time reconstruction codes, the passive structure model block (light blue block in figure 2.7) might contain a standard state-space model with a great number of variables, depending on the level of detail we consider when modeling the passive structures, typically causing an excessive time consumption for our scopes. One possibility to overcome this problem is through model order reduction. The main goal is to obtain a low dimensional system, starting from the initial one, that has the same response characteristics as the original one with far less storage requirements and much lower evaluation time. Besides delivering a reduced model, MOR methods should have the following properties:

- They should suggest a suitable choice of the reduced model order q.
- The reduction should be invariant to different representations of the starting model.
- A stable original model leads to a stable reduced model.
- It should be clear in what sense the reduced order model is *optimal*.
- The reduction algorithm is numerically robust and possibly not excessively time consuming. Moreover, the method should be *automatic*, which means that there are not many design parameters to play with.

During the last years, different MOR techniques have been developed. In particular, three different techniques have achieved great success:

1. Truncated Balanced Realization (TBR), based on the Hankel singular values of the system;
2. Hankel norm optimal reduction;

3. Selective Modal Analysis (SMA);

4. Krylov subspace methods.

TBR satisfies each requirement with some restrictions on the last one. Krylov subspace methods do not necessarily are invariant to different realizations of the original model and do not always lead to stable models starting from a stable one. Finally, SMA main benefit is that the retained variables in the reduced order model preserve their physical meaning. These techniques are developed and analyzed in the following sections.

3.1 Truncated balanced realization

In many applications, the most important requirement is that the input-output behavior is well approximated by the reduced model. Then we have to understand which states can be neglected without changing the transfer function of the original system significantly. Controllability and observability concepts give us a way to proceed. First of all we can remove uncontrollable and unobservable states of the system, without affecting the transfer function. Secondly, after the first step is done, the key idea is to also remove weakly controllable and weakly observable states.

Consider the standard space-state system

$$\dot{x} = Ax(t) + Bu(t)$$

$$y = Cx(t) + Du(t)$$

Suppose that A is Hurwitz. Let P and Q denote the controllability and observability Gramians, respectively. Then P and Q satisfy the following Lyapunov equations:

$$AP + PA^T + BB^T = 0$$

$$A^TQ + QA + C^TC = 0$$

where $P \geq 0$, $Q \geq 0$. Furthermore, the pair (A, B) is controllable iff $P > 0$, and (C, A) is observable iff $Q > 0$. Suppose the state is transformed by a nonsingular T to $\hat{x} = Tx$. Then the Gramians are transformed to $\hat{P} = TPT^T$ and $\hat{Q} = (T^{-1})^TQT^{-1}$. It's then easy to prove that $\hat{P}\hat{Q} = TPQT^{-1}$, and therefore the eigenvalues of the product of the Gramians are invariant under state transformation.

Now consider the similarity transformation T, which gives the eigenvector decomposition

$$PQ = T^{-1}\Lambda T, \quad \Lambda = diag(\lambda_1 I_{s_1}, \ldots, \lambda_N I_{s_N})$$

Although the eigenvectors are not unique, in the case of a minimal realization they can always be chosen such that

$$\hat{P} = TPT^T = \Sigma,$$
$$\hat{Q} = (T^{-1})^T Q T^{-1} = \Sigma,$$

When proceeding with this kind of reduction it is very useful to pass through a balanced realization of the original system, which is a realization of the original system where the controllability Gramian $\hat{P}$ and the observability Gramian $\hat{Q}$ satisfy the following identity:

$$\hat{P} = \hat{Q} = \Sigma,$$

where $\Sigma = diag(\sigma_1 I_{s_1}, \ldots, \sigma_N I_{s_N})$ and $\Sigma^2 = \Lambda$. In this way we have obtained a new realization of the same system with balanced controllability and observability Gramians. This realization is the so called balanced realization. The decreasingly ordered numbers, $\sigma_1 > \sigma_2 > \cdots > \sigma_N \geq 0$, are called the *Hankel singular values* of the system. The balanced realization implies that those states corresponding to the smallest singular values are less controllable and less observable than the others. Therefore, truncating those less controllable and observable states will not lose much information about the system.

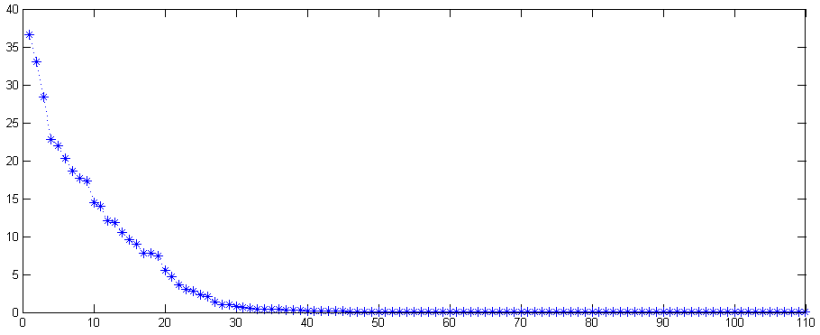

Figure 3.1: *Hankel singular values of the system with 110 states.*

In IAIA, the passive structure around the vacuum chamber is modeled with a stable standard space-state model with the following characteristics:

- $n = 110$ or $n = 1832$ states, which represent the metallic structures around the vacuum chamber. The number of states depends on the level of detail chosen during the design process to represent the passive structures.

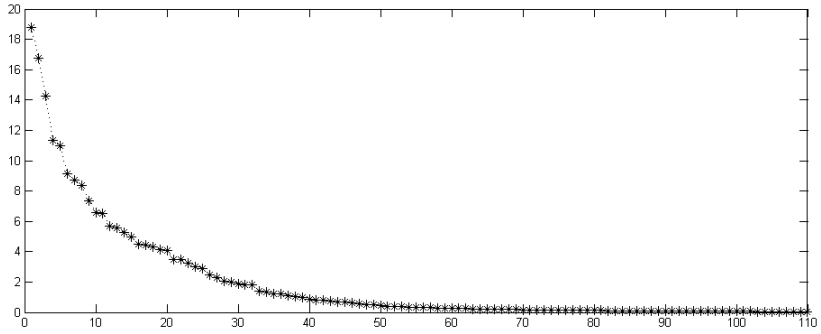

Figure 3.2: *First 110 Hankel singular values of the system with 1832 states.*

- $m = 114$ inputs, 100 are the current values of the filaments of the first guess plasma, while the remaining 14 inputs represent the currents flowing in the active coils.

- $p = 110$ or $p = 1832$ outputs, which correspond to the currents flowing in the metallic structures, depending on the level of detail chosen as before.

Both the models appear to be stable, controllable and observable, and so they are a minimal realization of their transfer function. Thus the gramians are positive definite. The state vector is then partitioned into x_1, to be kept, and x_2, to be discarded. All the matrices are then partitioned according to the partition of the state vector.

$$\begin{bmatrix} \dot{x}_1 \\ \dot{x}_2 \end{bmatrix} = \begin{bmatrix} A_{11} & A_{12} \\ A_{21} & A_{22} \end{bmatrix} \begin{bmatrix} x_1 \\ x_2 \end{bmatrix} + \begin{bmatrix} B_1 \\ B_2 \end{bmatrix} u$$

$$y = [C_1 \; C_2]x + Du$$

In figures 3.1 and 3.2 are represented the Hankel singular values of the systems we are dealing with. It is worth noticing that in both cases the first $30 - 40$ Hankel singular values decrease quite rapidly in magnitude and then the remaining ones are close to zero. Therefore it is clear that most of the information is contained in the first $30 - 40$ states of the systems, while the others can be discarded without affecting too much the systems input-output behavior. Figure 3.3 shows a comparison between the first 10 singular values of the original system, with 1832 states, and of the reduced model with 32 states only. The plots of the singular values of each system will be always made without considering the D matrix which directly links the inputs with the outputs, because it never changes during model order reduction operations.

Another approximation exists, where we do not simply discard the less controllable and less observable states to obtain the reduced order model, by using a slightly different approach. In this second approach we discard the specified states like in the first

method, then we alter the remaining states to preserve the DC gain of the full-order system. In particular, the derivative of x_2 is set to zero and then the resulting equation is solved for x_1. The reduced-order model is then given by

$$\dot{x}_1 = [A_{11} - A_{12}A_{22}^{-1}A_{21}]x_1 + [B_1 - A_{12}A_{22}^{-1}B_2]u,$$

$$y = [C_1 - C_2A_{22}^{-1}A_{21}]x_1 + [D - C_2A_{22}^{-1}B_2]u.$$

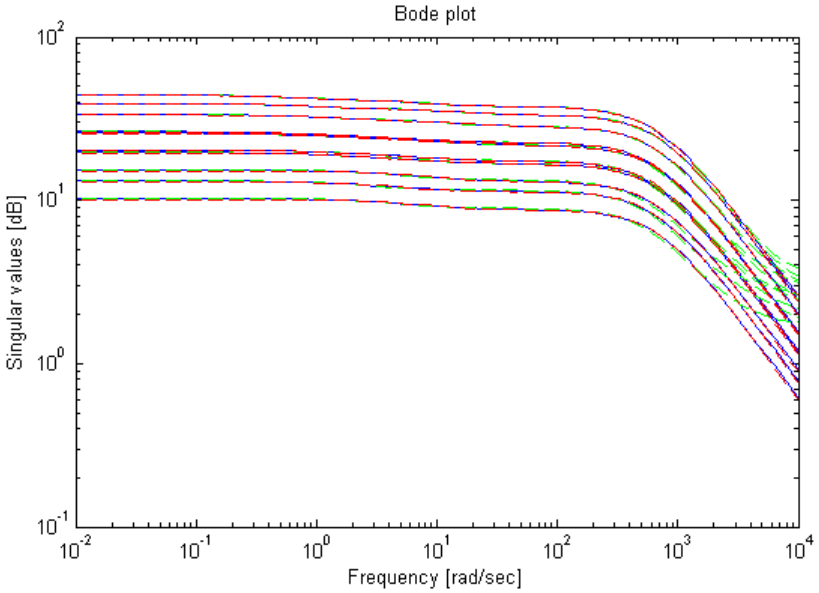

Figure 3.3: *First ten singular values of the full-order model (blue line), Hankel truncated reduced model (red-dashed), Hankel DC matched reduced model (green-dashed). [32 states].*

Figure 3.3 also shows that alterations made to preserve the DC gain of the full-order model have the drawback of producing a poorer performance at high frequencies, respect to the usual truncation approach. Obviously the choice between which approach to use depends on the particular application we are dealing with.

Furthermore, in figure 3.4 it is shown the behavior of the first 10 singular values, when we consider a reduced model of 20 states. The performance appears to be poorer as expected but quite acceptable, in particular the one of the truncated model, which approximates well enough the full-order model in a wide range of frequencies.

Finally, it can be shown that using the TBR method, based on the calculation of the original model Hankel singular values and on the truncation of these to the $k-th$ order, a H_∞ bound on the response of the error model is satisfied [12]:

$$||G(\omega) - G_k(\omega)||_\infty \leq 2 \sum_{i=k+1}^{n} \sigma_i.$$

where $||G||_\infty = \sup_\omega \sigma_{max}(G(j\omega))$.

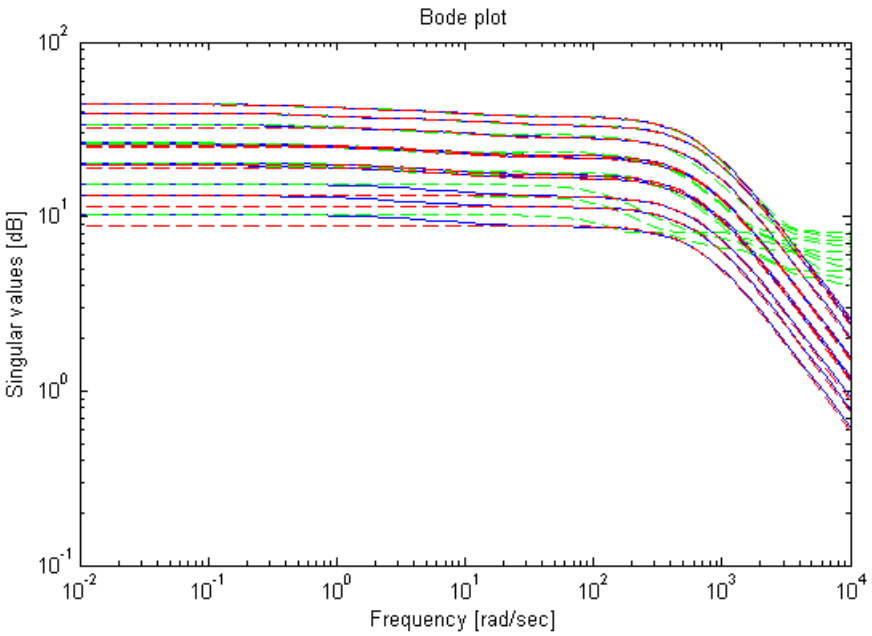

Figure 3.4: *Singular values of the full-order model (blue), Hankel truncated reduced model (red-dashed), Hankel DC matched reduced model (green-dashed). [20 states].*

3.2 Hankel optimal model order reduction

Balanced realizations choose a state coordinate based on the contribution of the states to the input/output energy flow. However, it is possible to focus only on the input/output map without explicitly considering the internal state of the system. From a mathematical point of view, Hankel optimal norm reduction is among the most appreciated model reduction procedures that exist today. As a matter of fact, it is one of the very few model approximation procedure that produce optimal approximate models, in relation to some well-defined criterion. In order to understand the reduction procedure, it is important to define the Hankel operator and the Hankel norm associated with a standard space-state dynamical system

$$\dot{x} = Ax(t) + Bu(t)$$

$$y = Cx(t) + Du(t).$$

The transfer function of $\Sigma = (A, B, C, D)$ is defined as $G(s) = C(sI - A)^{-1}B + D$ and the impulsive response is

$$H(\tau) = \begin{cases} 0, & if\ \tau < 0 \\ D\delta, & if\ \tau = 0 \\ Ce^{A\tau}B, & if\ \tau > 0 \end{cases}$$

In the following it is assumed that Σ is stable and that we're dealing with a minimal realization. Σ defines an input-output map defined in the time domain by the convolution

$y = H * u$, or in the frequency domain by the $y = Gu$. It is particularly interesting to express how *the past inputs influence future outputs*. Consider an input $u(t)$ that lives for times $t \in (-\infty, \infty)$ but vanishes for $t \geq 0$ and concentrate on the output $y(t)$, then

$$y(t) = \int_{-\infty}^{0} H(t-\tau)u(\tau), \qquad t \geq 0.$$

Therefore Σ defines a mapping, say $\mathcal{H}$, from past inputs $u : (-\infty, 0] \to \mathbb{R}^m$ to future outputs $y : [0, \infty) \to \mathbb{R}^p$. $\mathcal{H}$ is defined as the *Hankel operator* associated with Σ. Due to the assumption that Σ is stable, the outputs y converge to zero as time $t \to \infty$, for any given past input u. In particular, by restricting the past inputs to be square integrable signals (hence $u \in \mathcal{L}_2(-\infty, 0]$, where $\mathcal{L}_2$ is the space formed by all square-integrable functions with support on $(-\infty, 0]$), then the corresponding future outputs y will also be square integrable. Thus, the Hankel operator maps $\mathcal{L}_2(-\infty, 0]$ signals to $\mathcal{L}_2[0, \infty)$ signals it is possible to measure the maximal gain of this operator, defined as

$$||\Sigma||_H \triangleq \sup_{u \in \mathcal{L}_2(-\infty, 0]} \frac{||y||_2}{||u||_2}$$

Where $||\Sigma||_H$ is defined the *Hankel norm* associated with Σ and it reflects the maximal effect which past inputs can have on future outputs, with reference to the $\mathcal{L}_2 sense$. The Hankel norm of a system turns out to be equal to the greater Hankel singular value (σ_1 defined in the previous section).

Theorem 1. *If the system Σ is stable, then*

- *the Hankel operator $\mathcal{H}$ has rank at most n, and equal to n if and only if Σ is both reachable and observable.*
- $||\Sigma||_H = \sqrt{\lambda_{max}(PQ)} = \sigma_1$

Where P and Q are the controllability and observability Gramians. Therefore the Hankel norm can be easily computed directly from the product of the two Gramians.

In the previous section the model reduction by exploiting a balanced realization has been investigated. However, this algorithm does not allow for an interpretation as an optimal approximation. This means that the model obtained through the TBR procedure does not minimize a criterion in which we ascertain how far the $n-th$ order system Σ is from a $k-th$ order system Σ_k. On the other hand, the Hankel norm approximation does involve such criterion. Given a $n-th$ order stable system Σ, the objective is to find a $k-th$ order stable system Σ_k such that it minimizes the Hankel norm of the error $||\Sigma - \Sigma_k||_H$, where $\Sigma - \Sigma_k$ can be interpreted as the error system that has the difference of the outputs of Σ and Σ_k as its own output. A fundamental result in the theory of the Hankel norm is given by the following theorem.

Theorem 2 (AAK). *Let $G(s)$ be a matrix-valued function bounded on the $j\omega$-axis. Let $\sigma_1 \geq \sigma_2 \geq \cdots \geq \sigma_k \geq 0$ be the k largest singular values of the product PQ. Then σ_k is the minimum of $||G - G_k||_H$ among all stable systems G_k of order less than k.*

This theorem gives a lower bound on the error made by approximating a system Σ with transfer function G with a lower order system Σ_k with transfer function G_k. From this, it follows the main result of this section, given by the algorithm which was presented in [24]. Given a starting stable space-state system Σ, it provides the optimal Hankel-norm approximant $\Sigma_k = (A_k, B_k, C_k, D_k)$.

Algorithm 1. *Glover's algorithm.*
INPUT *The stable system$\Sigma = (A, B, C, D)$ where the pair (A, B) is controllable and the pair (A, C) is observable.*

Step 1 *Compute the Hankel singular values $\sigma_1 \geq \sigma_2 \geq dots \geq \sigma_n$ of Σ and assume that*

$$\sigma_k > \sigma_{k+1} = \sigma_{k+2} = \cdots = \sigma_{k+r} > \sigma_{k+r+1} \geq \cdots \geq \sigma_n > 0$$

i.e. σ_{k+1} has multiplicity r.

step 2 *Transform Σ to a balanced form where*

$$P = Q = \begin{bmatrix} \Sigma_1 & 0 \\ 0 & \Sigma_2 \end{bmatrix}$$

with $\Sigma_1 = diag(\sigma_1, \ldots, \sigma_k, \sigma_{k+r+1}, \ldots, \sigma_n)$ and $\Sigma_2 = \sigma_{k+1} I_r$.

Step 3 *Partition $\Sigma = (A, B, C, D)$ accordingly to the partitioned Gramians as*

$$A = \begin{bmatrix} A_{11} & A_{12} \\ A_{21} & A_{22} \end{bmatrix}, \quad B = \begin{bmatrix} B_1 \\ B_2 \end{bmatrix}, \quad C = \begin{bmatrix} C_1 & C_2 \end{bmatrix}$$

Now define

$$\Gamma = \Sigma_1^2 - \sigma_{k+1}^2 I.$$

From the definition its clear that Γ is non-singular. If $m \leq p$, proceed. If $m > p$, replace (A, B, C, D) by (A^T, C^T, B^T, D^T) and proceed.

Step 4 *Determine a unitary matrix U such that $B_2 + C_2^T U = 0$. Such a matrix exists.*

Step 5 *Let $\hat{n} \triangleq n - r$ be the state space dimension of the system defined as*

$$\begin{aligned}
\hat{A} &= \Gamma^{-1}(\sigma_{k+1}^2 A_{11}^T + \Sigma_1 A_{11} \Sigma_1 - \sigma_{k+1} C_1^T U B_1^T) \\
\hat{B} &= \Gamma^{-1}(\Sigma_1 B_1 + \sigma_{k+1} C_1^T U) \\
\hat{C} &= C_1 \Sigma_1 + \sigma_{k+1} U B_1^T \\
\hat{D} &= D - \sigma_{k+1} U
\end{aligned}$$

which is called as all pass dilatation *of (A, B, C, D). This means that the parallel interconnection between Σ and $\hat{\Sigma} = (\hat{A}, \hat{B}, \hat{C}, \hat{D})$ is all pass in the sense that the gain of the error transfer function is*

$$\sigma_{max}(G(j\omega) - \hat{G}(j\omega)) = \sigma_{k+1}$$

for all $\omega \in \mathbb{R}$. The system $\hat{\Sigma}$ is in general not stable.

Step 6 *Determine the stable subsystem of $\hat{\Sigma}$ by choosing a basis of the space-state such that*

$$\hat{A} = \begin{bmatrix} \hat{A}_- & 0 \\ 0 & \hat{A}_+ \end{bmatrix}, \quad \hat{B} = \begin{bmatrix} \hat{B}_- \\ \hat{B}_+ \end{bmatrix}, \quad \hat{C} = \begin{bmatrix} \hat{C}_- & \hat{C}_+ \end{bmatrix}$$

where $\hat{A}_+$ and $\hat{A}_-$ have all their eigenvalues on the open right and left complex plane, respectively. $\hat{A}_-$ will have dimension $\leq k$.
If $m \leq p$, proceed. Otherwise, replace $(\hat{A}, \hat{B}, \hat{C}, \hat{D})$ with $(\hat{A}^T, \hat{B}^T, \hat{C}^T, \hat{D}^T)$ and proceed.

OUTPUT *Set*

$$\begin{aligned}
A_k &= \hat{A}_- \\
B_k &= \hat{B}_- \\
C_k &= \hat{C}_- \\
D_k &= \hat{D}_-
\end{aligned}$$

Then, Σ_k defined by

$$\begin{aligned}
\dot{\xi} &= A_k \xi(t) + B_k u(t) \\
y(t) &= C_k \xi(t) + D_k u(t)
\end{aligned}$$

is a space-state representation of an optimal Hankel norm approximant of Σ with $||\Sigma - \Sigma_k||_H = \sigma_{k+1}$.

The existence and construction of $\hat{G}$ is crucial in the entire procedure. Its existence basically shows that it is possible to cancel any *resonance* of a stable system G by

connecting it in parallel with another system. In any case, in this way the lower bound of the AAK theorem is reached and an optimal Hankel norm approximant system is obtained. The algorithm is based on algebraic operations one the state space matrices, so it is fast and numerically simple. Finally, note that since the Hankel singular values of the original system can be easily computed, it's straightforward to get a priori insight in the achievable errors and to decide a suitable value of the number of states q in the reduced order model. Furthermore,the optimal Hankel norm approximation method gives a tighter guaranteed error bound in terms of the H_∞ norm respect to TBR method. In fact the following bound hold:

$$||G - G_k||_\infty \leq \sum_{i=k+1}^{n} \sigma_i$$

3.3 Selective Modal Analysis (SMA)

The fundamental idea laying behind the selective modal analysis approach is that the physical meaning of the state variables is preserved in the reduced model. Therefore, it is possible to employ this fact both in the analysis of the system properties and in the controller design. In SMA truncation is performed without a preliminary change of basis in the state space, thus granting the preservation of the physical meaning of the state variables. The problem is to decide which state variables are going to be preserved in the reduced model. The choice of the state variables to be retained in the reduced model is performed by considering two adimensional coefficients:

- the participation factor p_{ki} gives a measure of the contribution of the $k-th$ state in the $i-th$ mode. It is defined as the product of the $k-th$ components of the left and right normalized eigenvector (hereinafter indicated as w_{ki} and v_{ki} respectively) corresponding to the $i-th$ mode.

$$p_{ki} \triangleq w_{ki} v_{ki}$$

- the participation ratio ρ_{ri} gives a measure of the overall contribution of a set of r states in the $i-th$ mode, and is defined as

$$\rho_{ri} \triangleq \frac{\sum_{k=1}^{r} p_{ki}}{\sum_{k=r+1}^{n} p_{ki}}$$

  As a consequence, an absolute value of the participation ratio greater than one means that the selected states give a contribution to the $i-th$ mode greater than the contribution of the neglected ones.

The participation ratios and factors are used as a guideline to the aim of choosing the order of the reduced model. To begin the process of model order reduction, the states of the system are reordered so that the ones to be retained are the first *r* ($x = [x_1\ x_2]$, where x_1 incorporates the first r states). Consider now the invertible matrix of eigenvectors $V = [v_1\ v_2 \dots v_n]$, and let W be its inverse. It is then possible to reorder the eigenvectors of V, so that the first *r* eigenvectors correspond to the *r* eigenvalues $(\lambda_1, \dots, \lambda_r)$ to be retained in the reduced model. It follows

$$WAV = \Lambda = \begin{bmatrix} \Lambda_1 & 0 \\ 0 & \Lambda_2 \end{bmatrix}$$

where $\Lambda_1 = diag(\lambda_1, \dots, \lambda_r)$. Consequently, after partitioning the matrices in accordance to the partition of the eigenvalues, the matrices of the reduced model $S_r = (A_r, B_r, C_r, D_r)$ are given as follows:

$$\begin{cases} A_r = A_{11} + A_{12}V_{21}V_{11}^{-1} \\ B_r = V_{11}(W_{11}B_1 + W_{12}B_2) \\ C_r = C_1 + C_2V_{21}V_{11}^{-1} \\ D_r = D \end{cases}$$

The SMA is from a certain point of view a combination of basic modal truncation and singular perturbation approaches. In fact, the reduced system modes are exactly $(\lambda_1, \dots, \lambda_r)$, such as in the modal truncation approach. Furthermore the eigenvectors of A_r are $v_{1,i}$, which means they are composed by the first r components of the $i-th$ eigenvector of A associated to λ_i. The effect of the neglected dynamics on the retained variables is described by $H(s) = (sI - A_{22})^{-1}A_{21}$, that is the transfer function between x_1 and x_2. In the SMA procedure, the approximation is given by

$$H(s) \simeq H = V_{21}V_{11}^{-1}.$$

Thus the effect of x_2 on x_1 is totally preserved when only the retained modes are excited. For instance, consider the eigenpair $(\lambda_1, v_1 = [v_{11}^T v_{12}^T]^T)$. Then

$$\lambda_1 v_{12} = A_{21}v_{11} + A_{22}v_{12}$$

thus

$$v_{12} = (\lambda_1 I - A_{22})^{-1}A_{21}v_{11} = H(\lambda_1)v_{11}$$

Since $V_{21}V_{11}^{-1}v_{11} = v_{12}$, it follows that $Hv_{11} = H(\lambda_1)v_{11}$. Hence, the additional term $A_{12}V_{21}V_{11}^{-1}$ in the construction of the matrix A_r grants that the effect of x_2 on x_1 is totally preserved when only the selected modes are excited.

In some cases comparisons of different p_{ki} is made particularly easy by the structure of the problem. The following statement applies to the models considered here.

Proposition 1. *Assume that the matrix $A \in R^{n\times n}$ is such that*

$$A = -RL^{-1}$$

where $L = L^T$ is nonsingular and

$$R = \begin{bmatrix} 0 & 0 \\ 0 & R_2 \end{bmatrix}$$

where R_2 is a diagonal and positive definite matrix. If all the nonzero eigenvalues of A are real and distinct, then $p_{ki} \geq 0, \forall\ i, k$.

Proof *Let v, w be a right and left eigenvector of A respectively, associated with a nonzero simple eigenvalue λ, and let $w^T v = 1$. By partitioning v, w and L in accordance to the block structure of R and writing L^{-1} as*

$$-L^{-1} = \begin{bmatrix} M & N \\ N^T & P \end{bmatrix}$$

It is possible to find the following relations

$$\begin{cases} 0 = \lambda v_1 \\ R_2 N^T v_1 + R_2 P v_2 = \lambda v_2 \\ w_2^T R_2 P = \lambda w_2^T \\ w_2^T R_2 N^T = \lambda w_1^T \end{cases}$$

Remembering that $\lambda \neq 0$, the first relation gives $v_1 = 0$, and therefore it can be written

$$\begin{cases} \lambda v_2 = R_2 P v_2 \\ \lambda w_2^T = w_2^T R_2 P \end{cases}$$

So v_2 and w_2 are right and left eigenvectors of $A_{22} = R_2 P$ associated with λ. Therefore, the participation factors associated with nonzero eigenvalues depend on v_2, w_2 only. By defining $\phi = R_2 w_2$ and $\xi = R_2^{-1} v_2$, and by exploiting the previous relations, it is easy to obtain the following relations

$$\begin{cases} \lambda \phi = A_{22} \phi \\ \lambda \xi^T = \xi^T A_{22} \end{cases}$$

Then ϕ and ξ are right and left eigenvectors of A_{22} and they are associated with λ. Since λ is a simple eigenvalue it follows that ϕ and v_2 are proportional

$$\phi = R_2 w_2 = \alpha v_2$$

and so

$$v_2 = \frac{1}{\alpha} R_2 w_2$$

Now the following relation holds

$$w_2^T v_2 = 1 = \frac{1}{\alpha} w_2^T R_2 w_2$$

where $R_2 > 0$. *Then* $\alpha > 0$. *Denoting the* $i - th$ *component of vectors* v_2 *and* w_2 *as* $v_{2,i}, w_{2,i}$ *and with* $r_{2,i}$ *the* $(i,i) - th$ *entry of* R_2 *the previous relation yields*

$$v_{2,i} = \frac{1}{\alpha} r_{2,i} w_{2,i}$$

And finally, remembering that $r_{2,i} > 0$:

$$p_{\lambda i} = w_{2,i} v_{2,i} = \frac{1}{\alpha} w_{2,i}^2 r_{2,i} > 0, \quad \forall\, i$$

□

The fundamental step in SMA is the choice of the state variables to be retained in the reduced order model. A good method to determine the number of states to be retained is given by the participation ratios, which suggest the minimum number of states to be retained to have an absolute value greater than one. A reduced order model is obtained by retaining only the states with the greatest participation factors in the dominant modes (those contributing the most to the transfer function). Unfortunately, the models considered here are stable, so it is difficult to choose which modes have to be retained in the reduced model *a priori*. In such cases SMA is limited in practice by the difficulty to assess the modal dominance of the system. In other words, knowledge of which modes should be retained is not always clear, and consequently it is not easy to choose the states to be retained. In particular, the difficulty to choose the states increases because there are lots of closely-spaced eigenvalues. In many cases, it is the high frequency modes that are discarded, due to damping and bandwidth limitation of actuators and sensors.

3.4 Krylov subspace methods

Recently, Krylov subspace methods have become popular tools for computing reduced order models starting from really high order linear time invariant systems. They can be

used to find mapping from the high-dimensional space of a given state-space model to some lower dimensional space. This procedure of using mappings in order reduction is typically referred to as reduction by projection. The main advantages of Krylov reduction techniques are the following:

1. The number of operations needed to compute a reduced system of order q given a starting model of order n using the Arnoldi algorithm (which will be discussed in the following) is $O(qn^2)$, respect to $O(n^3)$ operations needed for the SVD based methods, such as TBR.

2. The building procedure of the reduced model is numerically robust, there is no need to compute the transformed $n-th$ order model and then truncate. Therefore, the ill-conditioning that arises in SVD methods can be avoided.

On the other hand, the main drawbacks are:

1. The reduced order system may not be stable, even when the original system is stable.

2. The reduced model is not invariant to different representations of the original model.

Considering the usual space-state model

$$\begin{aligned} \dot{x} &= Ax(t) + Bu(t) \\ y &= Cx(t) + Du(t) \end{aligned}$$

and then a projection as follows

$$x = Vx_r, \quad V \in \mathbb{R}^{n\times q},\ x \in \mathbb{R}^n,\ x_r \in \mathbb{R}^q$$

and applying it to the system considered above, also pre-multiplying the state equation by the transpose of $W \in \mathbb{R}^{n\times q}$, the general reduced order model by projection is calculated as follows:

$$\begin{aligned} W^TV\dot{x}_r &= W^TAVx_r + W^TBu \\ y &= CVx_r + Du. \end{aligned}$$

From this, the matrices identifying the reduced order model are the following

$$A_r = W^TAV, \quad B_r = W^TB, \quad C_r = CV$$

The question is how to calculate those matrices V and W. From a certain point of view, the Hankel model reduction can be seen as a method of reduction by projection.

By the way, the main difference between the two methods is that the Krylov subspace method requires a minor computational effort and the computation is numerically robust. A general Krylov subspace is defined as

$$K_q(\tilde{A}, \tilde{B}) = span\{\tilde{B}, \tilde{A}\tilde{B}, \ldots, \tilde{A}^{q-1}\tilde{B}\},$$

where $\tilde{A} \in \mathbb{R}^{n\times n}$ and $\tilde{B} \in \mathbb{R}^{n\times m}$. The vectors which span the subspace are called the basic vectors. With this definition, two Krylov subspaces $K_{q_1}(A^{-1}, A^{-1}B)$ and $K_{q_2}(A^{-T}, A^{-T}C^T)$ both with the same rank are used for model order reduction and are called input and output Krylov subspaces respectively. Therefore, the two projection matrix V and W are chosen as a basis of the Krylov subspaces K_{q_1} and K_{q_2} respectively.

The Krylov subspaces K_{q_1} and K_{q_2} are so chosen because they allow to match a certain number of moments of the full-order system with the reduced one. The number of matching moments directly depends on the number of variables retained in the low-order model and at the same time it depends on the number of inputs and outputs of the system. In linear space-state systems, moments (around zero) are defined as follows:

$$M_i = CA^{-(i+1)}B, \quad i = 0, 1, \cdots .$$

M_i is in general a $p \times m$ matrix, when we deal with MIMO systems. The moments are related to the coefficients of a Taylor series expansion around zero. The following theorem applies to SISO systems and can be generalized to MIMO case.

Theorem 3. *Let the projection matrix V be a basis of Krylov subspace $K_{q_1}(A^{-1}, A^{-1}b)$ with rank q. If W is chosen such that A_r is nonsingular, then the first q moments (around zero) of the reduced model coincide with the ones of the full-order one.*

Proof *The zeroth moment of the reduced system is*

$$m_{r0} = c_r^T A_r^{-1} b_r = c^T V (W^T A V)^{-1} W^T b$$

where b and c are the input and output matrices, which in a SISO model are reduced to a column and row vector respectively.

The vector $A^{-1}b$ can be written as

$$A^{-1}b = Vr_0, \quad r_0 \in \mathbb{R}^q$$

because it is in the Krylov subspace and so it can be expressed as a combination of the columns of V. Therefore,

$$(W^T A V)^{-1} W^T b = (W^T A V)^{-1} W^T (A A^{-1}) b = (W^T A V)^{-1} W^T A V r_0 = r_0$$

And then

$$m_{r0} = c^T V (W^T A V)^{-1} W^T b = c^T V r_0 = c^T A^{-1} b = m_0$$

By repeating these steps, it is possible to prove that the moments until $m_{r(q-1)} = m_{q-1}$ *match.*

□

It can be proved that when V is a basis of input Krylov subspace or W is a basis of output Krylov subspace then the first $\frac{q}{m}$ or $\frac{q}{p}$ moments match respectively and the reduction method is generally called *one-sided Krylov* method. This happens when only one of the two matrices is chosen as specified, while the other one is chosen arbitrarily (a typical choice is $V = W$). If both V and W are chosen as bases of the input and output Krylov subspace respectively, the method is called *two-sided Krylov* method and we have $\frac{q}{m} + \frac{q}{p}$ matching moments. From the previous observation it's clear that the Krylov subspace methods works well for general SISO systems or with systems which have a low number of either inputs or outputs, or both. The following theorems summarize two main results of Krylov methods:

Theorem 4. *If the projection matrix* V *is a basis of Krylov subspace* $K_{q_1}(A^{-1}, A^{-1}B)$ *with rank* q *and the projection matrix* W *is chosen such that* A_r *is nonsingular, then the first* $\frac{q}{m}$ *moments of the original and reduced order model match.* A *is assumed to be invertible.*

Theorem 5. *If the matrices* V *and* W *are bases of Krylov subspaces* $K_{q_1}(A^{-1}, A^{-1}B)$ *and* $K_{q_2}(A^{-T}, A^{-T}C^T)$ *respectively, both with rank q (where* q *is a multiple of* m *and* p*), then the first* $\frac{q}{m} + \frac{q}{p}$ *moments of the original and reduced order model match.* A *and* A_r *are assumed to be invertible.*

In MIMO systems the moments are matrices with $m \cdot p$ entries. Therewith, the number of matching scalar parameters is $m \cdot p \cdot \frac{q}{m} = p \cdot q$ for Theorem 4 and $m \cdot p \cdot (\frac{q}{m} + \frac{q}{p}) = p \cdot q + m \cdot q$ for theorem 5. Accordingly, each column of the matrices V and W allows to match one more row or column of scalar parameters. Therefore, by choosing the first q columns of the matrices V and W, it is possible to find a reduced model of order q to match $p \cdot q + m \cdot q$ parameters of the original model and there's no need to choose q such that it is a multiple of both, m and p. The choice of V and W using Krylov methods is very simple. However, the numerical calculation of the matrix-vector products involved in the Krylov subspaces turns out to tend to be unstable. Therefore, algorithms have been developed to reliably calculate those matrices. One of these is the Arnoldi algorithm.

Finally, Krylov subspace methods have another advantage. In fact, Krylov subspaces K_{q_1} and K_{q_2} can be adapted to match moments at a point different from zero,

which can be useful in some specific applications. To do so, it is necessary to consider the new input and output subspaces, which are respectively $K_{q_1}((A - s_0 I)^{-1}, (A - s_0 I)^{-1} B)$ and $K_{q_2}((A - s_0 I)^{-T}, (A - s_0 I)^{-T} C^T)$. There are other additional properties regarding in particular the differences between one-sided e two-sided methods which won't be discussed here and can be found in [4].

3.4.1 Arnoldi algorithm

When computing the projection matrices, it is desired to find an orthogonal basis, in order to avoid numerical problems. The classical Arnoldi procedure computes a set of orthonormal vectors which constitutes a basis for a given Krylov subspace with only one starting vector. This procedure must be expanded in order to deal with MIMO systems. For instance, consider a system with $B = [b_1 \ \dots \ b_m]$. The column vectors $b_1, \dots, b_m$ are called starting vectors. Consider the Krylov subspace $K_q(A, B)$ with m starting vectors. The Arnoldi algorithm finds a set of vectors orthogonal to each other, so that

$$V^T V = I$$

where the columns of V form a basis for the given Krylov subspace. In the Arnoldi algorithm, at every step a new vector is constructed, orthogonal to the previous ones and normalized to have length one. Its good accuracy results from orthogonality. When q is not small enough, it might happen that not all the basic vectors are independent. Thus, to avoid this problem the linearly dependent vectors must be deleted. This procedure is called *deflation*.

Algorithm 2. *Arnoldi algorithm with deflation using modified Gram-Schmidt procedure:*

0. *Delete the linearly dependent starting vectors in order to find m_1 independent vectors for the considered Krylov subspaces. Then set*

$$v_1 = \frac{b_1}{\sqrt{b_1^T b_1}}$$

where b_1 is the first starting vector after deleting the dependent ones.

1. *For $i = 2, 3, \dots,$ do*

   (a) *Compute the next vector: if $i \leq m_1$ the successive vector is the $i - th$ starting vector. Otherwise*

$$r_1 = A v_{i-m_1}$$

(b) Orthogonalization: set $\hat{v}_i = r_i$ *then for* $j = 1, \ldots, i-1$ *do*

$$h = \hat{v}_i v_j$$
$$\hat{v}_i = \hat{v}_i - h v_j$$

(c) Normalization: if vector $\hat{v}_i$ *is zero, reduce* m_1 *to* $m_1 - 1$ *and if* m_1 *is nonzero go to step* $1.a$*. If* m_1 *is zero break the loop. Otherwise, if* $\hat{v}_1 \neq 0$ *the* $i - th$ *column of matrix* V *is*

$$v_i = \frac{\hat{v}_i}{\sqrt{\hat{v}_i^T \hat{v}_i}}$$

(d) Increase i *and go to step* $1.a$*.*

An important property of Krylov subspaces is that, if the $i-th$ basic vector related to the starting vector b_j is linearly dependent from the previous basic vectors, then all other basic vectors p_{i+m_1}, p_{i+2m_1}, ... related to the vector b_j are linear combinations of the first $i-1$ basic vectors. In step $1.b$ of the Arnoldi algorithm, $\hat{v}_i = 0$ means that the $i - th$ basic vector is linearly dependent from the previous basic vectors and all basic vectors p_i, p_{i+m_1}, ... can be deleted in the following iterations. A way to do this is by reducing the parameter m_1. if $\hat{v}_i \neq 0$, the first i basic vectors are linearly independent and $\{v_1, \ldots, v_{i-1}, \hat{v}_i\}$ span the same space as the first i basic vectors and all of them are independent. The moments of a MIMO system are $p \times n$ matrices M_i, where each row and column is related to an output and an input respectively. Krylov subspace techniques make possible to match individual rows (and columns) up to a higher index i than other rows (or columns). Thank to this, for more important entries of the moment matrices the number of matched parameters can be increased, while decreasing the matched parameters for less important entries. This fact is very useful when dealing with MIMO systems with a great number of input or outputs.

For instance, consider an input Krylov subspace. For a system with m (linearly independent) inputs, there exist m starting vectors that must be orthonormalized, which yield the first m columns of matrix V, $v_1, \ldots, v_m$. For the successive vector, there are m candidates, $A^{-1}v_1, \ldots, A^{-1}v_m$, called $r_1, \ldots, r_m$, that can be chosen to construct vector v_{m+1}. One way to choose the next vector is by selecting the most linearly independent from all the previous ones. One way to identify this vector is through geometrical dominance measure. The angle between the candidate vectors and the hyperspace constructed by the previous ones gives a measure of the independence of each candidate vector from that hyperspace. The computation of the sine of this angle can be made within the Arnoldi algorithm as the division between the norm of the next vector before normalization ($\hat{v}_i$ in the algorithm above) and the norm of $r_i, i = 1, \ldots, m$. Consequently, $d_i = \frac{norm(\hat{v}_i)}{norm(r_i)}$ can be used as a dominance measure

to choose among the m candidates $r_1, \ldots, r_m$. Another dominance measure can be computed by exploiting SVD. In this case the SVD of the matrix $[\ v_1\ \cdots\ v_m\ r_i\ ]$ must be calculated for every candidate vector. The smallest singular value shows the linearly dependency of the columns. For proper comparison, it is better to normalize all vectors r_i before computing the SVD. Independently on the chosen method, once the dominance measure are calculated for all m candidates, the vector with the largest measure is chosen to become the next column vector of matrix V. Suppose that is r_j, then it must be substituted by the next candidate $A^{-1}v_{m+1}$, and the dominance measure must be renewed using by considering the $m+1$ columns of matrix V, and so on.

This selection procedure aims to choose the columns most contributing to the controllability subspace in every iteration. This method can obviously be applied also to the output Krylov subspace. Figure 3.5 shows a scheme of the selection procedure.

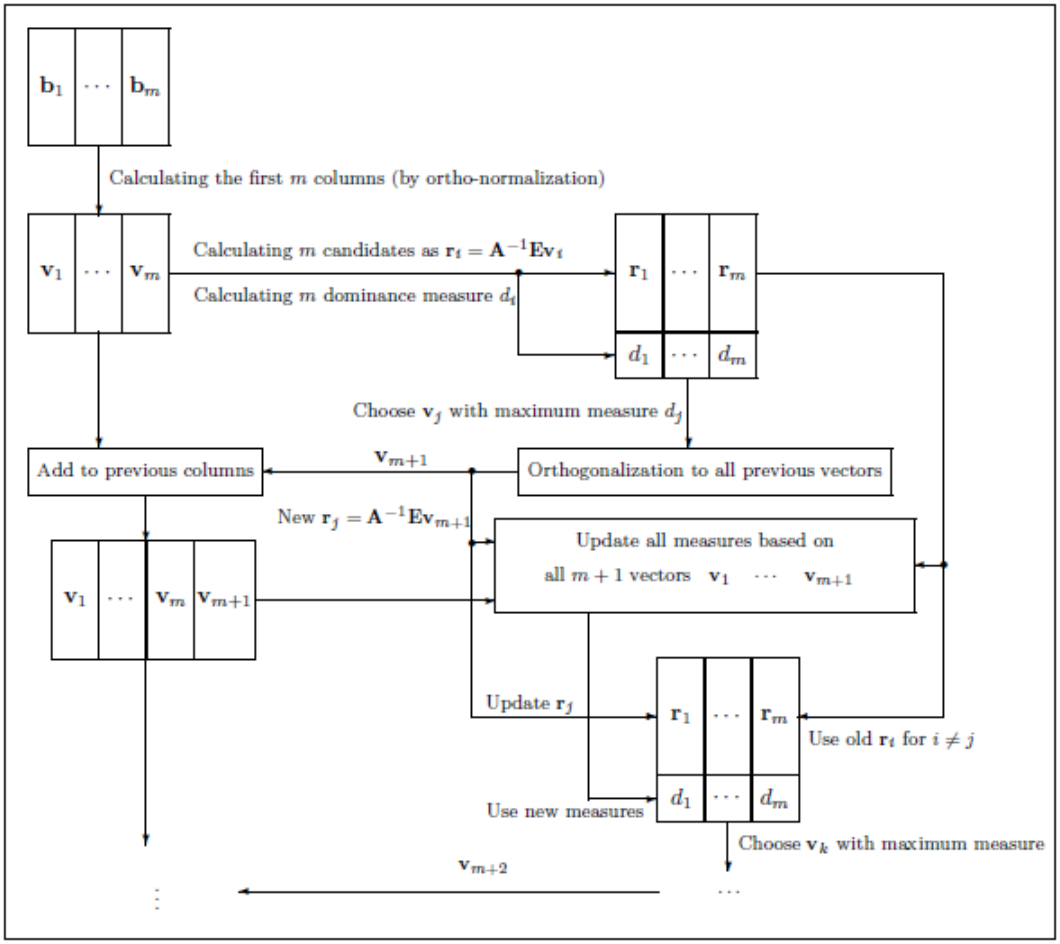

Figure 3.5: *Selection procedure with dominance measure.*

From a numerical of view, the computation of the inverse of the large matrix A can be affected by numerical issues or be excessively time-consuming. So direct calculation of this inverse isn't recommended. To solve the numerical problem, one solution is to use the LU-factorization and then solve two triangular linear equations. Obviously,

using this method in each iteration would lead to a slow algorithm. To cope with this problem the idea is to compute the LU factorization of the matrix A at the beginning of the algorithm and then solve only triangular linear equations in each iteration. In this way, time is saved and the algorithm is more robust to numerical issues. In the one-sided method $W = V$ is a common choice. In fact, this choice of W is useful because it allows to find the reduced order model with less computational effort, because $W^T V = I$.

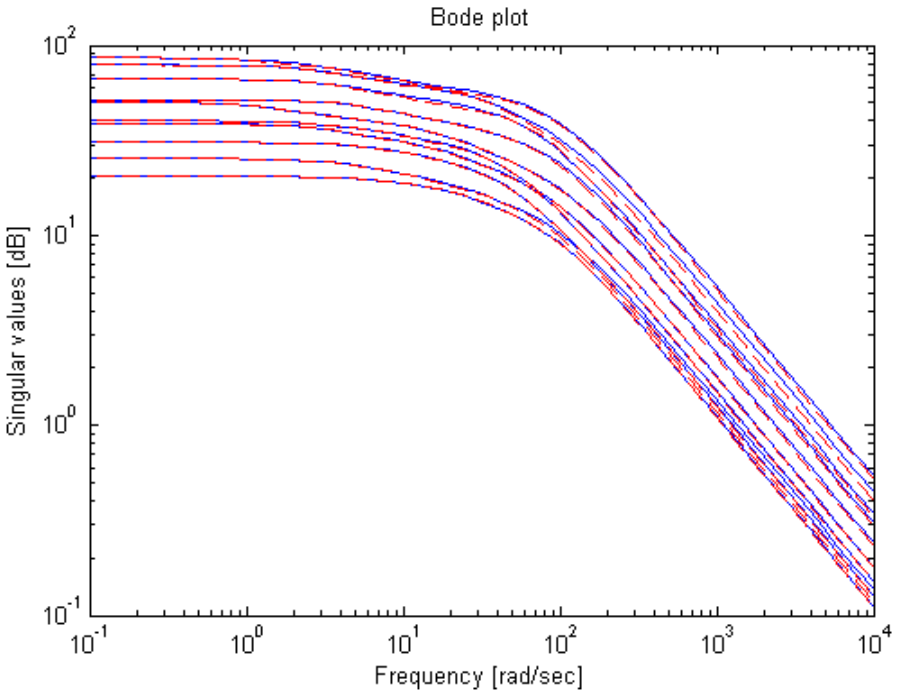

Figure 3.6: *Singular values of the full-order model [110 states] (blue) and Krylov reduced model (red-dashed, input-sided, 55 states).*

In figure 3.6 it is shown a comparison between the ten greater singular values of the full-order model (110 states) and of the input-sided Kyrlov reduced model, composed by 55 states, computed using the input Krylov subspace. The two models behave in a similar way in a wide range of frequencies. In particular, we can observe that the matching of the singular values is approximately perfect for low frequencies: in fact we are matching the moments of the original model around the origin, which leads to approximate the slow dynamics of the original system, so this was totally expected. For instance, in figure 3.7 it is shown the behavior of the reduced model when choosing to match the moments around $s = 10^2\,[rad/sec]$. By comparison with figure 3.6 it is clear that at high frequencies there is a better performance in terms of singular values, the drawback is that at low frequencies this new model has poorer results. The final choice of which model to use depends typically on the particular application.

There is one more important fact to be stressed. As explained above, Krylov re-

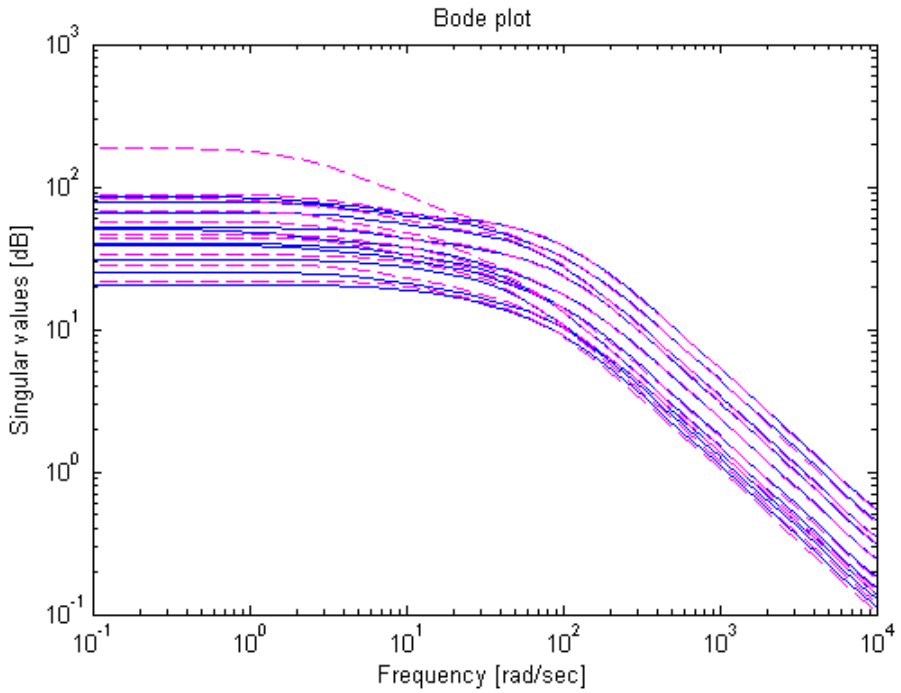

Figure 3.7: *Singular values of the full-order model [110 states] (blue) and Krylov reduced model (magenta-dashed, input-sided, 55 states). Here the moments are matched around* $s = 10^2$ *[rad/sec].*

duction technique aims to match the first moments of the reduced model with the ones of the full-order one. In doing so, the matrices V and W, or both, need to be suitably computed, to match the first $\frac{q}{m}$ or $\frac{q}{p}$ moments. The full-order model is in particular composed by $n = 110$ or $n = 1832$ states and by a corresponding number of outputs (which are independent). So, in order to match the first moment of the full-order model by using the output-sided method, it is necessary to consider a reduced order model that is the full-order model itself. So in this case the output-sided method is totally useless, showing a common weakness of Krylov subspace methods in dealing with lots of inputs or outputs. At the same time, the reason why we have achieved slightly better results in using one-sided input method is because the inputs are linearly dependent, leading to a better performance of the algorithm, but still not really satisfactory. To conclude, it's clear, from the previous observations, that the full-order model we are considering is not really suited for this kind of reduction techniques.

Chapter 4

Simulation results

Hereinafter the reduction techniques are applied to the RFX-mod and ITER models.

In particular the experiments on RFX-mod are mainly used as a validation and assessment of the procedure (despite their validity *per se*), and to gain a hands on experience on the MOR results. This approach has been motivated by the fact that MOR on ITER machine (which is the main objective of this work) has led to several numerical issues that inserted additional difficulties in the procedure.

In order to evaluate the goodness of the reduced models, there are considered comparisons between the Bode diagrams and step responses, where some inputs of the models are excited by a step of amplitude $1\,[A]$ at $t = 0\,[s]$.

4.1 TBR reduced models

4.1.1 Part A - technique validation on RFX-mod

The TBR approach was applied to the RFX-mod model with good results. To start the model reduction it is crucial to observe the Hankel singular values behavior, in order to have some hint on a suitable choice of the reduced model order q. In figure 4.1 it is shown the behavior of the Hankel singular values. The first ones show a fast decrease and so they rapidly come to near zero values. By comparing it with figures 3.1 and 3.2 it appears that this model is more suited for this kind of reduction. Given the knowledge of the Hankel singular values, three different reduced models were considered with different number of states: 20, 26 and 32. In figure 4.2 the singular values of the transfer matrix of the reduced models are compared with the ones of the full-order model, while some of the step responses are shown in figure 4.3. The step responses are generally good for each reduced model in particular when the amplitude of the response is relatively high, this meaning that the more important relations between inputs and outputs are well approximated by the reduced models, as

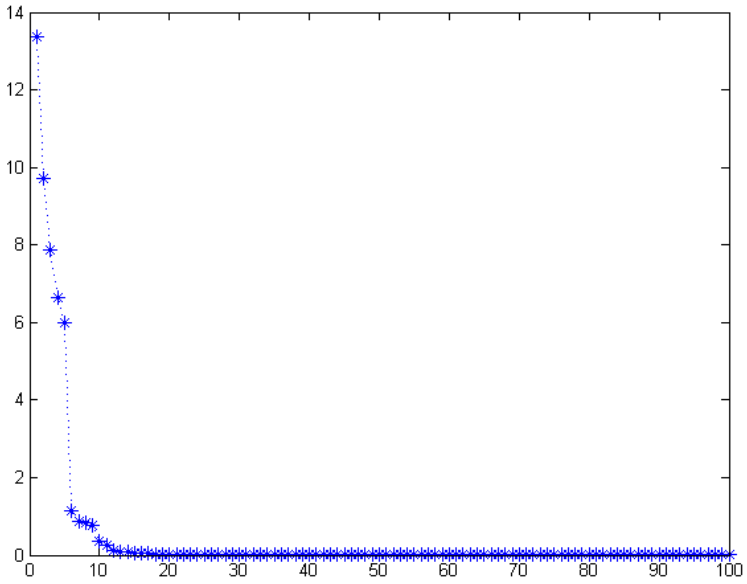

Figure 4.1: *RFX-mod: First 100 Hankel singular values of the RFX-mod model.*

expected. Obviously, when increasing the number of states in the reduced models, also less important dynamics start to be followed. As a further criterion of comparison, also the Bode plots are represented in figure 4.4. As it is shown, the Bode plots typically well approximates the full-order one until about a frequency of $10^2\,[rad/sec]$. This is also due to the fact that when the frequency increases, some of the outputs tend to be dumped (this translates in a decrease of the magnitude of the Bode plot when the frequency increases) and so they have small contributions in the overall response. These considerations are common to all the reduction techniques.

Finally, table 4.1 shows the errors made on the H_∞ norm and the relative error bounds.

number of states	H_∞ norm [dB]	error bound on H_∞
Full-order	26.7957	N/A
20	26.7820	0.1402
26	26.7950	0.0476
32	26.7954	0.0134

Table 4.1: *RFX-mod: H_∞ norm errors and relative error bounds in RFX-mod model. [TBR]*

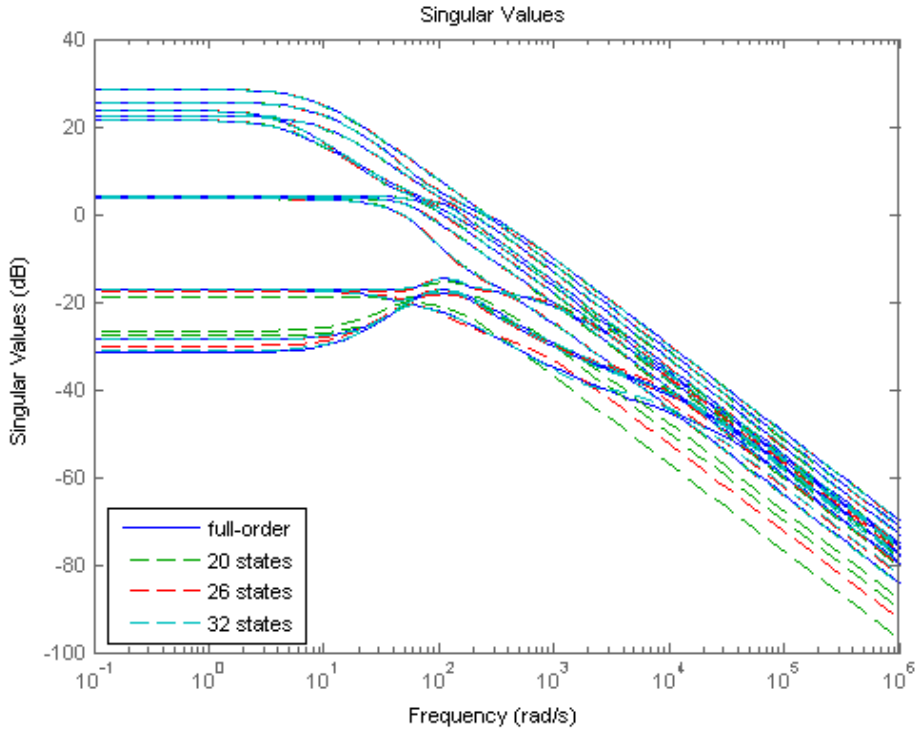

Figure 4.2: *RFX-mod: Comparison of the singular values between the full-order RFX-mod model and the three reduced models.*

4.1.2 Part B - technique approach on ITER models

The reduced models of the systems with $n = 110$ and $n = 1832$ states are here considered and the step responses and Bode plots are compared[1]. The Hankel singular values of these models have already been shown in section 3.1. Figure 4.6 shows the behavior of the currents in some of the states of the passive structures. The quality of the reconstructed currents is quite good compared to the full-order ones and the Bode plot are consistent with the step responses. Figure 4.5 shows the values of the 12 dominant singular values of the system with $n = 110$ states.

[1] We will refer to this two models as ITER110 and ITER1832.

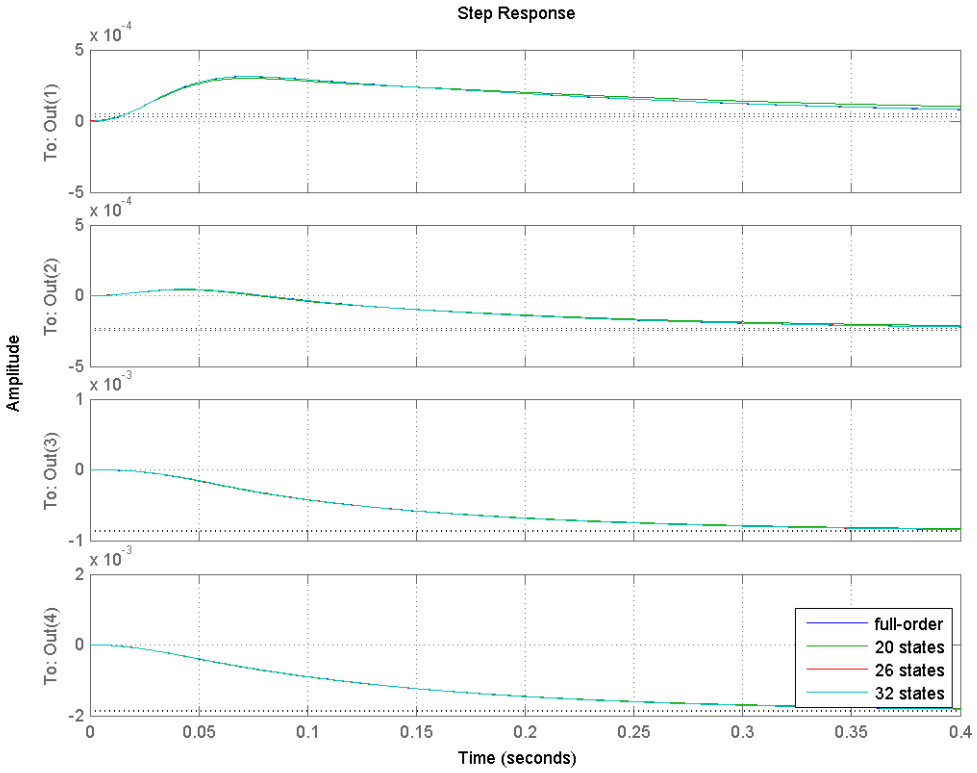

(a)

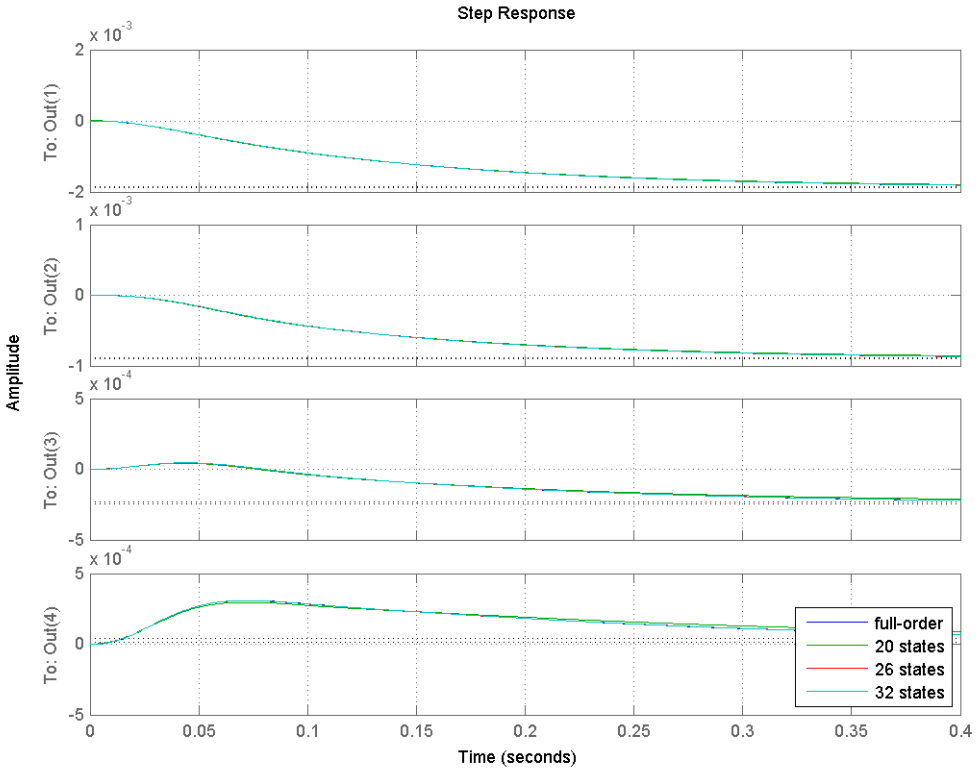

(b)

Figure 4.3: *RFX-mod: Step responses of the full-order and reduced systems of the outputs from 4 to 7 (a) and from 8 to 11 (b) when the first input is excited.*

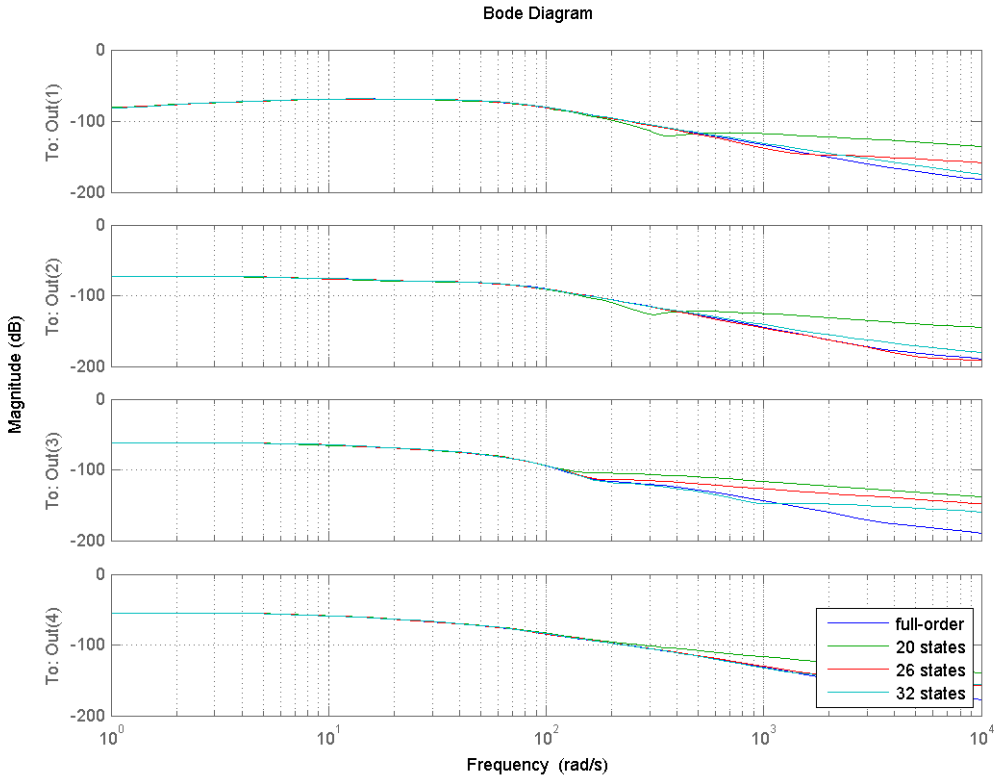

(a)

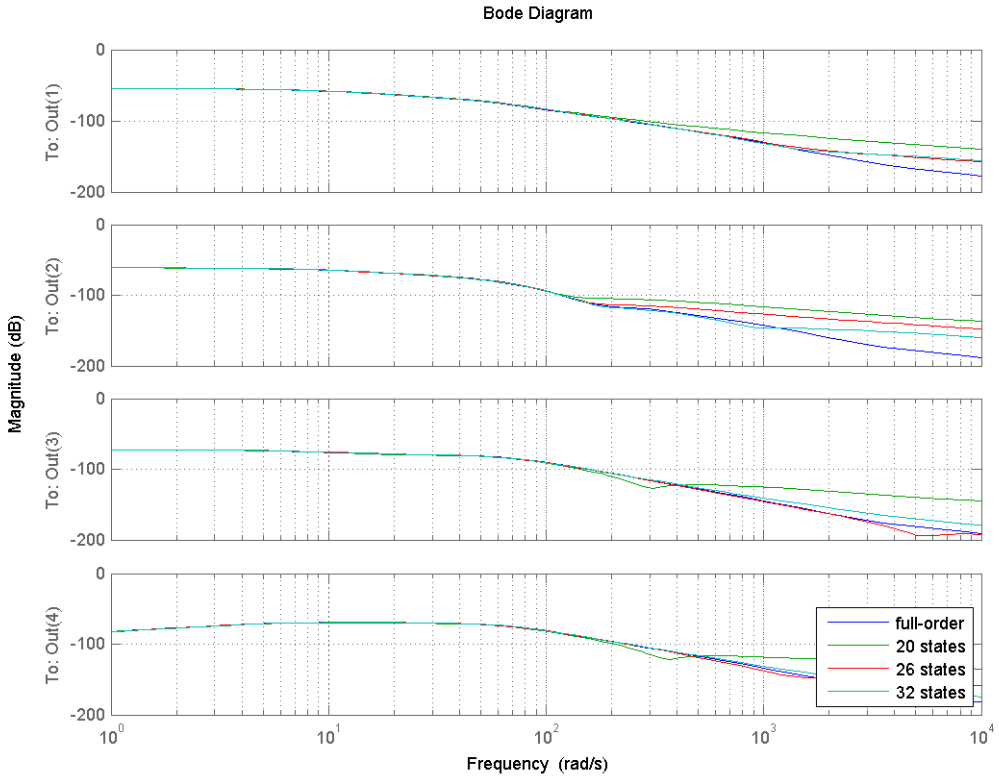

(b)

Figure 4.4: *RFX-mod: Bode plots (only the magnitude plots are represented) of the full-order and reduced systems between the first input and the outputs from 4 to 7 (a) and from 8 to 11 (b).*

number of states	H_∞ norm [dB]	error bound on H_∞
Full-order	86.0098	N/A
20	85.4773	56.5956
26	86.0047	19.5631
32	86.0085	8.8458

Table 4.2: *ITER110: H_∞ norm errors and relative error bounds in the ITER model with $n = 110$ states. [TBR]*

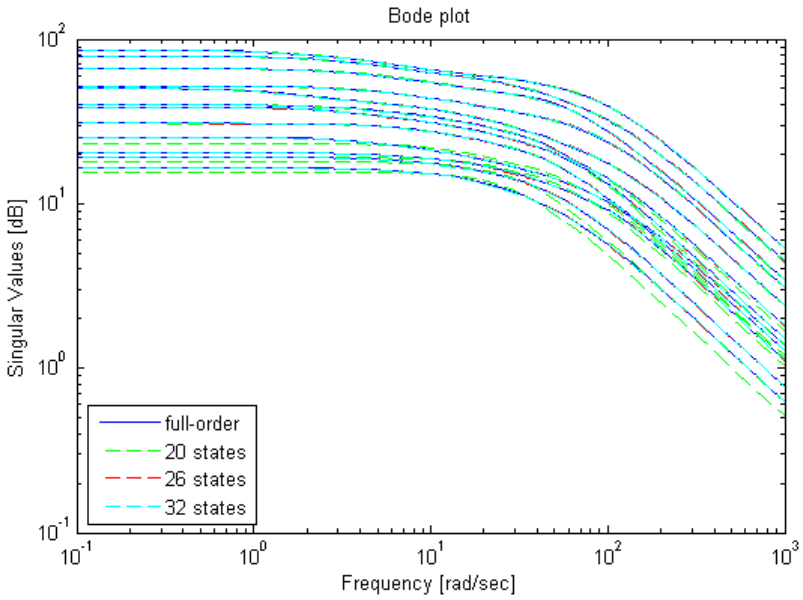

Figure 4.5: *ITER110: 12 dominant singular values of the full-order system with $n = 110$ states and of the reduced systems using TBR.*

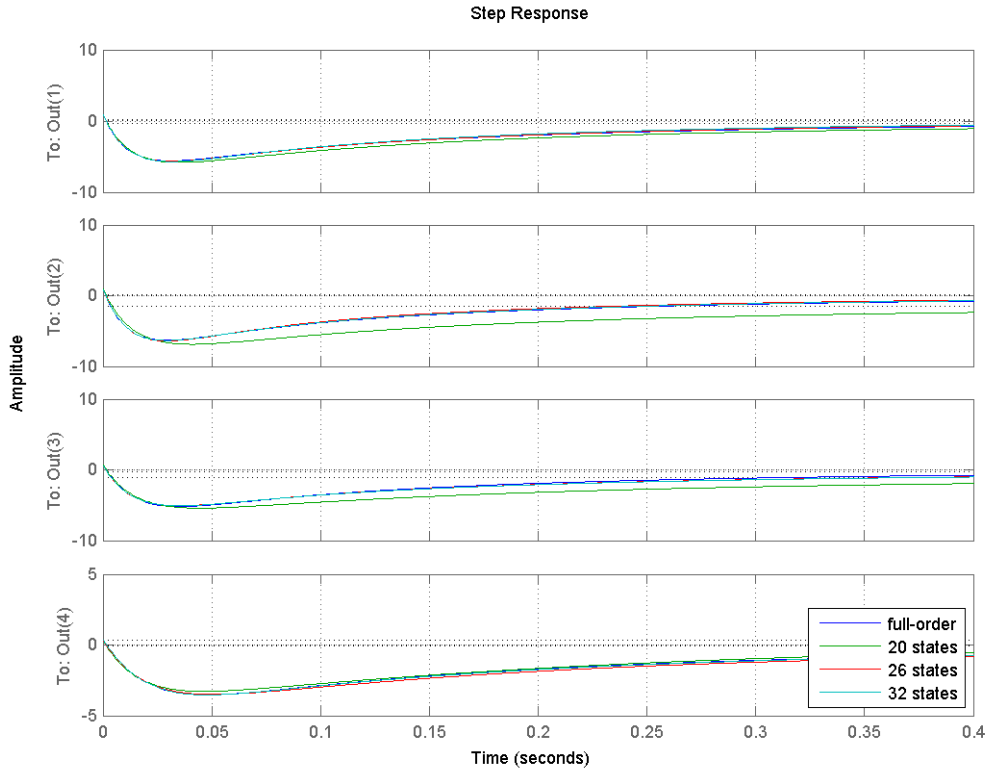

(a)

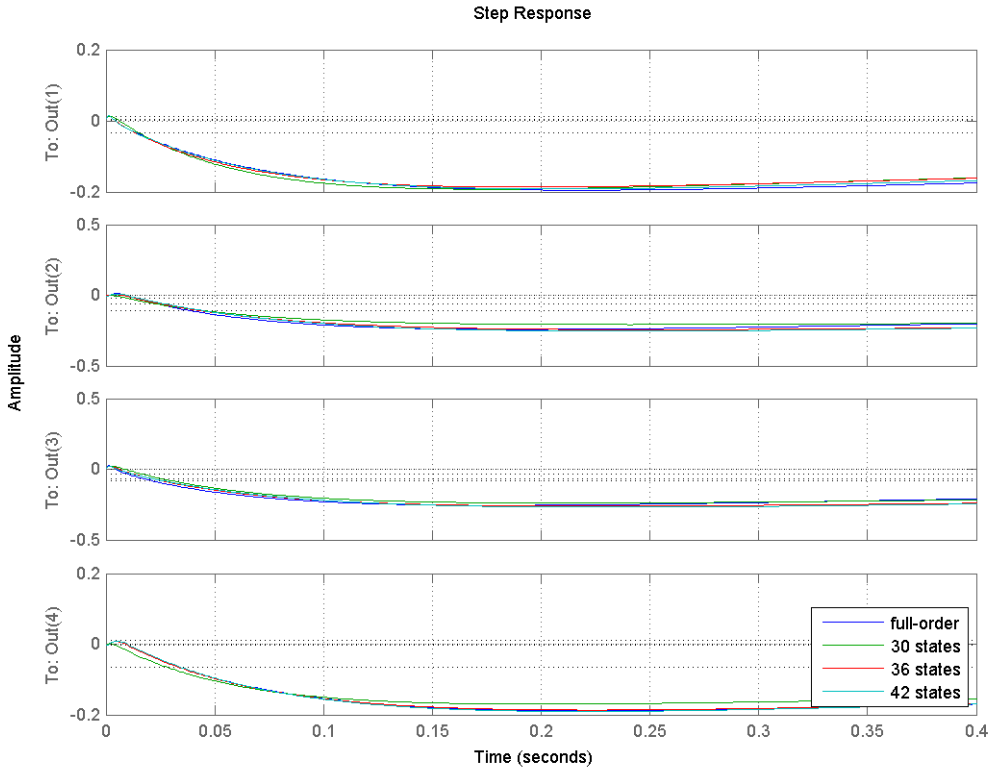

(b)

Figure 4.6: *ITER110/1832: Step responses of the full-order and reduced systems of the outputs from 1 to 4 when $n = 110$ (a) and $n = 1832$ (b), when the $101 - th$ input is excited (i.e. the first active coil). [TBR]*

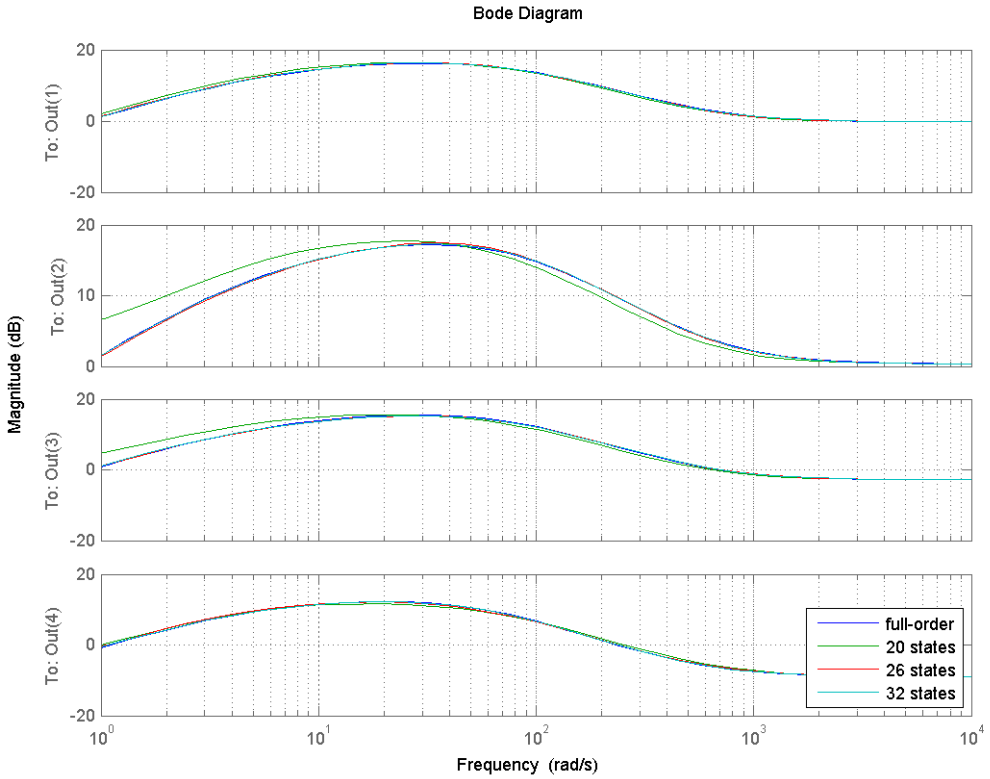

(a)

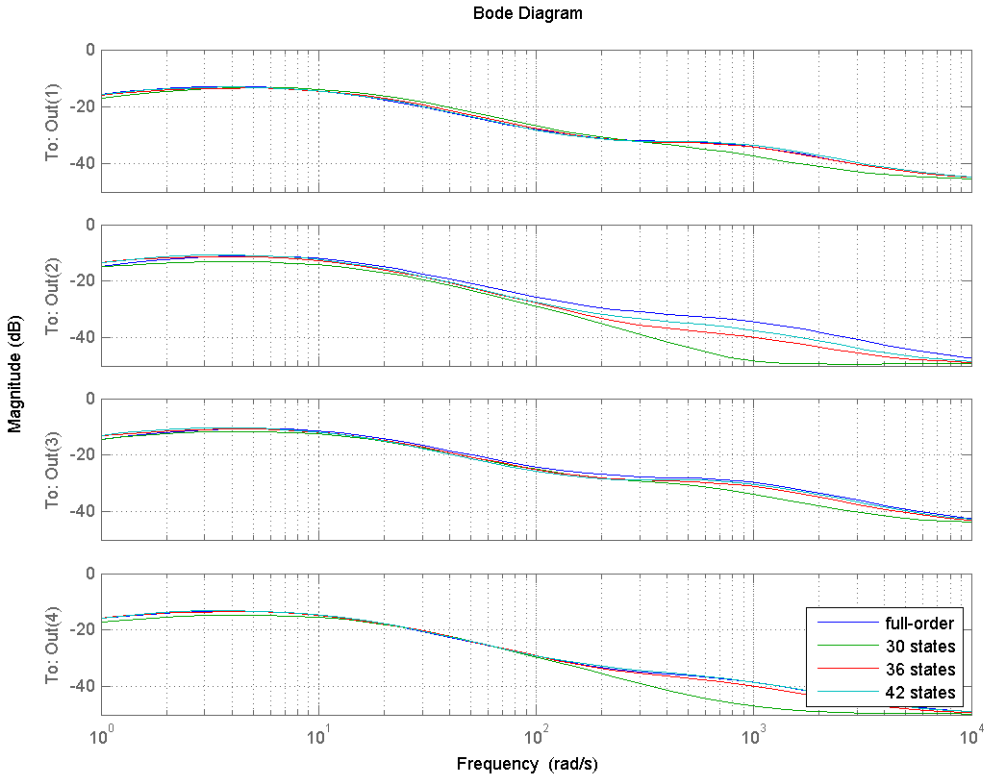

(b)

Figure 4.7: *ITER110/1832: Bode plot of the full-order and reduced systems between the* $101-th$ *input and the outputs from 1 to 4 when* $n = 110$ *(a) and* $n = 1832$ *(b) (i.e. the first active coil). [TBR]*

4.2 Hankel norm reduced models

4.2.1 Part A - technique validation on RFX-mod

The Hankel norm optimal reduction has been implemented with reference to the RFX-mod system and has given great results. In order to compare this model reduction technique with the previous one, reduced order models of the same order where considered. In figure 4.11 the comparison between the singular values of the full-order and reduced models is shown. Figures 4.9 and 4.10 show some step responses and Bode plots relative to the same inputs and outputs of figures 4.3 and 4.4. It is straightforward to verify that all the models produce similar and well performing reduced systems for both the model reduction techniques. In table 4.3 there are shown the value of the H_∞ norm and the relative error bound provided by the theory. So, from the point of view

number of states	H_∞ norm [dB]	error bound on H_∞
Full-order	26.7957	N/A
20	26.7842	0.0701
26	26.7935	0.0238
32	26.7952	0.0067

Table 4.3: *RFX-mod: H_∞ norm errors and relative error bounds in RFX-mod model. [Hankel norm]*

of the H_∞ norm, all the reduced models prove to be very good and show that the error bound is not really tight.

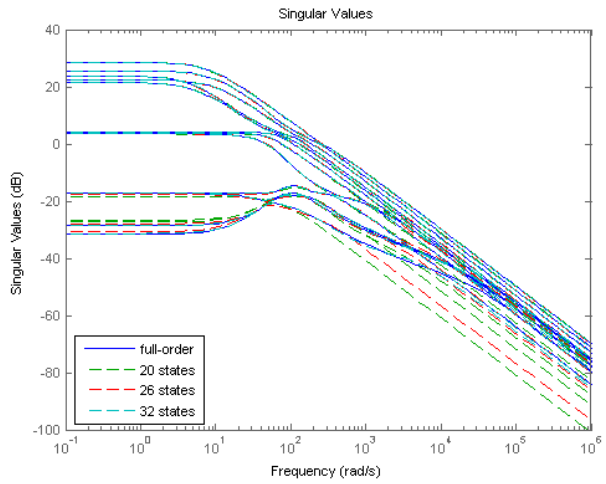

Figure 4.8: *RFX-mod: Comparison of the singular values between the full-order RFX-mod model and the three reduced models.*

4.2.2 Part B - technique approach on ITER models

The Hankel norm optimal reduction has been applied to both the ITER models with $n = 110$ and $n = 1832$ states. The step responses and Bode plots shown in figures 4.12 and 4.13 are good except for the models with the minor number of states, which shows some differences in both the time and frequency domains. Also the 12 dominant singular values in figure 4.11 show that by using only 20 states (when $n = 110$) there is a lack in the consistency between the reduced and full-order model. Similar conclusions can be made for the system with $n = 1832$. In any case, the results are greatly enhanced when considering the reduced models made of 26 and 32 states. From the H_∞ norm point of view, considering the system with $n = 110$ states, all the errors between the full-order model and the reduced models result to be almost zero.

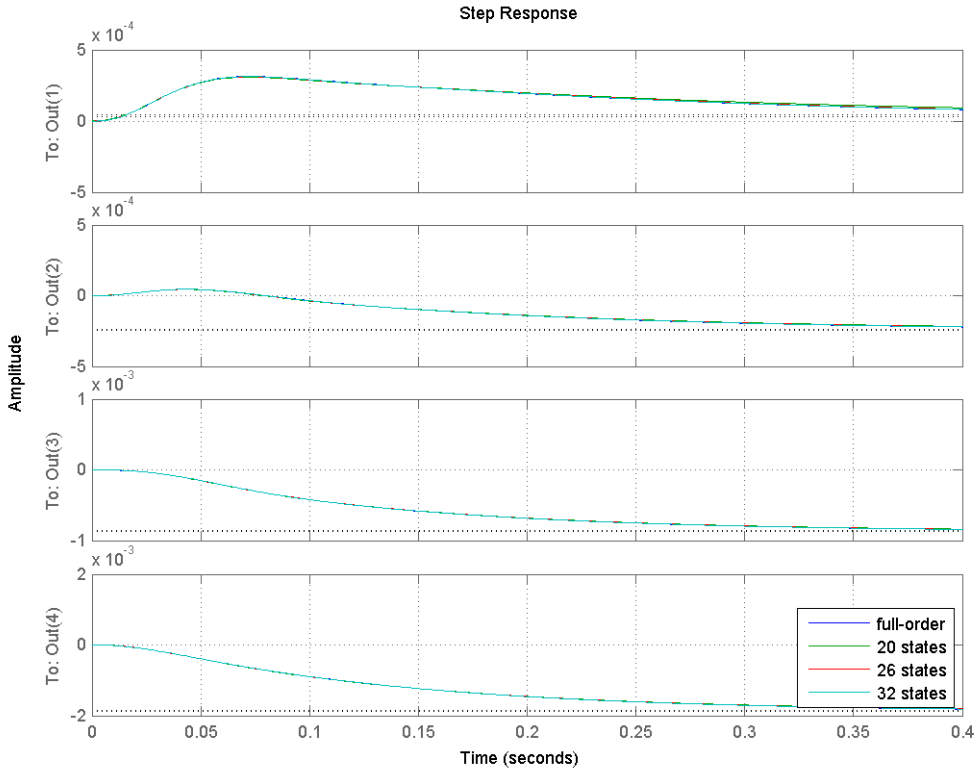

(a)

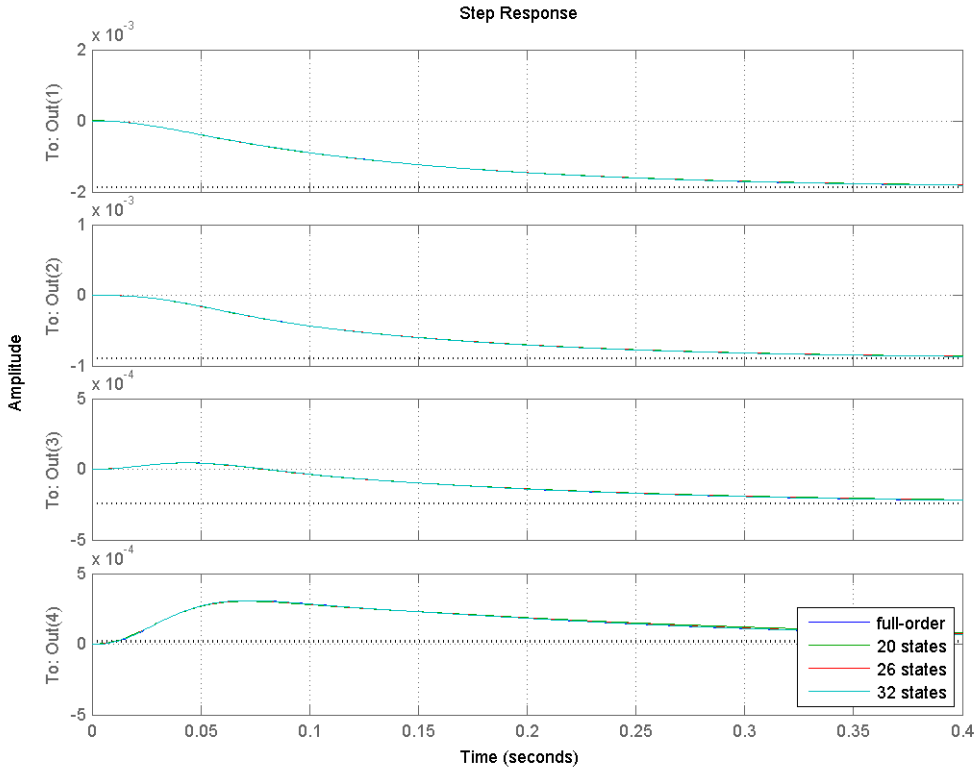

(b)

Figure 4.9: *RFX-mod: Step responses of the full-order and reduced systems of the outputs from 4 to 7 (a) and from 8 to 11 (b) when the first input is excited.*

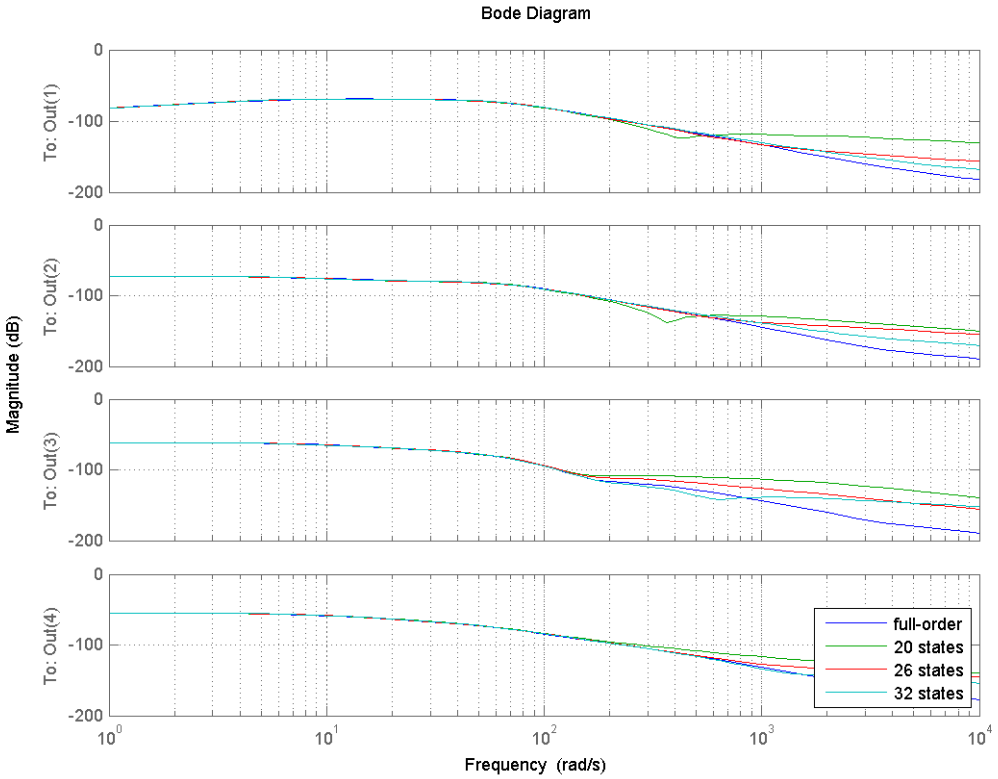

(a)

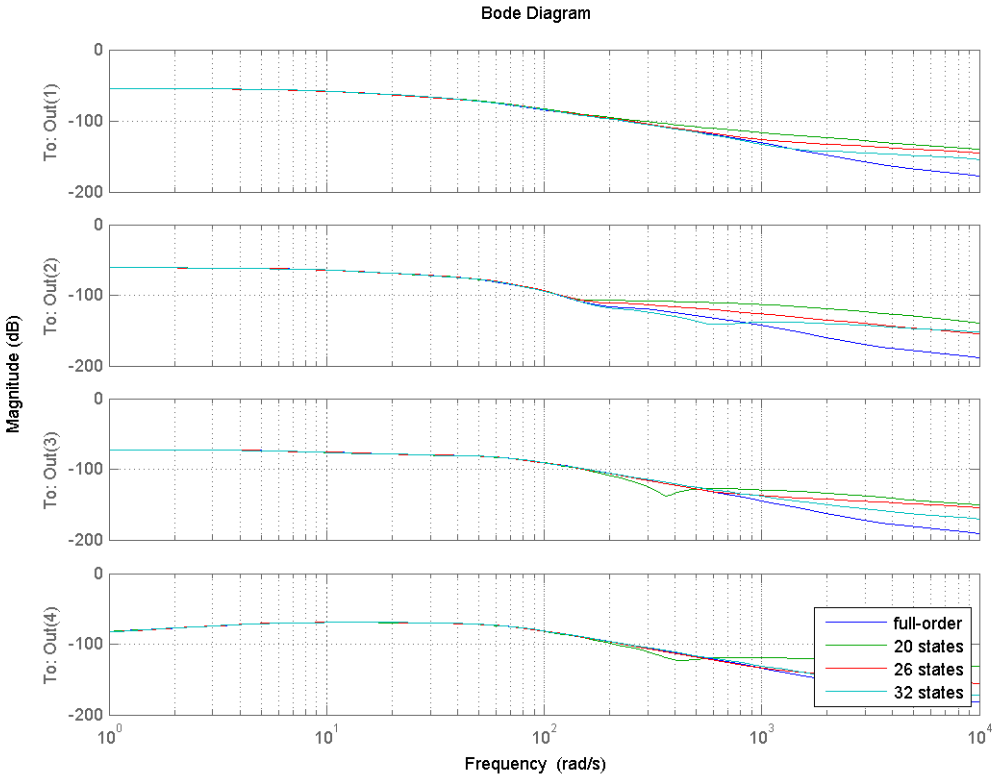

(b)

Figure 4.10: *RFX-mod: Bode plots (only the magnitude plots are represented) of the full-order and reduced systems between the first input and the outputs from 4 to 7 (a) and from 8 to 11 (b).*

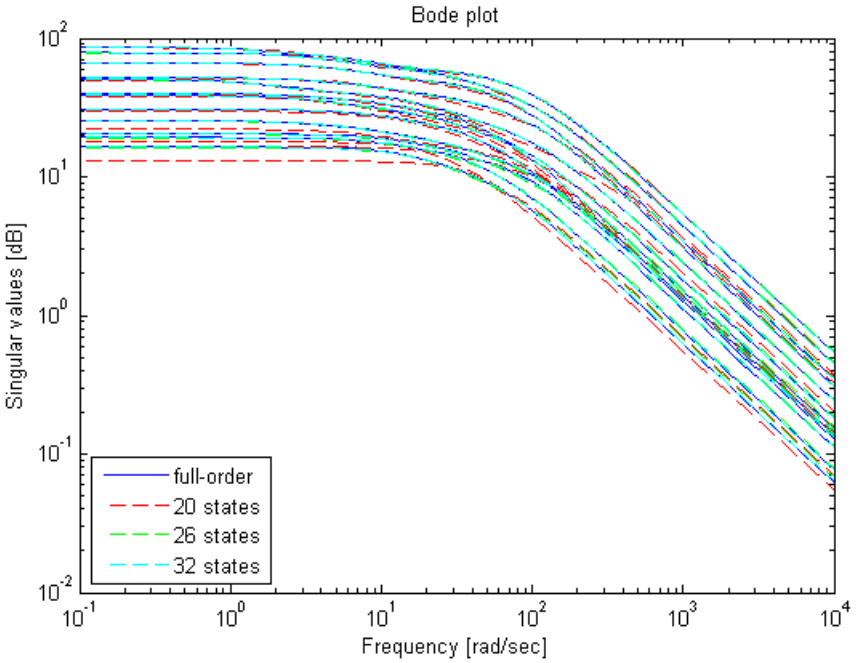

Figure 4.11: *ITER110: 12 dominant singular values of the full-order system with $n = 110$ states and of the reduced systems using the Hankel norm optimal reduction.*

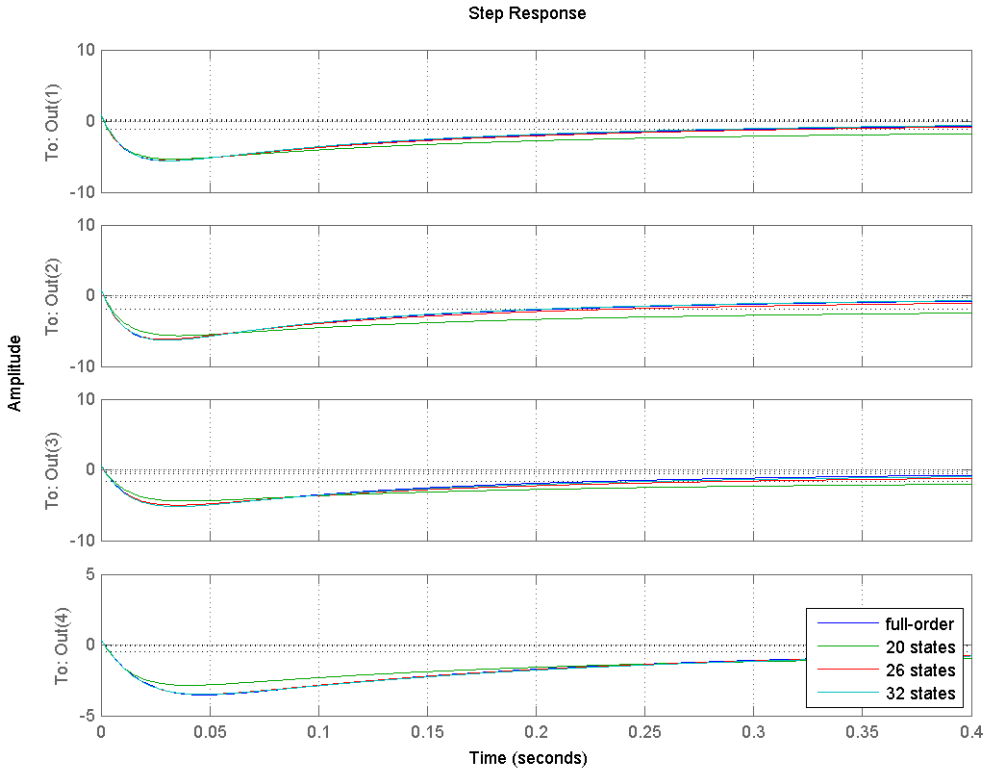

(a)

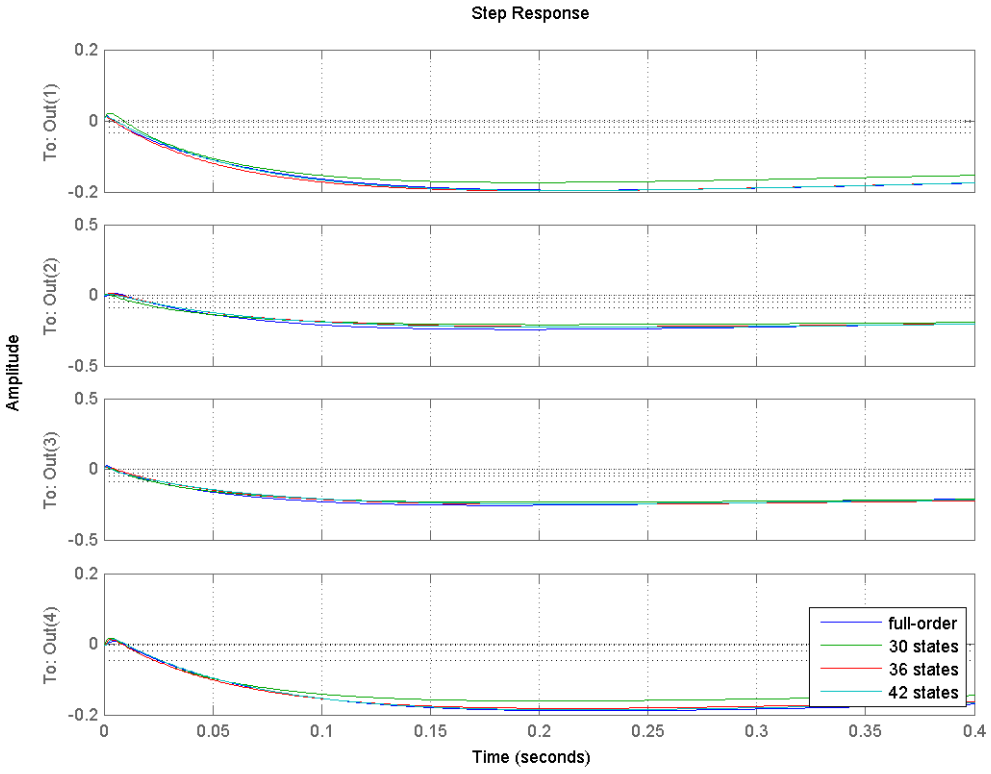

(b)

Figure 4.12: *ITER110: Step responses of the full-order and reduced systems of the outputs from 1 to 4 when $n = 110$ (a) and $n = 1832$ (b), when the $101 - th$ input is excited (i.e. the first active coil). [Hankel norm]*

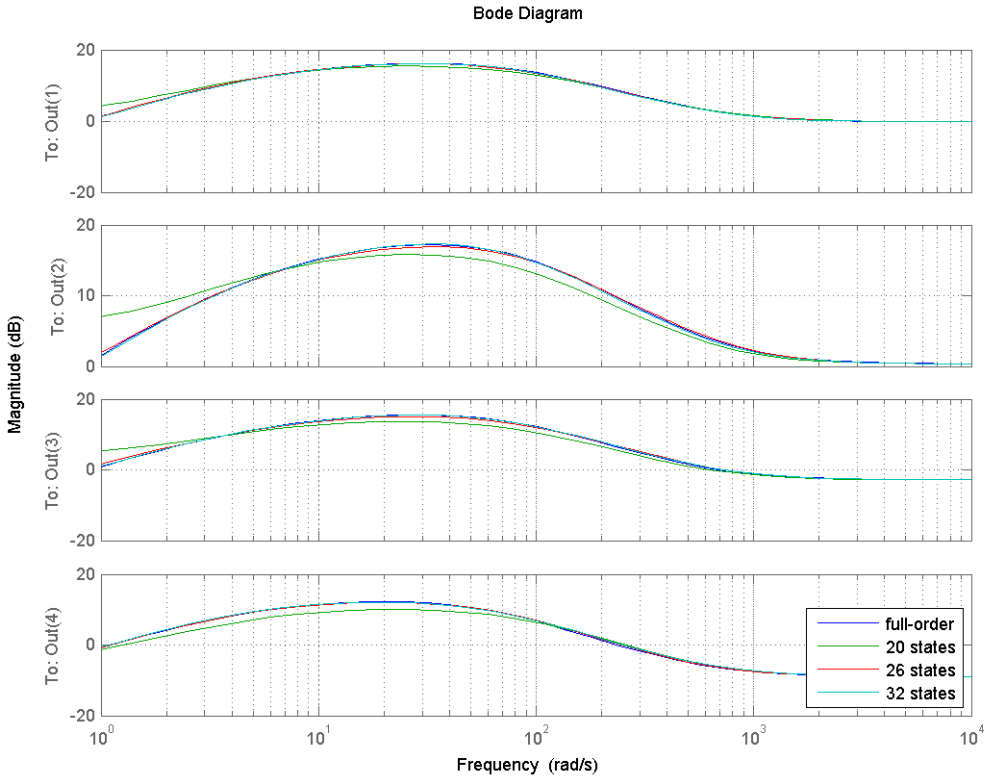

(a)

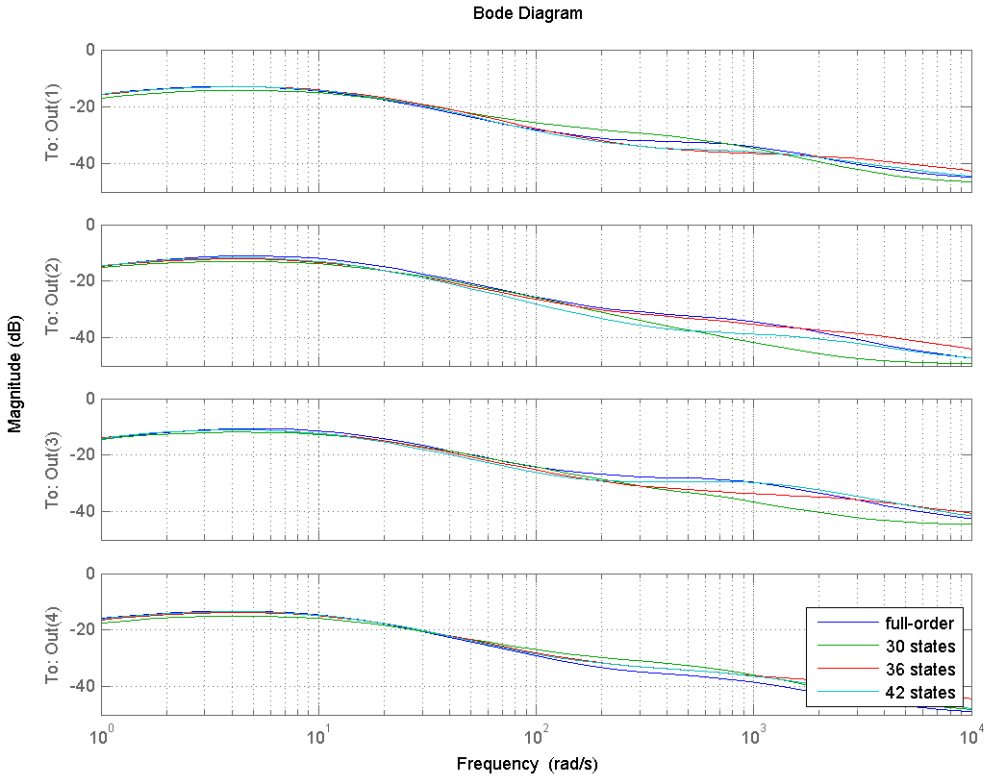

(b)

Figure 4.13: *ITER110: Bode plot of the full-order and reduced systems between the* $101-th$ *input and the outputs from 1 to 4 when* $n = 110$ *(a) and* $n = 1832$ *(b) (i.e. the first active coil). [Hankel norm]*

4.3 SMA reduced models

SMA reduction procedure allows to preserve in the reduced model the physical meaning of the full-order variables. This can be really helpful when designing or tuning a controller for a reduced system. On the other hand, this reduction method presents some drawbacks, in particular the computation of the eigenvalues of large systems can be difficult and subject to numerical issues. Moreover, this procedure is better suited for systems which have a particular structure, so that the participation factors can be easily studied (remember proposition 1). These are the cases of the IAIA passive structures model with $n = 1832$ states and the RFX-mod model, respectively.

Therefore, the only reduced model considered in this case is the model of the IAIA passive structures with $n = 110$ states.

4.3.1 Approach on ITER model with $n = 110$ variables

From the analysis of the systems we are considering (also the system with $n = 1832$ states is here discussed), some interesting results have emerged. In particular, it appears that low-frequency modes tend to be dependent, in a similar way (similar p_{ki} values), from a great number of states, while high-frequency modes usually depends on a minor number of states, which have a great influence on them, granting high participation ratios. From now on, we will consider the modes of the full-order system ordered decreasingly, so that the first mode will be the slower, and the last one the faster.

particip. ratio	states	mode 1	mode 35	mode 110	mode 600	mode 1832
ρ	110	1.137	2.797	$\simeq 8 \cdot 10^8$	N/A	N/A
ρ	1832	1.585	4.156	1.867	12.595	$\simeq 4.228 \cdot 10^{13}$

Table 4.4: *Participation ratio of 6 different modes, computed by considering the* 30 *and* 500 *states with the major influence for each mode in the systems with* 110 *and* 1832 *states respectively.*

As we can see from table 4.4 the first mode is awfully dependent on a very large number of states, in particular when $n = 1832$. This behavior is common to almost all low frequency modes. The consequence is that *to obtain a participation ratio on the first mode greater than one, we have to retain about 400 states*. So by retaining 400 states we can only achieve a participation ratio slightly greater than one for the first mode, and at the same time we have low participation ratios for all the remaining

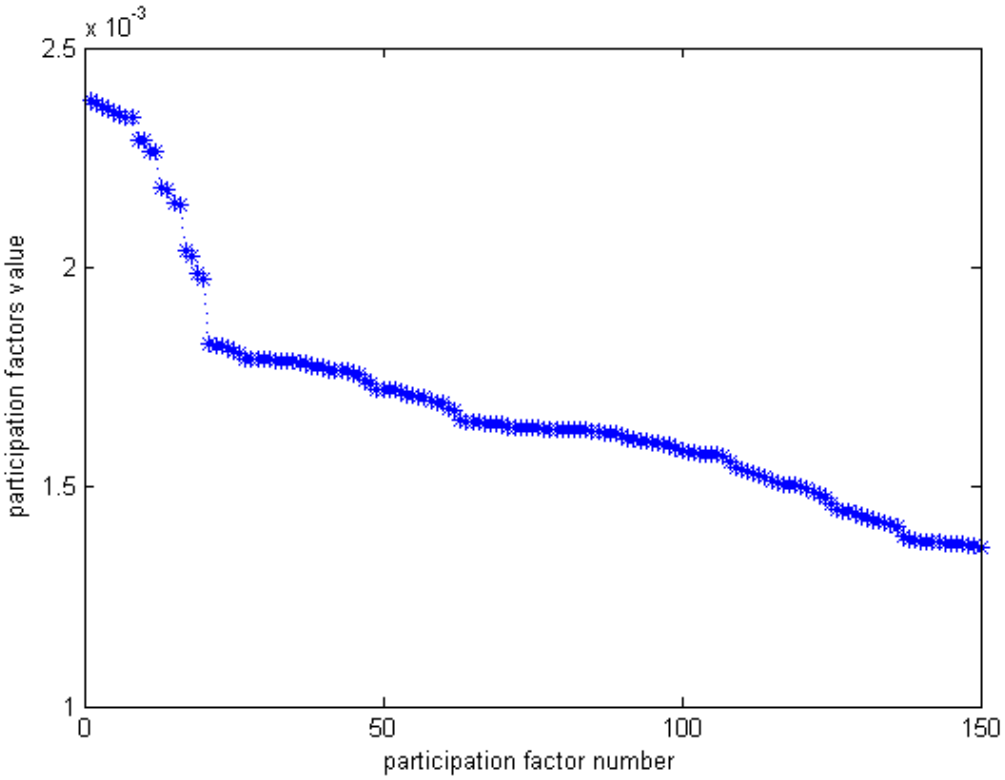

Figure 4.14: *ITER1832: Greater participation factors corresponding the to first mode of the system with $n = 1832$ states. The behavior is extremely smooth and the values are very small.*

modes. Thus, to obtain a reduced model which well approximates the original one, there is the need to retain a number of states ridiculously high. Figure 4.14 shows the behavior of the 150 greater participation factors in the first mode. The values of the participation factors are very small and the decrease is very smooth, leading to a difficulty in the choice of the number of states to be retained.

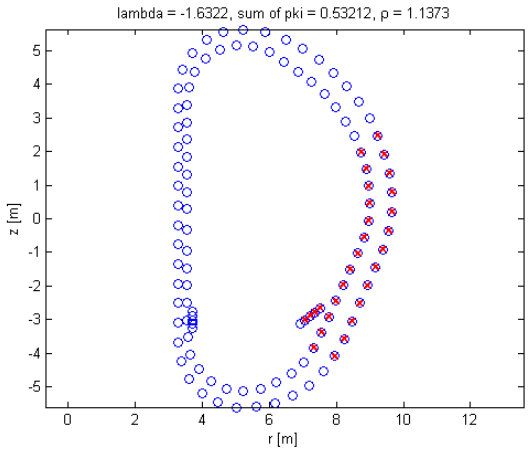

(a) *Map of the* 30 *states with higher participation ratio (crossed circles) in the modes associated with the eigenvalue* $\lambda = -1.6322$.

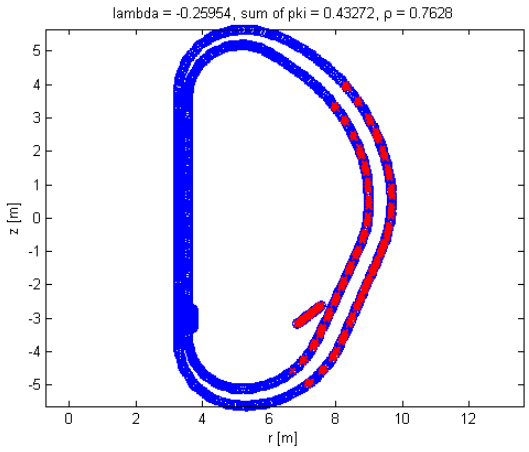

(b) *Map of the* 300 *states with higher participation ratio (crossed circles) in the modes associated with the eigenvalue* $\lambda = -0.2595$.

Figure 4.15: *areas of major influence on the first mode of the two systems*

From the Figures above we can observe that:

- low-frequency modes depend on states which typically present symmetries with respect to radial or vertical axes, such as in Figure 4.15 or in Figure 4.16 (b);
- middle-frequency modes depend on states that are quite evenly distributed in the metallic structures, like in Figures 4.16 (a) and 4.17 (a) and (b);
- high-frequency modes behave in a similar way like the middle-frequency ones, except for the very high-frequency modes, which appear to be dependent on localized currents without any symmetric pattern. In particular, it appears that the vertical structure has a great influence on the majority of them. Figures 4.17

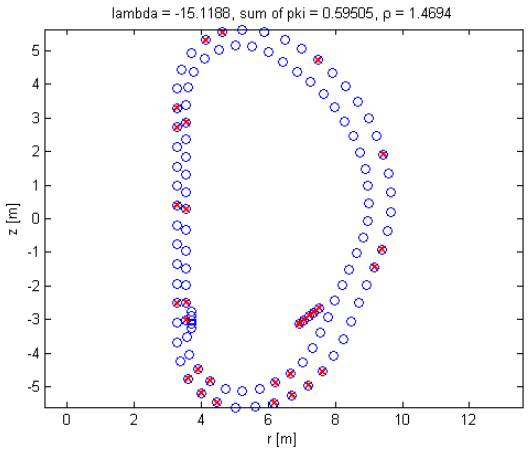

(a) *Map of the* 30 *states with higher participation ratio (crossed circles) in the modes associated with the eigenvalue* $\lambda = -15.1188$.

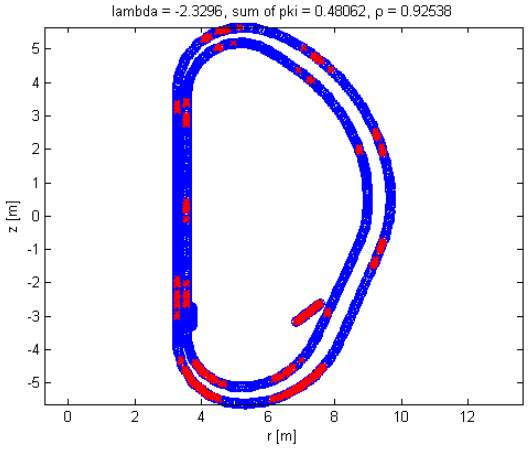

(b) *Map of the* 300 *states with higher participation ratio (crossed circles) in the modes associated with the eigenvalue* $\lambda = -2.3296$.

Figure 4.16: *areas of major influence on the tenth mode of the two systems*

(c) and (d) shows this particular behavior. Furthermore, when considering this modes, we can achieve really high participation ratios with only few states.

Dissimilarly from the high-frequency modes, the low-frequency modes behave in a different way. Considering these modes, to achieve participation ratios greater than 1, we need to include in the reduced model a greater number of states. This is caused by the fact that the single states have small and similar participation factors in relation to low-frequency modes. Because of this we have to retain a greater number of states in the reduced model respect to the optimal model obtained with the Hankel procedure. For instance in figure 4.18 is represented the sum of the 30 greater participation factors for each mode of the system with 110 states.

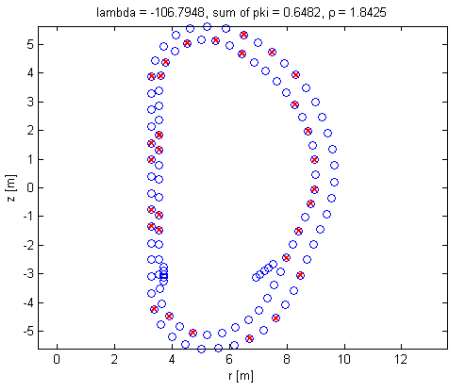

(a) *Map of the* 30 *states with higher participation ratio (crossed circles) in the modes associated with the eigenvalue* $\lambda = -106.7948$.

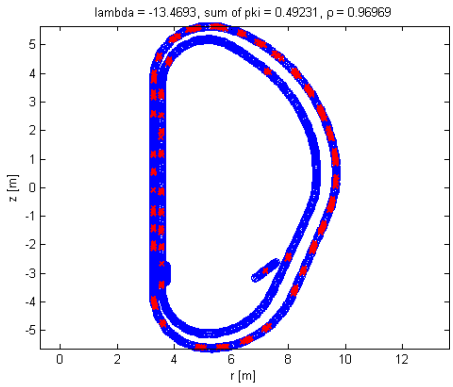

(b) *Map of the* 300 *states with higher participation ratio (crossed circles) in the modes associated with the eigenvalue* $\lambda = -13.4693$.

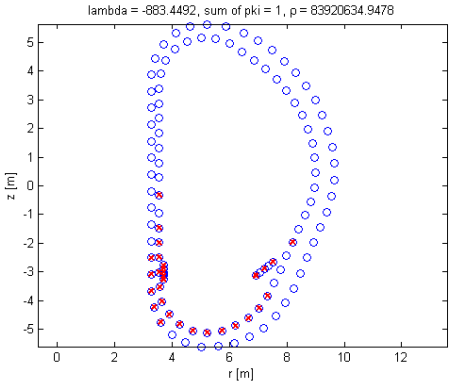

(c) *Map of the* 30 *states with higher participation ratio (crossed circles) in the modes associated with the eigenvalue* $\lambda = -883.4492$.

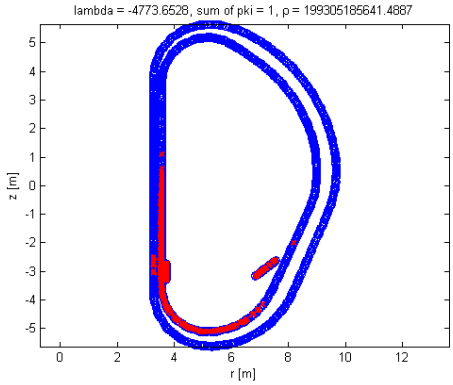

(d) *Map of the* 300 *states with higher participation ratio (crossed circles) in the modes associated with the eigenvalue* $\lambda = -4773.6528$.

Figure 4.17

In order to determine the number of variables to be retained in the reduced model the participation factors of the first eigenvalues were considered. In particular, the participation factors relative to the first eigenvalues of the systems appear to decrease very smoothly and this behavior is common to almost all low and middle frequency eigenvalues. Only high frequency eigenvalues tend to be dependent from a small number of states, probably because they are due to local artifacts of the magnetic field.

As the physical meaning of the state variable is preserved, it is possible to use as a guideline in the selection of the variables to be retained the available *a priori* knowledge on the machine structure. The key issue is to find a criterion for selecting which states belonging to the metallic structures can be neglected while retaining the most relevant dynamic behavior of the system. A typical choice for stable system is to retain the variables which are the most influential on the low frequency eigenvalues of the system, which are the dominant ones in the dynamic of the system.

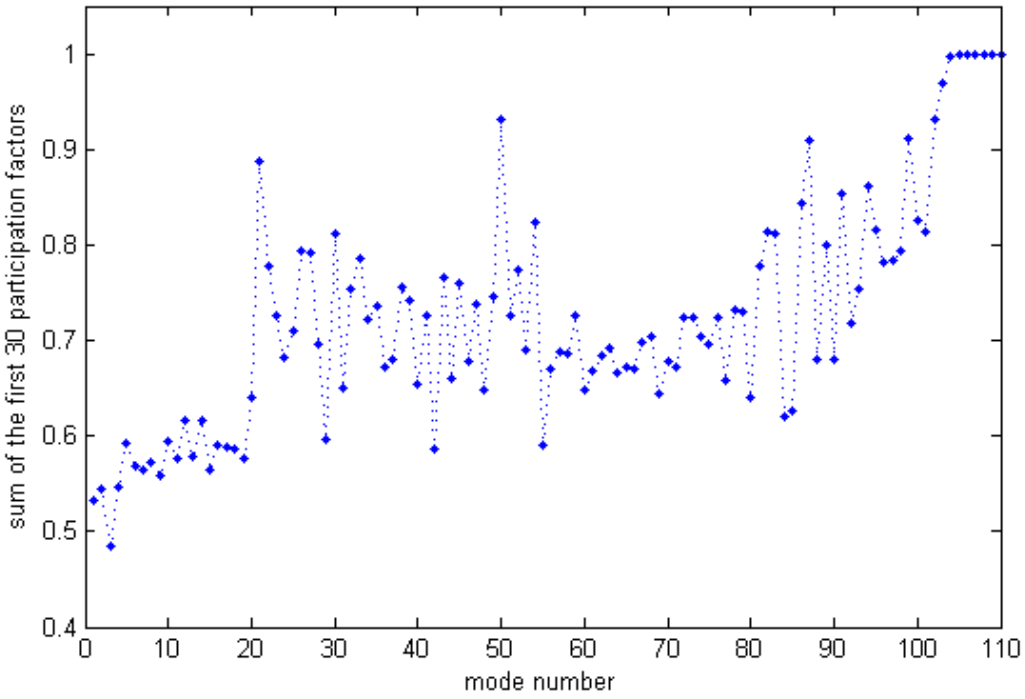

Figure 4.18: *ITER110: sum of the* 30 *greater participation factors for each mode of the system with* 110 *states.*

From these considerations it's clear that to achieve a reduced order model which reproduces the full-order one, a higher number of variables must be retained in the reduced model respect to the previous MOR techniques. There is the necessity to make a choice that mediates between the contrasting needs of reducing the number of variables and obtaining a good approximation of the original system. A good solution is to retain the most relevant variables with respect to the 10 dominant eigenvalues of the model with $n = 110$ states. This led to a model composed of 63 states, so in this way almost half the number of starting variables was removed while conserving the physical meaning of the remaining ones. In figure 4.19 it is shown the comparison between the dominant singular values of the two models. Figure 4.20 shows the behavior of the step responses in the same situation of the previous section (for instance, see figure 4.6). The relative Bode plot is shown in figure 4.21. The behaviors of the Bode plots and of the step responses are quite similar to the ones achieved using the previous techniques, but now we are retaining a far greater number of variables in the reduced order model. In conclusion, with this kind of system the SMA procedure grants us the possibility to preserve the physical meaning of the retained variables, with the drawback of the need to retain a higher number of variables to achieve a satisfactory result.

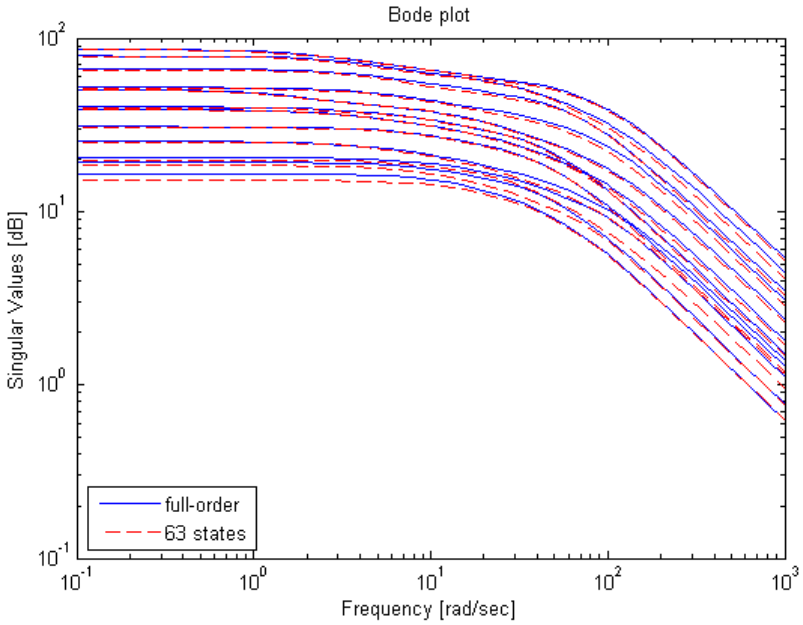

Figure 4.19: *ITER110: 12 dominant singular values of the full-order system with $n = 110$ states and of the reduced system using SMA.*

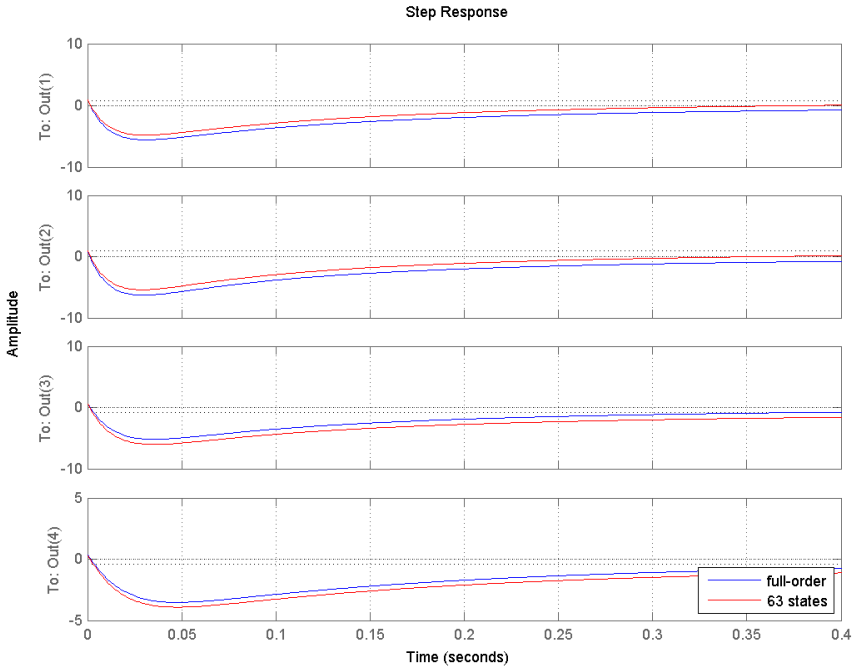

Figure 4.20: *ITER110: Step responses of the full-order and reduced system of the outputs from 1 to 4.*

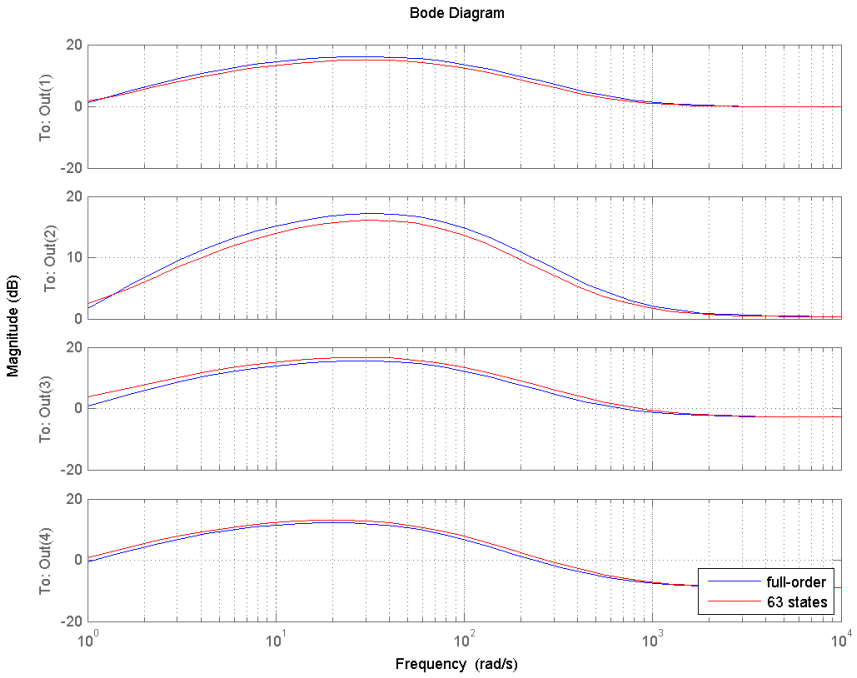

Figure 4.21: *ITER110: Bode plot of the full-order and reduced system between the* $101-th$ *input and the outputs from 1 to 4.*

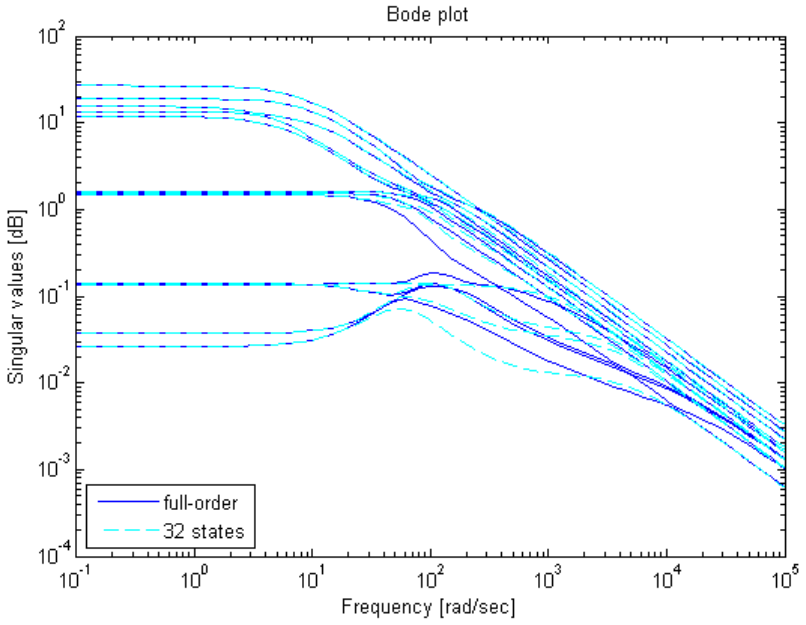

Figure 4.22: *RFX-mod: comparison of the 12 dominant singular values of the starting system and of the input-sided reduced one with 32 states.*

4.4 Krylov reduced models

4.4.1 Part A - technique validation on RFX-mod

Krylov techniques aim to compute reduced order models in which the first moments of both the original and reduced model match. This allows to easily determine the desired order of the reduced model and may also give some hint outside the mathematical meaning of the reduction procedure. The moments of the reduced system were forced to match around $s = 0$ because of the desire to approximate the dominant dynamics of the original system. Also, the input-sided Krylov technique has been implemented because of the lower number of inputs which grants better performance respect to the output-sided one. For the sake of consistency, three reduced models of the same order seen in the Hankel sections were considered, with 20, 26 and 32 states. However, the systems with 20 and 26 states resulted to be unstable (remember the drawbacks of Krylov techniques), leading to unacceptable behaviors, so only the comparison with the remaining reduced system is plotted in the following. In figure 4.22 there is shown the comparison between the 12 greater singular values of the original and reduced model. Note that for low frequencies the singular values matching is almost perfect and starts to deteriorate at frequencies slightly higher than 10 $[rad/sec]$. This is in total accordance with the fact that by using a reduced model of 32 states having 12 distinct inputs, approximately the first three moments are matched. Furthermore, this is also confirmed by the Bode plots of figure 4.22, where the approximation of the original system begins to deteriorate in the range of frequencies from 10^1 to 10^2.

The fact that only the first two or three moments are matched is reflected also by the step responses of figure 4.24. Some responses of the reduced model presents slight differences in the really first instants after the application of the input step. This is due to the appearance of different high frequencies dynamics in the reduced model, which usually can be neglected after about 0.1 [s] or less. Obviously, by increasing the number of variables in the reduced system (i.e. by increasing the number of matched moments), these effects can be reduced or almost totally eliminated.

4.4.2 Part B - technique approach on ITER models

The Krylov subspace methods can also be applied to the ITER models. However, the results are not so good as in the previous case. This is caused by the fact that in these models there is the need to face a extremely high number of inputs (active coils and filamentary currents) and outputs (a number of outputs equal to the number of state variables). As a consequence, the Krylov technique suffers this model structure. Indeed, to match the same number of moments as in the RFX model, there is the need

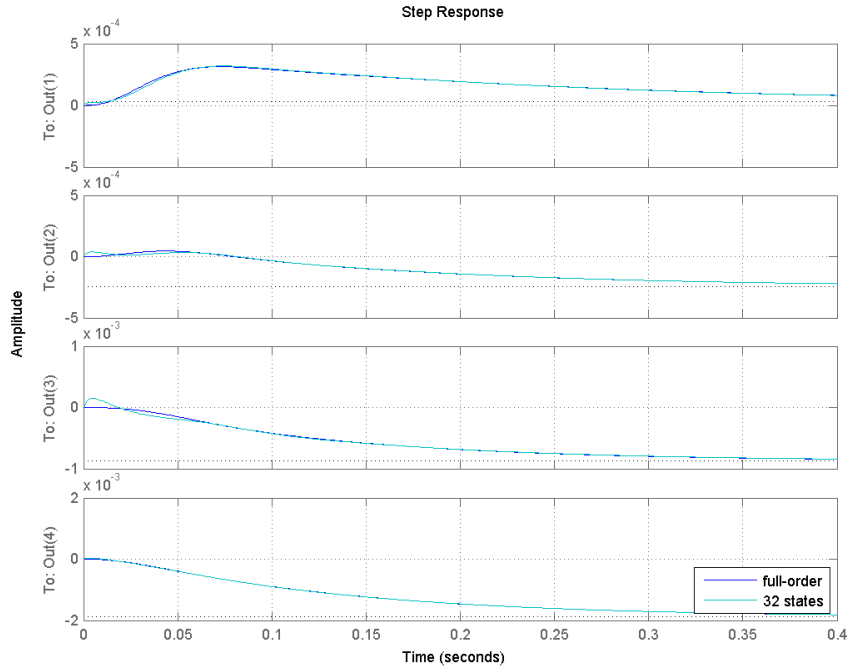

(a)

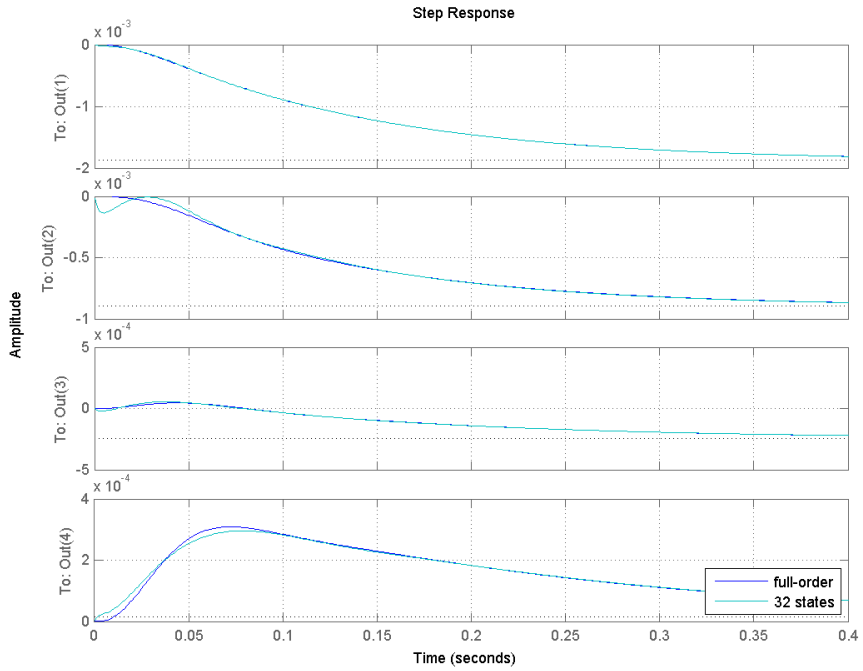

(b)

Figure 4.23: *RFX-mod: Step responses of the full-order and reduced systems of the outputs from 4 to 7 (a) and from 8 to 11 (b) when the first input is excited.*

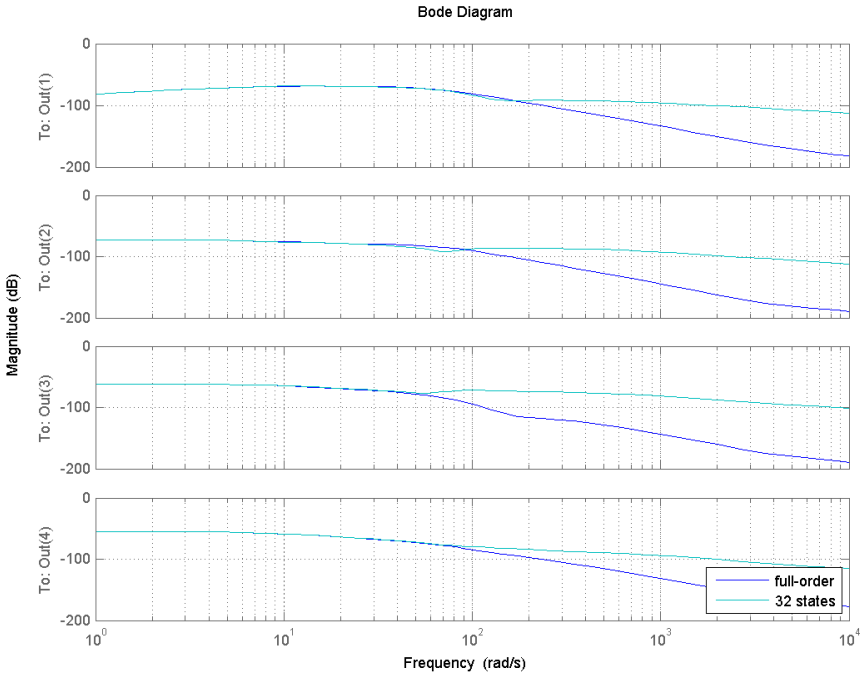

(a)

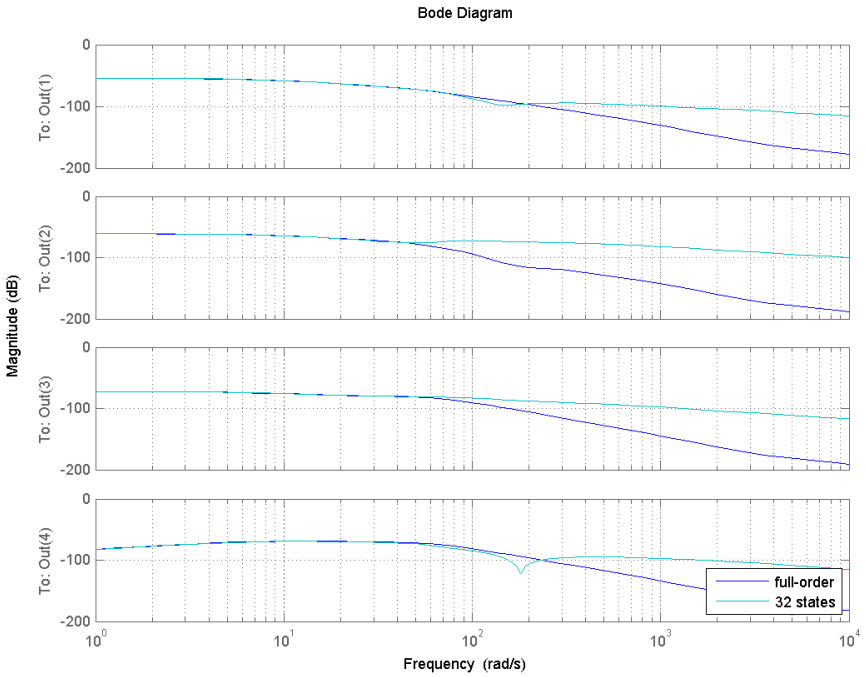

(b)

Figure 4.24: *RFX-mod: Step responses of the full-order and reduced systems of the outputs from 4 to 7 (a) and from 8 to 11 (b) when the first input is excited.*

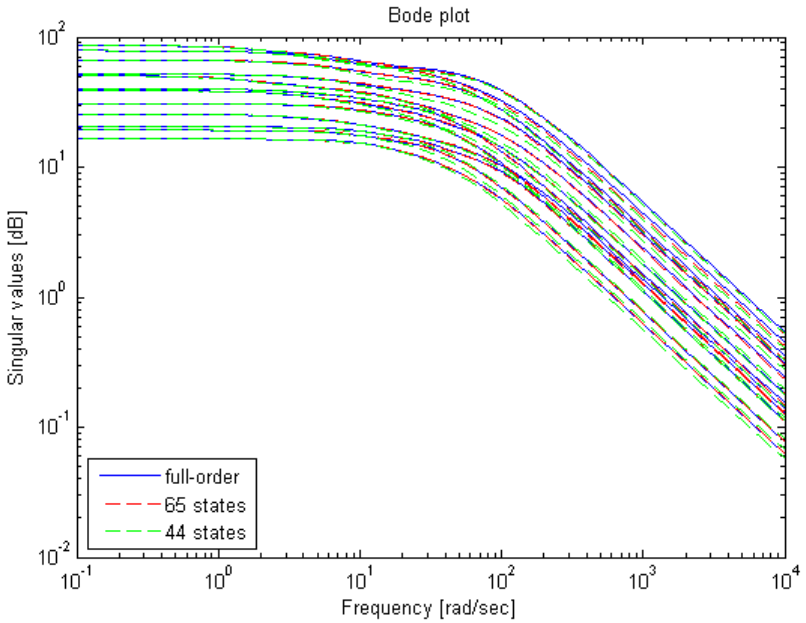

Figure 4.25: *ITER110: 12 dominant singular values of the full-order system with $n = 110$ states and of the reduced systems using Krylov input-sided subspace.*

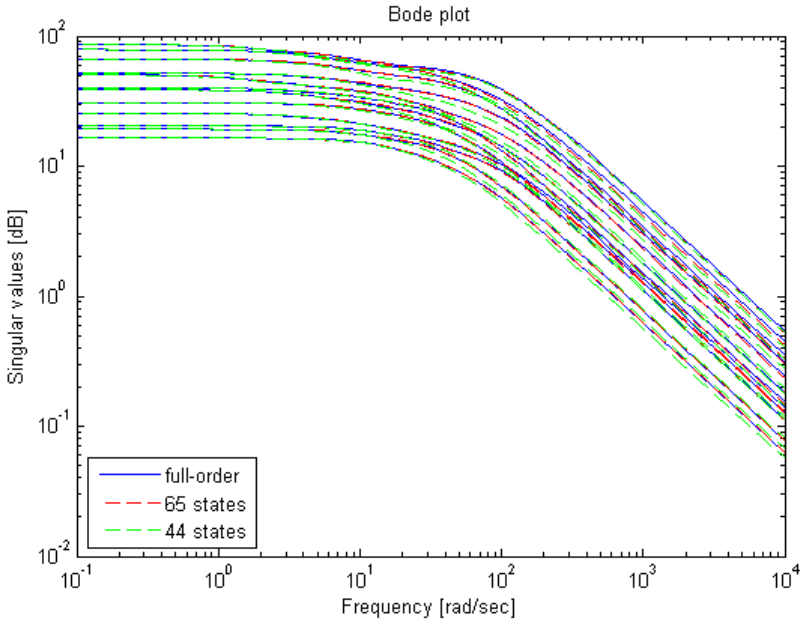

Figure 4.26: *ITER1832: 12 dominant singular values of the full-order system with $n = 1832$ states and of the reduced systems using Krylov input-sided subspace.*

to build reduced order models with a higher number of state variables. Therefore, the output-sided method was discarded a priori. Only the input-sided method has been applied to both the systems with $n = 110$ and $n = 1832$ states. In the first one, the number of starting vectors (i.e. independent inputs) is $m_1 = 34$, which is still to big to hope in really efficient reduced systems. The situation is similar in the second system, where the number of starting vectors rise to 104. This means that only to match the first moment we have to deal with a reduced system consisting of 104 variables. By the way, keeping in mind this considerations, some reduced models were built. In figures 4.27 and 4.28 the step responses of the full-order models and reduced ones are represented. In both cases two possible reduced systems are considered. In the case of $n = 110$ a reduced system of 65 states gives discrete results, comparable to the SMA reduction. On the other hand, there is no preservation of the variables physical meaning, so it is suggested to use the SMA procedure. The system with $n = 1832$ states can be approximated sufficiently well by using about 260 states, which lead to match the first two moments and about half parameter of the third one. This represents a step ahead respect to the SMA, but the reduction is far less performing respect to the Hankel techniques.

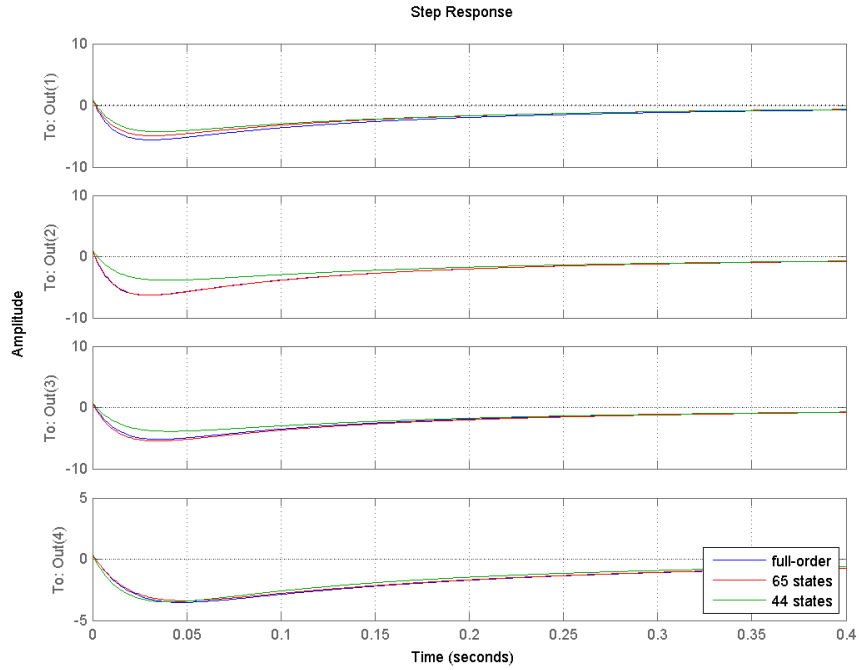

(a)

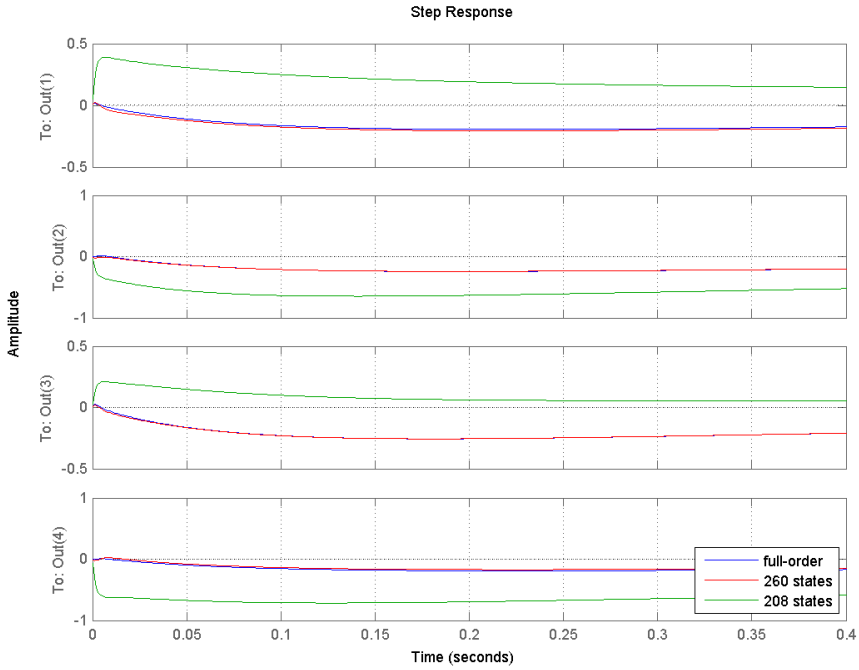

(b)

Figure 4.27: *ITER110/1832: Step responses of the full-order and reduced systems of the outputs from 1 to 4 when $n = 110$ (a) and $n = 1832$ (b), when the $101 - th$ input is excited (i.e. the first active coil). [Krylov]*

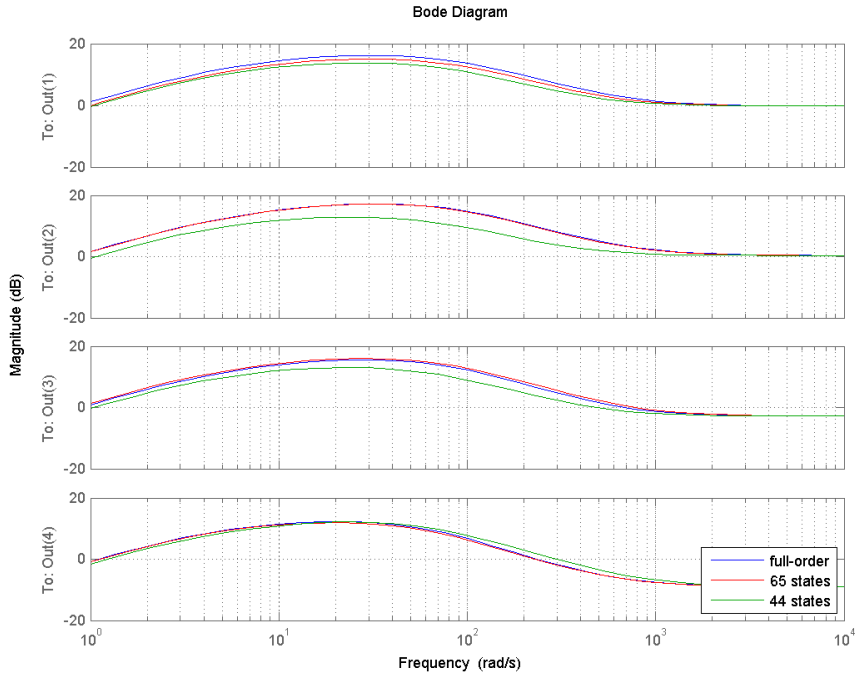

(a)

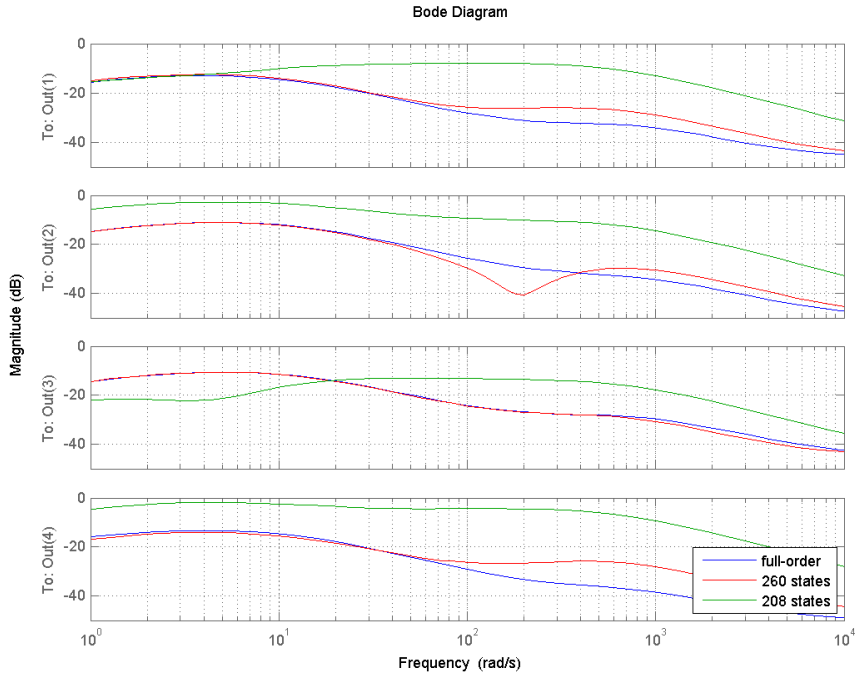

(b)

Figure 4.28: *ITER110/1832: Bode plot of the full-order and reduced systems between the* $101-th$ *input and the outputs from 1 to 4 when* $n = 110$ *(a) and* $n = 1832$ *(b) (i.e. the first active coil). [Krylov]*

Conclusions

Nuclear fusion is considered a key technology in the development of new form of long-lasting sources of energy. Therefore, the study of nuclear fusion devices capable of generating fusion-derived energy has rapidly grown in the last 50 years. Several problems are involved in the construction and operation of tokamaks, ranging from the handling of safety aspects to the control of the main plasma parameters.

As a consequence, numerous algorithms and modeling techniques have been developed to cope with such problems and in particular capable of accurately identifying the plasma shape and boundary position. These algorithms need to face real-time constraints because the plasma shape and boundary position must be quickly identified in order to implement useful feedback loops to modify the plasma boundary shape as desired. Unfortunately, the large passive structures surrounding the vacuum chamber are affected by large eddy currents flowing in the metallic structures, which in particular influence the magnetic diagnostic used to reconstruct the plasma boundary position, leading to wrong or bad reconstructions. Therefore, these currents need to be somehow modeled. A typical choice is to split the metallic structure into toroidally symmetric elements which are exploited to estimate the currents flowing in the overall passive structure.

The problem is now how to take into account many elements in this kind of procedure. In fact, a large number of elements would lead to a more detailed but also complex model, thus causing a too high computational burden, hardly suitable with real-time constraints. One way to cope with this problem is by exploiting model order reduction techniques, which allow to compress high order models into more compact ones, thus leading to a balance between the contrasting needs of dealing with real-time constraints and at the same time the necessity to accurately describe the involved dynamics. Several MOR techniques have been developed, which face the problem of model reduction with different approaches due to the difficulty of establishing a unique criterion.

This thesis addresses the problem in relation to the models developed for the IAIA code, which is an algorithm capable of reconstructing the plasma boundary position, in order to improve its real-time performance. As a consequence, some reduced model are

derived starting from different original models, with different complexity. Also, several MOR techniques have been implemented, in order to compare their performance and to exploit the main advantages of each one. The Hankel based techniques have proved to be the most effective, granting reduced models able to well-approximate the starting ones, using a very reduced number of variables. One of the reasons of this behavior is that it seems that such techniques are well suited for almost every kind of model, meaning that they're not really affected by the model structure, in relation, for instance, to the number of inputs and outputs of the system. Moreover, they give useful hints on a suitable order of a well-performing reduced model. Contrary to Hankel techniques, Krylov subspace methods show some difficulties in reducing large MIMO systems. These issues are directly linked to the reduction procedure, which aims to match the first moments of both the original and reduced models by exploiting the so called input and output Krylov subspaces, which in the case of large MIMO systems lead to a still too high complexity of the reduced model, making sometimes even impossible to reduce the starting system with acceptable results. Finally, the selective modal analysis has been implemented. The strength of this technique is that it allows to preserve the retained variables physical meaning in the reduced model, thus simplifying the successive design or tuning of the controller. On the other hand, this technique does not give a hint in the choice of which modes of the system is better to retain. The choice that was made was to discard those states which showed to be less influent in the slow dominant dynamics of the starting model. The key definition in SMA is that of the participation factor which measures the contribution of the single states in the construction of each mode. In relation to the IAIA models there have been some issues. In particular, the participation factors have proved to be very smooth in relation to the slow dynamics of the system, leading to the necessity of retaining a number of variables higher than the one obtained in the models achieved through Hankel reduction. At the same time, this behavior of the participation factors was observed also in the system with $n = 1832$ states, making impossible to get a reduced order model with an acceptable number of variables. Therefore, the SMA reduction technique applied in this specific case poses the problem of achieving a reduced model where the variables meaning is preserved, at the cost of having a more complex reduced model.

Interestingly, on average the number of states to be retained after the reducing procedure is in the range $20-40$, which basically corresponds to the number of degrees of freedom of many large scale nuclear devices (e.g. ITER, JET) linked to the dimension of the operative space of the machine (in terms of shape/magnetic control capabilities).

As for the future work, from the MOR point of view, a study can be carried forward about the passive model which takes as input both the currents flowing in the active

coils and the magnetic measurements, which leads to a compact version of the IAIA algorithm by merging three modules into a single one. Such model might be more suited to model order reduction and moreover it would allow to study the dependence of the modes of the passive model in relation to the different geometrical position or number of the magnetic measurements as input.

In addition, by exploiting a different approach, the IAIA time consumption can be improved also by modifying some of its internal parameters, in particular in relation to the plasma filamentary model. In this sense, an analysis was made in the IAIA algorithm version which doesn't make use of the eddy currents to estimate the plasma boundary position. The fixed grid in which the filamentary currents can be put was halved in a homogeneous way while keeping the same number of filamentary currents. The algorithm seems to be still efficient in static conditions, but showing some lack in the precision of the estimation with the increase in the value of the eddy currents. This is probably related to the absence of the estimate of the passive currents flowing in the metallic structures, which makes the algorithm particularly sensitive to dynamic conditions.

In the near future, one way to improve the algorithm real-time performance is to think about a filamentary model where the grid of position in which the currents can be put changes adaptively, in relation to the plasma boundaries estimated in the preceding iterations, leading to a minor number of calculations.

Appendix A

Sensitivity of the IAIA code to variations of the internal parameters

In this section, we consider the reconstruction code IAIA with the purpose of reducing its computation burden.

In order to reduce the time consumption of the IAIA algorithm, MOR is not the only way. In fact, in the iterative procedure of the algorithm, two sets of equivalent currents are placed along the rad-lines. The first set is fixed and placed well inside the plasma domain, in an area basically included in any plasma cross section shape, while the second set is placed along the rays in a position approximately midway between the starting point of the rays and the currently identified boundary, which is computed on-line at every iteration. The number of iterations can be chosen to be fixed or depending on some convergence criterion with reference to some distance measurement between two consecutive iterations.

Following this discussion, another method to optimize the time consumption is to reduce the number of points on the rad-lines. In the developed code there are 80 rad-lines and each one is composed of 120 points where each one of the outer filaments of current can be put. Obviously, the reduction in the number of degrees of freedom should lead to a worsening in the precision of the reconstructed boundary. In particular, in the following we will be interested in the assessment of the code precision while reducing the number of the algorithm internal parameters. In figure A.1 (a) it is represented the cross section of the ITER tokamak together with a representation of the rad-lines. From now on a different version of the IAIA algorithm will be considered, in which the eddy currents are not considered in the identification of the plasma boundary.

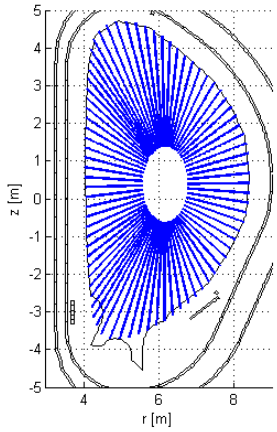

(a) *The blue lines represent the* 80 *rad-lines of IAIA.*

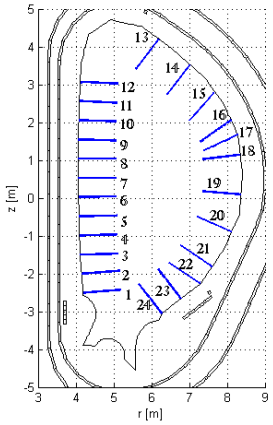

(b) *Location of the 24 gap-lines.*

Figure A.1: *Rad-lines and gap-lines in IAIA.*

A.1 rad-lines points reduction

One way to decrease the time consumption is to reduce the number of points of which the rad-lines are constituted. In this way, there are still 80 outer currents like in the full algorithm, and its possible to keep an homogeneous distribution of the points along the cross section of the tokamak. The comparison between different reconstructed boundaries is made in terms of boundary to first-wall distances called *gaps*. A gap-line is a segment that starts at the FW and ends near the center of the vacuum chamber, as shown in figure A.1 (b). So they are used as descriptors of the plasma shape.

To give some numerical results, a comparison between the reconstructed boundary of the full-code with the new one has been carried forward:

- The sum of the distances between the reconstructed position of the boundary along the 24 gaps in the 137 equilibria is $d = 5.8935$ [m].
- Consequently, the mean error in the reconstruction of every Gap position is of about 0.0017 [m].
- Unfortunately, in some cases there are too large errors. The greatest is of about 0.08 [m].

Thus, the performance is quite good in most cases, but sometimes there is a great difference in the reconstructed boundary. As a matter of fact, there are still 80 outer currents like in the full-code, so at first similar results are expected in terms of currents values in the filaments, and so it is. For instance, in figure A.2 the inner and outer filamentary currents are compared with the ones of the full-code.

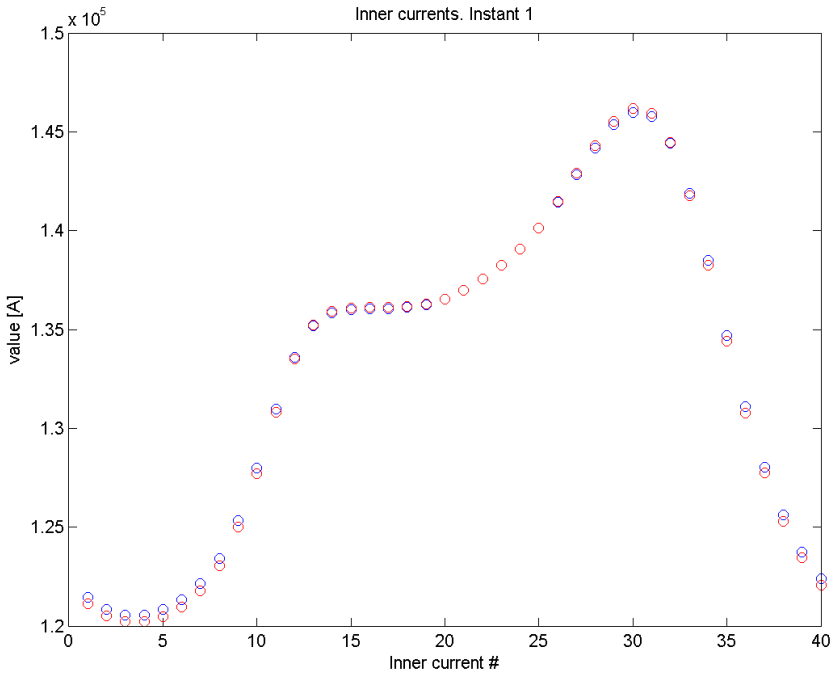

(a) *Red circles represent currents in the inner filaments when considering only half the number of points, while blue circles represent currents in the inner filaments of the full-code.*

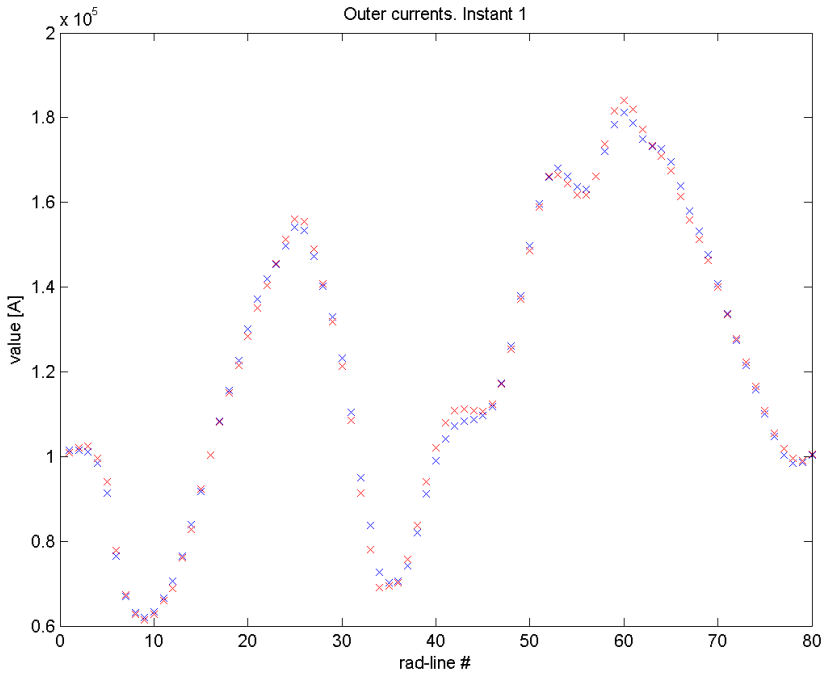

(b) *Red crosses represent currents in the outer filaments when considering only half the number of points, while blue crosses represent currents in the outer filaments of the full-code.*

Figure A.2: *Comparison of inner and outer currents at equilibrium* 1.

To assess the quality of the reconstruction the differences between the boundary reconstructed by the full-code and the new code were analyzed. In figure A.3 three pictures of the errors made in gaps 1, 10 and 20 are shown. The reconstruction is quite accurate in the first 65-70 equilibria, while presenting a lack of accuracy in the successive reconstructions until about the equilibrium 110. In particular, it appears that around gap 1 the algorithm presents more difficulties in reconstructing the boundary position. Most of the greatest errors in the gap values are confined between the time intervals 60 and 120. This is due to the fact that in the considered scenario this time interval corresponds to quite strong dynamical events in the evolution of the plasma inside the vacuum vessel. So, the algorithm appears particularly sensitive to variations of the parameters in dynamical situations. This can be explained by remembering that the eddy currents aren't actually involved in the identification of the plasma boundary. As a consequence, this version of the IAIA algorithm seems to be quite sensitive to modifications of the number of points in the rad-lines when dealing with a dynamical scenario, but preserves a good performance in static conditions.

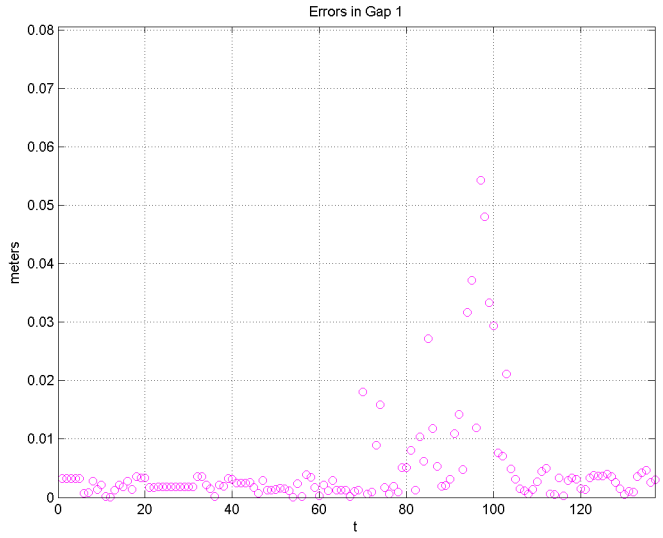

(a) *Errors in Gap 1*

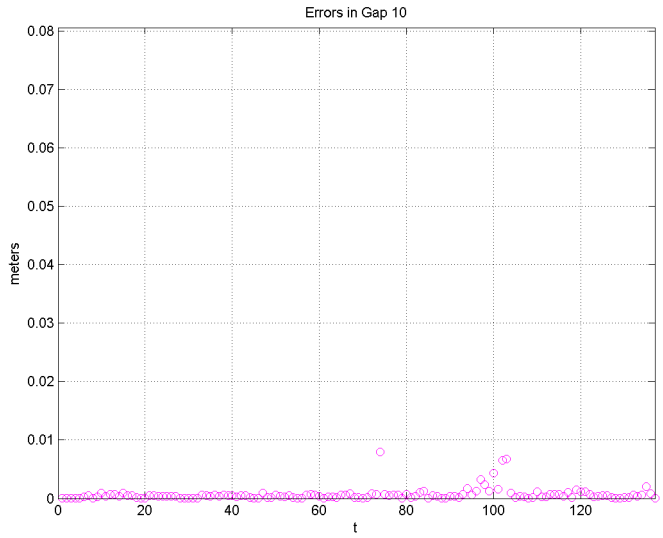

(b) *Errors in Gap 10*

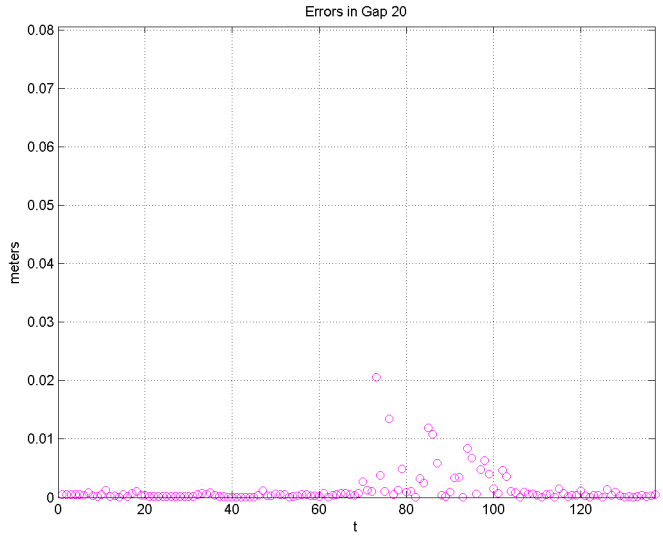

(c) *Errors in Gap 20*

Figure A.3: *Errors in three random gaps, in all 137 equilibria of the scenario considered.*

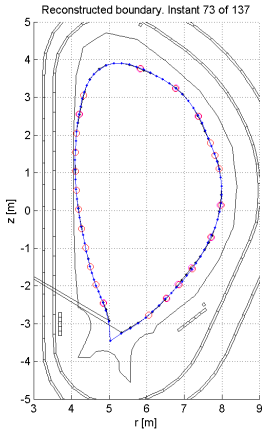

(a) *Equilibrium 73.*

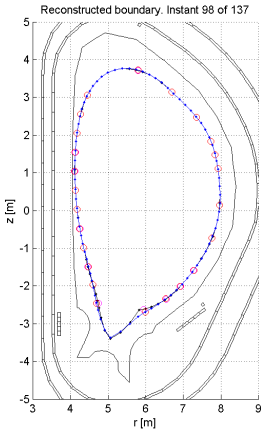

(b) *Equilibrium 98.*

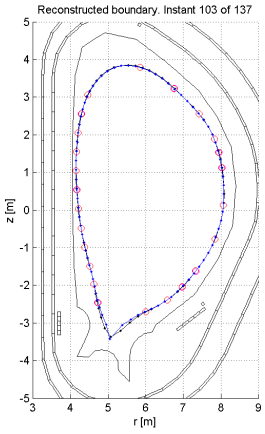

(c) *Equilibrium 103.*

Figure A.4: *Reconstructed boundaries by the full-code (blue line) and by the one with only half the number of points (black line).*

Unfortunately, some boundaries are badly reconstructed, like the ones represented in figure A.4. The algorithm works quite good but there are some points of non-convergence, like in equilibrium 73, near the $x - point$ (this error is due to a thresholding effect).

Figure A.5 finally shows the greatest errors among the 24 gap-lines. 21 of 137 are badly reconstructed. It means that there is an error of at least 1 $[cm]$ in at least one gap. Typically the greatest errors are placed along the gaps 1 and 24, which are the closest to the $x - point$ region, that is a crucial region for the algorithm performance. For instance, compare figure A.3 (a) and A.5. It's clear that in static conditions the biggest errors in the gaps are less than 1 $[cm]$ and so the reconstruction is good enough. When this is not, the algorithm performance decreases. In particular, during dynamical events in the plasma behavior, the algorithm appears to be particular sensitive in the

computation of the flux values along the grid predisposed to find the value of the flux at the boundary when dealing with a diverted plasma.

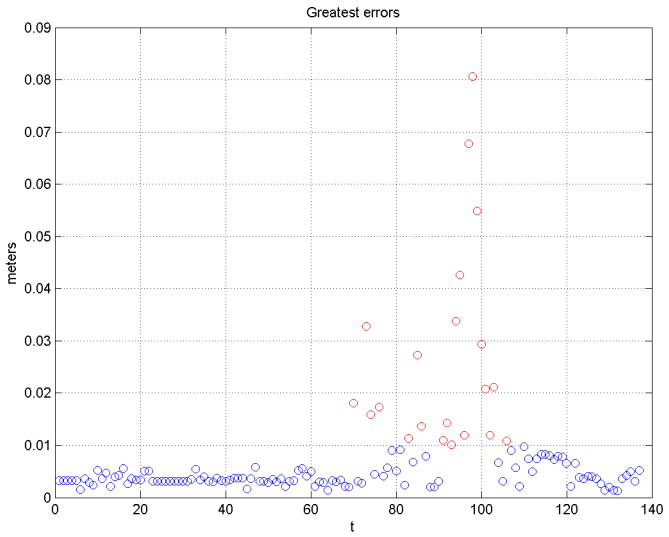

Figure A.5: *Greatest errors among the* 24 *gap-lines in each time instant. The blue circles represent errors smaller than* $1\ [cm]$*, while red circles are above this threshold.*

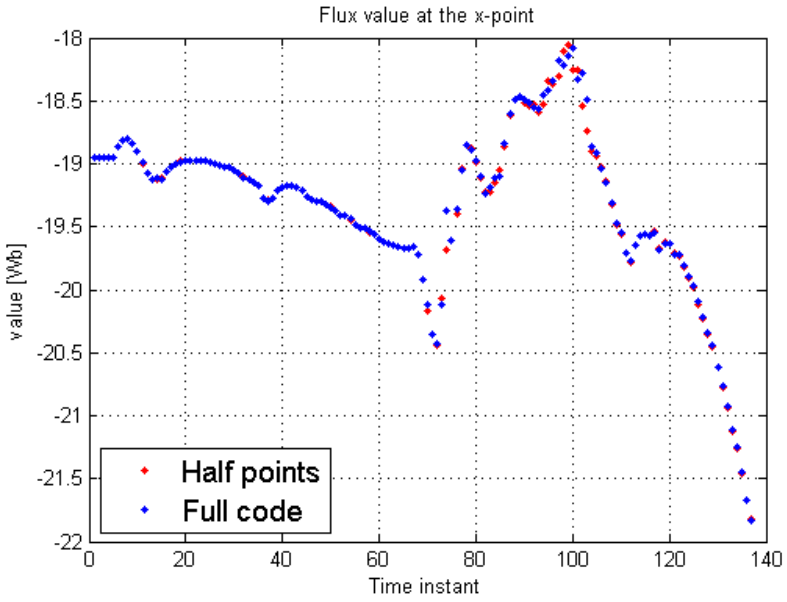

Figure A.6: *Flux estimated values at the* $x-point$*.*

As is shown in figure A.6, considerable errors in the evaluation of the boundary flux are made exactly in those equilibrium corresponding to dynamical events, and they lead to the errors seen in figure A.5.

Acronyms

ITER	International Thermonuclear Experimental Reactor
PF	Poloidal Field
MOR	Model Order Reduction
MHD	Magnetohydrodynamics
IAIA	Iterative Axisymmetric Identification Algorithm
TBR	Truncated Balanced Realization
pMOR	Parametric MOR
PDE	Partial Differential Equations
ODE	Ordinary Differential Equations
GS	Grad-Shafranov
SVD	Singular Value Decomposition
FE	Finite Element
SMA	Selective Modal Analysis
MIMO	Multiple-Input Multiple-Output
SISO	Single-Input Single-Output
TF	Toroidal Field
CS	Central Solenoid
FW	First Wall
RFX	Reverse Field eXperiment
RFP	Reverse Field Pinch

List of Figures

List of Tables

Bibliography

[1] B. Lohmann and B. Salimbahrami, *Introduction to Krylov Subspace Methods in Model Order Reduction*, Bremen, Germany, 2001.

[2] Z. Bai and D. Skoogh, *Krylov Subspace Techniques for Reduced-Order Modeling of Nonlinear Dynamical Systems*, Davis, USA, 2001.

[3] A. Beghi, *An Application of Selective Modal Analysis to Tokamak Modeling and Control*, Padua, Italy, 2001.

[4] B. Lohmann and B. Salimbahrami, *Krylov Subspace Methods in Linear Model Order Reduction: introduction and Invariance Properties*, Bremen, Germany, 2002.

[5] A. C. Neto, F. Sartori, F. Piccolo, et al., *Marte: A multiplatform real-time framework*, IEEE Trans. Nucl. Sci., vol. 57, no. 2, pp. 479–486, 2010

[6] L. Zabeo, G. Artaserse, A. Cenedese, et al., *A new approach to the solution of the vacuum magnetic problem in fusion machines*, Fusion Engineering and Design, vol. 82, pp.1081–1088, 2007

[7] P. Merlo, *Plasma Boundary Reconstruction and Shape Control of Tokamak Discharges in RFX-MOD*, Padua, Italy, 2011.

[8] A. Pironti and M. Walker, *Fusion, Tokamaks, and Plasma Control*, IEEE Control System Magazine, 2005.

[9] M. G. Safonov, R. Y. Chiang and D. J. N. Limebeer, *Optimal Hankel Model Reduction for Nonminimal Systems*, IEEE Trans. Automat. Contr., vol.35, 1990.

[10] A. Beghi, A. Cenedese, *Advances in real-time plasma boundary reconstruction: From gaps to snakes*, IEEE Control Systems Magazine, vol. 25(5), 2005.

[11] A. Beghi, A. Cenedese, *Iterative Axisymmetric Identification Algorithm (IAIA) for real-time reconstruction of the plasma boundary of ITER*, Padua, Italy, 2005.

[12] M. G. Safonov et al., *Optimal Hankel model reduction for Nonminimal Systems*, IEEE Transactions on automatic control, 35, 1990.

[13] A. Beghi, M. Cavinato and A. Cenedese, *Nonlinear dynamic modeling for control of fusion devices*, Cancun, Mexico, 2008.

[14] J. B. Lister, A. Portone and Y. Gribov, *Plasma Control in ITER*, IEEE Control System Magazine, 2006.

[15] G. Ambrosino and R. Albanese, *Plasma Current, Position, and Shape in Tokamaks*, IEEE Control System Magazine, 2005.

[16] W. Gressick, J. T. Wen and J. Fish, *Order Reduction for Large Scale Finite Element Models: a Systems Perspective*, International Journal for Multiscale Computational Engineering, Rensselear Polytechnic Institute, NY, 2005.

[17] M. M. M. Al-Husari, B. Hendel, I. M. Jaimoukha, E. M. Kasenally, D. J. N. Limebeer and A. Portone, *Vertical stabilization of Tokamak plasmas*, 30th Conference on Decision and Control, Brighton, England, December 1991.

[18] I. M. Jaimoukha and E. M. Kasenally, *Oblique projection methods for large scale model reduction*, SIAM journal on Matrix Analysis and Application, Vol. 16, No. 2, pp. 602-627, April 1995.

[19] R. D. Slone, Jin-Fa Lee and R. Lee, *A Comparison of Some Model Order Reduction Techniques*, ElectroScience Laboratory, Department of Electrical Engineering, Ohio, USA, 2002.

[20] D. OBrien, J.J. Ellis, J. Lingertat, *Local expansion method for fast plasma boundary identification in JET, Nuclear Fusion*, vol. 33, no. 3, pp. 467, 1993

[21] H. Wu and A. Cangellaris,*Model-Order Reduction of Finite-Element Approximations of Passive Electromagnetic Devices Including Lumped Electrical-Circuit Models*, IEEE Transactions on Microwave Theory and Techniques, Vol. 52, No. 9, September 2004.

[22] S. Janardhanan, *Model Order Reduction and Controller Design Techniques*.

[23] L. E. Zacharov and V. D. Shafranov, *Equilibrium of a toroidal plasma with noncircular cross section*, Sov. Phys. Tech. Phys., vol. 18, no. 2, pp. 151–156, 1973.

[24] K. Glover, *All Optimal Hankel Norm Approximations of Linear Multivariable Systems and their $\mathcal{L}_\infty$ Error Bounds*, International journal of control, Vol. 39, pp. 1115-1193, 1984.

[25] A. Polidoro, *Algoritmi per la riduzione del modello*, Padua, Italy, 2013.

[26] N. Singh, R. Prasad and H. O. Gupta, *Reduction of large scale systems using Hankel norm approximation*, Electrical Engineering Departiment, IIT Roorkee, India.

[27] S. H. Aydin, M. Tezer-Sezgin, *Numerical solution of Grad-Shafranov equation for the distribution of magnetic flux in Nuclear Fusion Devices*,Turkish Journal of Engineering and Environmental Sciences, 2008.

[28] L. Boncagni, S. Galeani, G. Granucci, G. Varano, V. Vitale and L. Zaccarian, *Plasma Position and Elongation Regulation at FTU Using Dynamic Input Allocation*, IEEE transactions on control system technology, Vol. 20, No. 3, May 2012

[29] P. Bettini, A. Formisano, R. Martone, et al., *Identification of the plasma magnetic contour from external magnetic measurements by means of equivalent currents*, European Physical Journal of Applied Physics, vol. 13, pp. 51–57, 2001

[30] A. Cenedese, F. Sartori and M. Macuglia, *Development of fixed- position filamentary plasma model based on the current moment description*, IEE Proc.-Sci. Meas. Technol., vol. 151, pp. 484–487, 2004

[31] H. Wu and A. Cangellaris,*Krylov Model Order Reduction of Finite Element Models of Electromagnetic Structures with Frequency-Dependent Material Properties*, University of Illinois, Department of Electrical and Computer Engineering, June 2006.

[32] K. Zhou, *Essential of Robust Control*, California, USA, Prentice Hall, 1998.

[33] B. Lohmann, B. Salimbahrami and T. Bechtold, *Two-Sided Arnoldi in Order Reduction of Large Scale MIMO Systems*, Bremen-Freiburg, Germany, 2002.

[34] J.P. Freidberg, *Ideal Magneto-Hydro-Dynamics*, New York: Plenum Press, 1987.